

Evaluation of SAS1B as an Immunotherapeutic Target for the Treatment of Cancer

Kiley Anderson Knapp
Barre, Vermont

Bachelor of Science, University of New Hampshire, 2009

A Dissertation Presented to the Graduate Faculty of the University of Virginia in
Candidacy for the Degree of Doctor of Philosophy

Experimental Pathology
University of Virginia
May, 2018

Dedication

I dedicate my work to daughter, Harper, my husband, Brook, and to my parents Kristin and Michael Gilbar and Thomas and Holly Anderson. My successes are owed in large part to my family; I sincerely thank them for their continued unconditional love and support.

Acknowledgements

Firstly, I offer thanks to my late mentor, Dr. John C. Herr (1948-2016), for the many lessons learned not only in science but also in leadership, perseverance, and expert-level gardening. For those of us working in Dr. Herr's lab, his passion for and dedication to his research served as regular inspiration and motivation. His vision and expertise inspired this work and I am grateful to have had the opportunity to work with him.

I also thank Dr. Timothy Bullock for serving as an exceptional mentor to me after Dr. Herr's passing. I am grateful that despite his busy schedule, Dr. Bullock was regularly available and willing to offer guidance. Dr. Bullock went above and beyond with regard to intellectual support, research guidance, and invaluable assistance with manuscript and dissertation preparation for which I thank him.

Dr. Eusebio Pires has also been a great mentor and friend of mine throughout this work and I am grateful to him for that. I thank Dr. Pires for patiently teaching me, answering my relentless questions, and for the endless discussions. Many of the protocols utilized in this work were adapted from Dr. Pires' previous work. Dr. Pires' general scientific support was crucial to this research.

I also thank the following members of my dissertation committee: Dr. James Mandell, Dr. Timothy Bullock, Dr. J. Thomas Parsons, Dr. Janet Cross, Dr. Amy Bouton, Dr. Charles Landen, and Dr. Barry Hinton for their continued support and scientific counseling. I am grateful for the discussions with and suggestions from the committee which helped guide the research aims and the progress of this work.

A number of people contributed experimentally to this work whom I would also like to thank. Dr. Pires performed the experiments represented in Supplemental Figure 2.1.

Dr. Walter Olson and Aaron Stevens performed the work shown in Figures 3.2 and 3.3, respectively. Dr. Jagathalpa Shetty performed the experiments in Figure 3.11. Dr. Michael Harding contributed the hypothesis regarding SAS1B's active role as a metalloprotease which cleaves ZP domain containing proteins in cancer.

I would like to thank Dr. Scott Vande Pol and Nicole Brimer at UVA for providing neonatal keratinocytes and offering support for cell growth and expansion.

I am grateful to Dr. Jagathpala Shetty, Dr. Ryan D'Souza, and Dr. Michael Harding, and Dr. Arabinda Mandal for continued general intellectual support and guidance.

I also thank the members of the following UVA Core Facilities: the Research Histology Core, the Flow Cytometry Core, the Cell Culture core, the Microscopy Facility, and the Biorepository and Tissue Research Facility.

Abstract

Immunotherapeutic options for the treatment of cancer, which remains a major global health challenge, offer the allure of greater tumor specificity and less associated toxicity than is typically achieved with traditional chemo- and radio-therapeutic strategies. The success of some immunotherapies, such as ADCs and CAR-Ts, rely on identification and selection of targets which are highly tumor-specific with limited or no expression in normal tissues. Cancer germline antigens represent potential ideal targets for targeted immunotherapy as CGAs are expressed in cancer cells but show limited or no expression among normal tissues. Although many cancer-testis antigens have been described, SAS1B is the first, and only, cancer-oocyte antigen identified to-date. Owing to the limited expression of SAS1B among normal tissue combined with expression in a number of cancer indications, we propose that SAS1B is an attractive immunotherapeutic target.

We have shown that, in addition to previous work published in female reproductive cancers, SAS1B is expressed in a majority of pancreatic and head and neck cancers. SAS1B localized to both the cytoplasm and the cell surface in PDAC and HNSCC cell lines by IIF and flow cytometry, suggesting potential utility of SAS1B targeted immunotherapeutic strategies. Furthermore, an ADC targeting SAS1B administered to pancreatic cancer cell lines was internalized and subsequently caused significant cell death in a manner correlated with SAS1B cell surface expression. Thus, SAS1B represents a novel therapeutic target for the treatment of PDAC and HNSCC. These data support further development of a SAS1B-ADC including *in vivo* assessment using mouse xenograft systems.

Although we have shown proof of concept that SAS1B-ADC induces cytotoxicity in pancreatic cancer cell lines, addressing multiple fundamental biological questions which remain regarding SAS1B expression will also inform production of SAS1B targeted therapies. For example, we have identified six ASTL splice variants in cancer, known as SV-A to SV-F, and have shown differential cellular localization of recombinant SV-A and SV-C proteins (cell surface vs. cytoplasm, respectively). Further studies characterizing major SAS1B protein isoform(s) expressed at the cell surface in cancers may lead to development of more effective immunotherapies utilizing mAbs generated against cell surface, cancer-associated form(s) of SAS1B. Our work suggests SAS1B expression in a broad range of cancer indications and demonstrates efficacy of a SAS1B-ADC *in vitro*, thus supporting further assessment of SAS1B as an immunotherapeutic target for the treatment of cancer.

Table of Contents

List of Figures.....	3
Chapter 1: General Introduction	
Cancer: Statistics and Common Therapeutic Options.....	6
Select Immunotherapeutic Options for Cancer Treatment.....	7
Antibody Drug Conjugates.....	10
SAS1B.....	14
Astacin Family of Metalloendopeptidases.....	17
Tumor Neoantigens.....	19
Chapter 2: Evaluation of SAS1B as a target for antibody-drug conjugate therapy in the treatment of pancreatic cancer (modified from <i>Oncotarget</i> submission)	
Abstract.....	23
Introduction.....	24
Results.....	26
Discussion.....	46
Methods.....	53
Chapter 3: ASTL/SAS1B: Expression in normal cells and additional cancers	
Introduction.....	63
Results.....	69
Discussion.....	105
Methods.....	121

Chapter 4: Future Directions

What is the pattern of expression and cellular localization of ASTL splice variants and SAS1B isoforms in cancer.....	130
What is the functional role of SAS1B in cancer.....	132
How is SAS1B regulated in cancer.....	138
Is SAS1B expressed in pancreatic cancer stem cells.....	141
What is the threshold of SAS1B surface expression needed for ADC cytotoxicity in PDAC cell lines and how does this relate to potential cutoff for which patients will be treated.....	143
Does a SAS1B-ADC effectively stop tumor growth or shrink tumors <i>in vivo</i>	145
Final Summary.....	148
Chapter 5: References.....	152

List of Figures

Figure 1.1: SAS1B protein domain structure.....	16
Figure 2.1: SAS1B was expressed in a majority of pancreatic cancers and was not detected in normal pancreas ductal epithelium by IHC.....	29
Figure 2.2: SAS1B signal in pancreatic cancer tissue was blocked by pre-incubating anti-SAS1B mAb, 6B1, with rSAS1B.....	31
Figure 2.3: ASTL/SAS1B expression in pancreatic cancer patient derived xenografts...	32
Figure 2.4: SAS1B localized to the cytoplasm and to the cell surface in pancreatic cancer cell lines.....	35
Figure 2.5: SAS1B surface expression in pancreatic cancer cell lines correlated to anti-SAS1B ADC cell killing <i>in vitro</i>	41
Figure 2.6: Anti-SAS1B mAb, SB2, signal in live mPanc96 cells was blocked when pre-incubated with rSAS1B protein.....	42
Figure 2.7: ADCs with different anti-SAS1B mAbs are also cytotoxic to mPanc96 cells.....	43
Figure 2.8: Anti-SAS1B mAb, SB2, alone was not cytotoxic to pancreatic cancer cell lines.....	44
Figure 2.9: Cytotoxicity of an anti-SAS1B ADC was blocked in pancreatic cancer cell lines when SB2 mAb was pre-incubated with a SAS1B peptide.....	45
Supplemental Figure 2.1: SAS1B mAb 6B1 preferentially recognizes cytoplasmic SAS1B.....	60
Figure 3.1: ASTL gene expression data from GTEx database.....	70
Figure 3.2: SAS1B localizes to the cytoplasm, but not to the cell surface, in a small population of human PBMCs.....	73
Figure 3.3: Mouse SAS1B was expressed intracellularly in dendritic cells.....	76

Figure 3.4: ASTL/SAS1B was expressed in a high percentage of patient HNSCCs.....	81
Figure 3.5: HNSCC cell lines expressed ASTL/SAS1B.....	82
Figure 3.6: SAS1B is predicted to be heavily O-glycosylated.....	83
Figure 3.7: SAS1B localized to the cytoplasm and to the cell surface in OSC-19.....	87
Figure 3.8: ASTL/SAS1B was expressed in leukemia patient samples and cell lines....	89
Figure 3.9: Improved RT-PCR amplification of ASTL achieved by optimizing reverse transcription assay.....	92
Figure 3.10: ASTL splice variants identified in cancer cells.....	95
Figure 3.11: Transfection of 293T cells with ASTL SV-A and SV-C mammalian expression constructs resulted in expression of SAS1B proteins.....	99
Figure 3.12: siASTL knock-down in mPanc96 cells reduced total cell number.....	104

Chapter 1

General Introduction

Cancer: Statistics and Common Therapeutic Options

Cancer, a major public health problem globally, causes 1 in 8 deaths [1] and is the second leading cause of death worldwide [2]. In 2017, an estimated 1.69 million Americans will be diagnosed with cancer and approximately 600,000 will die [3]. For decades, the mainstay of cancer treatment has been surgery, radiation therapy, and/or chemotherapy. Although treatment plans will vary depending on tumor type, tumor stage, and patient health, surgery and radiotherapy are often used when a tumor remains locally while chemotherapy is used for metastatic disease. Many early-detected, primary and localized tumors can be effectively treated with surgery, even cured. Prognosis for these patients is generally very good, especially if the entirety of the tumor is surgically removed before metastasis has occurred. Tumors prone to early dissemination are likely to receive combination treatment of surgery and/or radiation to treat the primary tumor followed by chemotherapy to treat potential metastatic disease [4]. Neoadjuvant therapy, in which radio- or chemo-therapy is administered before surgery, may be used to shrink tumors prior to surgical removal. Patients who have metastatic disease at the time of diagnosis typically have a far less favorable prognosis and are more difficult to treat. In this case, chemotherapy and/or radiation therapy are utilized, often in combination or followed by newer therapeutic approaches [4]. Lymphoma and leukemia, the so-called liquid cancers, are generally treated with systemic chemotherapy and potentially newer targeted therapies as well. However, for many patients with metastatic disease, even if initial therapeutic response is good, development of drug-resistance and relapse are common [5]. Surgery, chemotherapy, and radiation therapy have been the mainstay of cancer treatment for

decades; however, chemo- and radio-therapy lack tumor specificity leading to problematic off-tumor toxicity.

Many current anti-cancer drugs, namely chemotherapeutics, have nonspecific toxicity as a consequence of targeting proliferating cells which often includes healthy cells in addition to tumor cells. As such, these drugs have a low therapeutic index and a narrow therapeutic window which limits their efficacy. Due to lack of specificity, most anti-cancer drugs are used near their maximum tolerated dose which is typically lower than what would sufficiently eradicate the tumor [6, 7]. Because dose-limiting toxicities of the gastrointestinal tract and bone marrow are relatively common, chemotherapy can often be difficult for patients to endure; therefore, new treatments including targeted immunotherapeutic approaches (e.g. antibody drug conjugate (ADC)) have become highly attractive due to their specificity [5].

Select Immunotherapeutic Options for Cancer Treatment

Despite the signing of the National Cancer Act in 1971, which increased efforts to eradicate cancer as a major cause of death, the war on cancer has clearly not been won; however, recent advancements in novel treatment modalities, such as immunotherapy, have provided renewed hope for prolonging patient survival. Development of novel therapeutics should focus on cancer cell-specific targeted therapies to avoid pitfalls of current treatment standards (e.g. chemotherapy) including, lack of selectivity/specificity and unwanted toxicity. Although it has long been known that cancer cells have the ability to suppress the host's immune response, immunotherapeutic strategies saw numerous failures early on. However, several recent clinical successes using immunotherapies such

as sipuleucel-T, the autologous cellular immunotherapeutic option for prostate cancer, ipilimumab, the anti-cytotoxic T lymphocyte-associated protein 4 (CTLA-4) antibody for melanoma, and antibodies against the anti-programmed cell death protein 1 (PD1) also for melanoma treatment, have gained widespread attention and have rejuvenated the field.

While there are multiple immunotherapeutic options for treating cancer, common research areas including passive approaches such as antibody-drug conjugates (ADC) and chimeric antigen receptor T cells (CAR-T) or active approaches like cancer vaccines, have been given widespread attention in hopes of developing more specific and less toxic therapeutics [8, 9]. These approaches are unified by their dependence on the identification and selection of appropriate targets which have high tumor specificity and expression with no or limited expression in normal tissues. Newly discovered, tumor-specific antigens are of great value and may be purposed for both active and passive immunotherapies, with the exception of mutation driven neoantigens that are solely T cell targets. Immunotherapies represent a promising approach to achieve a more selective, and potentially more potent, treatment than has been seen before with radio- and chemo-therapy.

Cancer vaccines with tumor antigens work to specifically activate T cells of the host immune system. The first FDA approved autologous cellular immunotherapy, sipuleucel-T (2010), provides a significant survival benefit in prostate cancer patients but did not significantly decrease tumor volume or disease response in randomized clinical trials [10]. There is minimal associated toxicity and treatment with sipuleucel-T is of short duration [8]. Despite excitement generated by sipuleucel-T approval, vaccine development has been slowed, in part, due to lack of appropriate tumor antigens. Requirements of ideal tumor antigens include: high tumor expression, high patient incidence, no to low

expression among normal tissues, and cancer cell growth or survival dependent to avoid antigen downregulation associated immune escape [8].

In contrast to vaccination, the adoptive cell therapy known as CAR-T, circumvents the need for functional antigen processing machinery in tumor cells or major histocompatibility complex (MHC) antigen expression. In CAR-T therapy, tumor cell surface antigens are recognized by the antibody variable domain portion of the CAR and then the T-cell receptor (TCR) constant domain portion of the CAR results in T-cell activation via intracellular signaling chains [8, 11]. Antigen selection is crucial to the success of CAR-T therapy, which has greatly limited by the lack of tumor specific antigens not expressed on essential normal tissues. Expression of CAR-T targets in normal tissues, even at low levels, can result severe on-target, off-tumor toxicity. Thus, the ideal CAR-T antigen will be exclusive to cancer cells; however, an antigen shared between cancer cells and nonessential normal cells may also be a potential CAR-T target [11]. The CD19 antigen expressed in the vast majority of B cell malignancies, is a prominent example of a CAR-T antigen shared between cancer cells and nonessential normal cells as it is also expressed on B cells at all stages of differentiation. Effectiveness of targeting CD19 with CAR-T therapy has been demonstrated in patients with follicular lymphoma, large-cell lymphomas, chronic lymphocytic leukemia, and acute lymphocytic leukemia [12-15]. Cytotoxicity of normal CD19^{pos} B cells is countered by periodic administration of immunoglobulin infusions into patients receiving treatment thus demonstrating potential clinical applications for targets which are shared between cancer cells and nonessential, normal cells. Antigens which are highly specific for cancer cells are of high value for

immunotherapeutic approaches including cancer vaccines, CAR-T, and ADCs; the nature of the target will help guide development of the most effective immunotherapeutic option.

Antibody Drug Conjugates

ADCs represent a subset of immunotherapies whose functional activity is not dependent upon targeting oncogenic pathways that drive tumorigenesis, but via the recognition of proteins that are uniquely expressed by tumors, leading to direct or indirect immune-mediated destruction. The use of ADCs for therapeutic purposes is a fast growing field that has seen recent successes in pre-clinical studies as well as clinical trials. Success is owed, in part, to optimization of the various components of ADCs: the monoclonal antibody (mAb), the drug, and the linker. In general, the monoclonal antibody portion of the ADC binds to the target antigen expressed on cancer cells and the ADC is internalized followed by release of the toxin culminating in cell death. Based on the specificity of the target, ADCs have the potential to selectively kill cancer cells while sparing normal cells which do not express the tumor specific antigen.

The method of action of the ADC becomes complex as the ADC must travel through various conditions from the blood stream to the target cancer cells with challenges existing at each step: circulation, antigen binding, internalization, drug release, and drug action. The stability of the linker in the blood is crucial to prevent nonspecific cell killing and associated cytotoxicity which may result from premature release of the toxin [7]. ADCs need to have a half-life long enough to reach the target tissue and shouldn't be immunogenic, both of which were overcome by generating humanized antibodies for use in substitution of murine antibodies originally utilized [6, 16].

Once at the target tissue, the antigen and monoclonal antibody become more important. Ideal targets will be tumor specific and not expressed on the surface of normal cells, internalized, not shed into the blood, and of sufficient concentration at the cell surface for ADC induced cytotoxicity. Naked antibody-antigen binding at the cancer cell surface leads to cell lysis via one of three mechanisms: 1) stimulation of immune response leading to antibody-dependent cellular cytotoxicity (ADCC), 2) complement-dependent cytotoxicity (CDC), or 3) triggering an apoptotic signaling cascade [16]. Monoclonal antibodies can have high binding specificity for tumor specific antigens but can be therapeutically ineffective alone; improved cytotoxicity can be achieved by attaching a toxin to the mAb [7, 16, 17]. In addition to high target selectivity, mAbs may also display favorable pharmacokinetics. Notably, a humanized antibody can circulate in humans with a half-life of several days to weeks. Other advantages of mAbs include lack of toxicity while in circulation as they are only functional upon target binding and internalization [6]. The conjugated mAb needs to retain high immunoaffinity for the target such that attaching a toxin does not interfere with antigen binding [7]. Antigen concentration at the tumor cell surface must be high enough such that, following internalization, there is a sufficient amount of intracellular cytotoxin to cause cell death.

In contrast to being stable in the neutral pH of the blood, the ADC has to efficiently release the cytotoxin once internalized into a cancer cell; thus, a balance between plasma stability and efficient active drug release at the target cell must be achieved. Linker technology is incredibly important to the overall efficacy and safety of the ADC and as such, continues to be extensively studied. Because most ADCs are internalized by receptor-mediated endocytosis [18], many linkers are designed to be sensitive to the

proteolytic enzymes present in the acidic lysosomal compartment or alternatively utilize the highly reducing environment of the cell itself [16]. The four groups of linkers are either cleavable or non-cleavable. Acid-labile hydrazine linkers, early cleavable linkers, were shown to be associated with non-specific release of the drug in clinical studies [7, 19]. Newer cleavable linkers are disulfide-based or peptide based and have greater *in vivo* stability. Disulfide-based linkers are cleaved intracellularly due to high concentration of glutathione while peptide-based linkers are cleaved by lysosomal proteases. Peptide-based linkers are advantageous over disulfide-based because they have greater systemic stability and rapidly release the drug inside the target cell [16]. Non-cleavable linkers are thioether-containing and proteolytic degradation is likely the cause of toxin release [20, 21]. The therapeutic index of the ADC may be improved with a non-cleavable linker due to greater stability in circulation suggesting higher tolerance and lower nonspecific toxicities [20, 22, 23]. It is likely that assessment of each individual mAb-antigen pair will afford the best optimization of ADCs for particular cancer types.

In addition to the target antigen, the mAb, and the linker, the appropriate cytotoxic payload must also be chosen. Multiple drugs suitable for conjugation exist but those currently being used in ADCs are generally either target microtubules or DNA. Because the concentration of the released drug may be quite low due to low target antigen expression, the use of very potent drugs with subnanomolar IC₅₀ (as free drug) becomes necessary [7]. Antibodies can be linked to highly toxic drugs, toxins which are 100 to 1000 times more cytotoxic than traditional anticancer agents, which would otherwise be too harmful to be used *in vivo* [24-26]. Drugs are linked to the constant region (Fc) of the antibody to minimize potential interference with antigen binding which occurs in the

variable region (Fv). Studies have shown that attaching 2-4 drug molecules per antibody provides optimal pharmacokinetics giving the best therapeutic window [27, 28]. Many insights into developing effective, stable, and safe ADCs have been gained over the last two decades and ongoing research continues to contribute to producing clinically significant ADCs, two of which are currently in use today.

Two FDA approved ADCs, brentuximab vedotin (Adcetris) targeting the tumor necrosis factor CD30 and trastuzumab emtansine (Kadcyla) targeting the human epidermal growth factor receptor 2 (Her2/neu), have revolutionized treatment for Hodgkin's lymphoma and breast cancer, respectively [26]. Trastuzumab and Kadcyla, however, target molecules found on normal and cancer cells and can result in on-target/off-tumor side effects [29]. In addition to cell surface localization on breast cancer cells, Her2 is expressed in many normal human tissues which can lead to a variety of adverse drug effects including cardiomyopathy [30]. CD30, the target of Adcetris, is expressed on normal activated immune cells (T-/B-cells, natural killer cells, and monocytes) as well as Hodgkin's lymphomas and systemic anaplastic large-cell lymphomas [29]. Potential adverse drug effects associated with CD30 targeting include neutropenia and sepsis. Interleukin (IL)-13 receptor $\alpha 2$ [31] is a promising therapeutic target which is expressed in a majority of incurable glioblastoma multiforme tumors [32-34] as well as other solid tumors [35] and is largely absent in normal tissues except for the testes [36]. Despite some potential adverse effects, the clinical successes of Adcetris and Kadcyla have helped promote greater effort to identify and validate novel targets for ADCs. Development of ADCs and other immunotherapies depends largely on identification of appropriate targets; to deliver highly cytotoxic drug concentrations with limited off-tumor effects, ideal targets are tumor

specific and are not expressed on normal tissues. Cancer-germline antigens, described below, represent a class of proteins, which show specificity for tumor cells over normal cells, of which some members may be target candidates for immunotherapies.

SAS1B

SAS1B (sperm acrosomal SLLP1 binding; aka ovastacin, *ASTL*, GenBank ID NM_001002036.3) is an oocyte membrane-associated zinc metalloprotease which interacts with the intra-acrosomal sperm ligand SLLP1 prior to gamete fusion, contributing to fertilization [37, 38]. An additional population of SAS1B has been shown to be exocytosed from oocyte cortical granules, which are peripherally located subcellular organelles unique to ovulated eggs, after fertilization to aid in the block to polyspermy by cleaving zona pellucida protein 2 (ZP2) surrounding 2-cell embryos [39, 40]. SAS1B, a 431 amino acid protein, is comprised of a signal peptide (amino acids 1-23) at the N-terminus, pro-peptide (24-90), proteinase domain (91-279) containing a Hex-box catalytic site (HEXXHXXGXXH; zinc atoms are coordinated at positions 182, 186, 192), and a unique C-terminal domain (280-431) (Figure 1.1). The prodomain (pro-peptide) is predicted to be endoproteolytically cleaved to activate SAS1B's enzymatic function, as commonly occurs with other astacin family zinc metalloproteases [38].

Among normal tissues, SAS1B expression is thought to be limited to the ovary and only at specific stages of folliculogenesis: secondary, pre-antral, and Graffian follicles. Expression of SAS1B first occurs within the cytoplasm of oocytes within follicles that have entered the transition between primary and secondary follicle stages at when the formation of two granulosa cell layers is initiated. Thus, SAS1B is absent in all oocytes within

primordial follicles that comprise the quiescent ovarian reserve [38]. Post-fertilization, distribution of SAS1B becomes patchy on the blastomere membranes and is undetectable in mouse embryos by the late blastocyst stage [37]. The precise timing of expression of SAS1B during folliculogenesis in follicles at the primary to secondary transition has been observed in a range of ovaries from different species and stages – post-natal, pubertal, or adult mouse, as well as in all eutherian species examined (humans, mice, rats, hamsters, sheep, dogs, cats) [38].

SAS1B was not detected in a variety of additional normal human tissues from a tissue microarray (TMA) by immunohistochemistry (IHC) [41] and no *ASTL* expressed sequence tags (ESTs) have been deposited in NCBI Unigene database from normal tissues [42]. Some ESTs from uterus matched SAS1B sequence but these deposits were determined to be from uterine cancers, leading to further investigation of SAS1B in female reproductive cancers.

SAS1B Protein Domain Structure (amino acids)

Figure 1.1 SAS1B protein domain structure

Schematic diagram of SAS1B protein domain structure with amino acid positions listed in parentheses. At the N-terminus, SAS1B begins with a signal peptide (pink), which likely directs SAS1B to the cell membrane or to be secreted, followed by a propeptide domain (blue) which is likely cleaved to produce an active enzyme. The proteinase domain (green) contains a conserved catalytic region (light green dashed-line box; amino acids 182-192 with zinc binding at amino acids 182, 186, and 192). The C-terminal region (orange) is unique to SAS1B as compared to other metalloproteinases.

In addition to localization within the ovary, SAS1B has also been shown to be expressed in a majority uterine tumors (66-85%) [41]. In a uterine tumor cell line SNU539, SAS1B was shown to be localized to the cell membrane and internalized via the endocytic pathway; thus, cell surface SAS1B may be used to deliver cargo (e.g. cytotoxins via ADC) into the interior of tumor cells. SNU539 cells were sensitive to growth arrest and cell death in the presence of an indirect antibody-saporin (drug) conjugate using a rabbit polyclonal antibody targeting SAS1B. Markedly increased LDH levels in supernatants were observed. No effect of the ADC was seen with normal endometrial stromal cells, media alone, normal rabbit IgG-saporin, or secondary-drug conjugate alone [41]. A pilot *in vivo* study using SNU539 tumor cells injected into athymic nude mice showed tumor development with expression of ASTL/SAS1B transcript and proteins (Pires et. al, unpublished data). This pilot study suggests that human tumors xenografted in mouse maintain ASTL/SAS1B expression and therefore represent a suitable system for studying effects of anti-SAS1B therapies *in vivo*. These preliminary studies position SAS1B as a viable target of an immunotoxin and support the study of ADCs for the treatment of SAS1B positive tumors. Because of limited expression in normal cells plus expression in cancer cells, SAS1B was the first described protein in a new class known as cancer-oocyte antigens (COA) which is the ovary counterpart of the well-known group of cancer-testis antigens (described below) [41].

Astacin Family of Metalloendopeptidases

ASTL/SAS1B belongs to the astacin family of zinc metalloproteinases (MEROPS family M12) and the metzincin superfamily [43-45]. Included in the metzincin superfamily

are the ADAMs (a disintegrin and metalloproteinase), the MMPs (matrix metalloproteinases), the pappalysins (pregnancy associated plasma proteins), the serralysins (bacterial enzymes), the leishmanolysins (protozoan and metazoan proteinases), and the astacins [46]. The astacin family, which is made up of mostly secreted or plasma membrane bound proteins, was named from the prototypical digestive enzyme, astacin, identified from crayfish, *Astacus astacus L.* Astacins have roles in both mature and developmental systems with several enzyme family members crucial for embryonic development, tissue differentiation, and extracellular matrix (ECM) assembly [45, 47]. Characterized by a ~200-residue catalytic region, including a highly conserved Hex-box sequence, and an N-terminal propeptide region, several hundred astacins have been identified in animals and bacteria. However, for most, functional roles have not been determined experimentally but domain structure and localization can be used to hypothesize physiological roles. In addition to the catalytic and propeptide domains, most eumetazoan astacins have multiple additional domains including complex C-terminal regions. These C-terminal elongations, which also roughly reflect different functional roles, have been used sort astacins into three major groups: tolloids/BMP1 (bone morphogenetic protein), hatching enzymes, and meprins [45].

The six known astacin family genes in humans and mice include two meprins, three BMP-1/tolloid-like, and one SAS1B (a.k.a ovastacin) [46]. Since meprins (α and β , encoded by two separate genes) were first discovered in epithelial cells of kidney tubules [48, 49] and of the small intestine [50], meprin expression has been documented in colon [45], intestinal leukocytes [51], skin [52], and cancer [53]. Via hydrolysis, meprins are able to activate or inactivate a variety of growth factors, vasoactive peptides, cytokines,

ECM proteins, and secreted protein kinases [54]. More recent work indicates meprin expression is much broader with suggested roles in angiogenesis, cancer, inflammation, fibrosis, and neurodegenerative diseases [52]. BMP-1/tolloid-like proteinases are involved with ECM assembly by activating pro-collagens, pro-proteoglycans, and other matrix protein precursors via cleavage [55, 56]. Humans express BMP-1 as well mammalian homolog of tolloid (mTLD) which is a splice variant encoded by the same gene. BMP-1, mTLD, plus two additional genes encoding mammalian tolloid-like 1 and 2 (mTLL-1, mTLL-2), comprise the human BMP-1/tolloid-like proteinase subfamily sometimes referred to as BTPs [57]. While BTPs are secreted, meprins are either secreted or localized to the plasma membrane. Hatching enzymes degrade embryonic envelopes during the hatching process and aid in skeletal formation [45]. Initially, ASTL transcript detected in human and mice ovaries was named ovastacin and was predicted to be involved in hatching [43] but was subsequently shown to play a role in fertilization, rather than in zonal hatching [37, 39]. Thus, the Herr group advocates the name SAS1B which conveys the protein's biological interactions better than the name ovastacin. Unlike the other astacin family members, SAS1B is a unique members in that it has been described as a cancer-oocyte antigen based on its' limited localization among normal tissues plus expression in cancer.

Tumor Neoantigens

Neoantigens were defined by Boyse and Old as new antigens that appeared on tumor cells as a result of de-differentiation or trans-differentiation [58]. More recently, neoantigens have been defined as peptides that are entirely absent from the normal human genome which are created by tumor-specific DNA alternations resulting in novel proteins

[59]. A rich literature exists on a class of neoantigens known as cancer testis antigens (CTAs). SAS1B represents one of the first defined antigens in a new class of cancer-oocyte antigens [41]. Cancer germline antigens (CGA), exemplified by the well-studied, numerous CTAs, are normally expressed discretely in germ cells and trophoblasts but are re-expressed in various human cancers [60, 61]. The first CTA, MAGE-A1 (melanoma antigen 1), was discovered in 1991 and since then, over 130 CTA genes have been described belonging to 83 gene families [60, 61]. It is theorized that CGAs are aberrantly expressed in tumors when the silenced gametogenic program in somatic cells is activated, and that this program acquisition, in part, contributes to tumorigenesis [62, 63]. Somatic cell-to-germline dysregulation has come to be regarded as a general feature of many human tumors and is associated with highly malignant phenotypes [64-66].

CTAs are expressed in a wide variety of human malignancies with different histological origins. Common regulatory mechanisms result in coordinated expression of some CTAs [67]. Embryonic cells, before implantation, are similar to cancer cells in that both are deprogrammed to a stem cell state and have the potential to become immortal and invasive [68]. Numerous studies have shown CTAs to be silenced by epigenetic mechanisms, particularly DNA methylation, and have observed demethylation at the promoter regions of CTAs in various cancers [69-74]. Similarly, genome-wide demethylation also occurs in oocytes in very early development [68]. CGAs with no to low expression among normal tissues are considered widely applicable targets for both cancer immunotherapy and vaccination with little risk of harmful side effects [66, 75]. Numerous anticancer immunotherapeutic strategies are currently being developed and have progressed to clinical trials [75].

Immunotherapeutic approaches to treating cancer are attractive, in part, because they rely on targets which are largely specific to cancer cells thereby theoretically resulting in fewer side effects as compared to traditional chemo- and radio-therapeutics. SAS1B, a cancer-germline antigen, represents a potential immunotherapeutic target that is expressed in cancer but has limited expression among normal tissues. Initial reports show SAS1B expression in female reproductive cancers. Our subsequent work focuses on expanding the range of cancer indications, including more solid tumors like pancreatic cancer and head and neck cancer, as well as hematological malignancies, which could potentially benefit from a SAS1B targeted therapeutic. We also seek to understand biological properties of SAS1B, which will guide development of successful SAS1B-immunotherapies, such as characterization of SAS1B isoform expression patterns and cellular localization in both cancers and normal tissues.

Chapter 2

Evaluation of SAS1B as a target for antibody-drug conjugate therapy in the treatment of pancreatic cancer

Kiley A. Knapp¹, Eusebio S. Pires^{2,3}, Sara J. Adair⁴, Arabinda Mandal², Anne M. Mills¹, Walter C. Olson⁴, Craig L. Slingluff Jr.⁴, J. Thomas Parsons⁵, Todd W. Bauer⁴, Timothy N. Bullock¹, John C. Herr^{1,2}

Departments of Pathology¹, Cell Biology², Obstetrics and Gynecology³, Surgery⁴, and Microbiology⁵ at the School of Medicine, University of Virginia, Charlottesville, Virginia USA

(Modified from manuscript published in *Oncotarget* **9**:10. January, 2018.)

ABSTRACT

Successful therapeutic options remain elusive for pancreatic cancer. The exquisite sensitivity and specificity of humoral and cellular immunity may provide therapeutic approaches if antigens specific for pancreatic cancer cells can be identified. Here we characterize SAS1B (ovastacin, *ASTL*, astacin-like), a cancer-oocyte antigen (COA), as an attractive immunotoxin target expressed at the surface of human pancreatic cancer cells, with limited expression among normal tissues. Immunohistochemistry shows that most pancreatic cancers are SAS1B^{POS} (68%), while normal pancreatic ductal epithelium is SAS1B^{NEG}. Pancreatic cancer cell lines developed from patient-derived xenograft models display SAS1B cell surface localization, in addition to cytoplasmic expression, suggesting utility for SAS1B in multiple immunotherapeutic approaches. When pancreatic cancer cells were treated with an anti-SAS1B antibody-drug conjugate, significant cell death was observed at 0.01-0.1 $\mu\text{g/mL}$, while SAS1B^{NEG} human keratinocytes were resistant. Cytotoxicity was correlated with SAS1B cell surface expression; substantial killing was observed for tumors with low steady state SAS1B expression, suggesting a substantial proportion of SAS1B^{POS} tumors can be targeted in this manner. These results demonstrate SAS1B is a surface target in pancreatic cancer cells capable of binding monoclonal antibodies, internalization, and delivering cytotoxic drug payloads, supporting further development of SAS1B as a novel target for pancreatic cancer.

INTRODUCTION

Pancreatic cancer continues to pose a serious clinical challenge, being the fourth leading cause of cancer-related deaths in the United States. Total deaths due to pancreatic cancer are predicted to increase dramatically, with the expectation that it will become the second leading cause of cancer-related deaths by 2030 [76]. Pancreatic ductal adenocarcinoma (PDAC) originates in the exocrine pancreas and accounts for 95% of all pancreatic cancers [77]. Endocrine pancreatic tumors, typically arising from islet cells, account for only 2-4% of total pancreatic cancer incidence [78]. The overall five-year survival rate has remained resistant to improvement, from 2% in 1975 to only 8% currently; for most pancreatic cancer patients, life expectancy is measured in months [3, 79].

Conventional treatment approaches, such as surgery, radiation, chemotherapy, or a combination of these, have had little impact on this aggressive tumor due to: 1) late stage diagnosis, which precludes surgery as a viable option, 2) lack of effective early detection biomarkers, 3) early and frequent metastases, and 4) eventual therapeutic resistance [9, 80, 81]. Almost 100% of patients eventually succumb to advanced metastatic disease with death from debilitating metabolic effects of the tumor [82]. At time of diagnosis, less than 10% of patients present with localized disease, approximately 30% with regional metastatic disease, and 50-60% with distant metastatic disease [3, 78]. More than 85% of tumors cannot be resected at time of diagnosis because of metastases, common sites including the liver, peritoneum, and the lungs. The only available option for patients with metastatic disease remains chemo- and/or radio-therapy, yet it rarely has any impact on survival [9, 83]. Gemcitabine, a nucleoside analog, has been the standard chemotherapy for all stages of PDAC, yet alone or in combination with additional chemotherapy, has shown lack of

significant response to therapy [78]. Radiotherapy, although previously used regularly, poses toxicity threats due to the closely adjacent radiosensitive organs [84, 85]. The need for effective, novel treatments for PDAC is clear.

Recent advances in the treatment of metastatic disease using combination chemotherapeutics have only increased overall survival in terms of months [86, 87]. The dense desmoplastic tumor stroma, characteristic of PDAC, contributes to inadequate therapeutic penetration and promotes resistance to chemo- and radiotherapy [80, 88]. However, combination of these more aggressive chemotherapies with therapies that engage novel targets may represent a promising therapeutic strategy for the treatment of PDAC [80].

Recent clinical success using the ADCs Adcetris and Kadcylla to treat Hodgkin's lymphoma and breast cancer, respectively, has sparked greater focus on developing ADCs. ADCs are an attractive molecular therapeutic option when the target is largely cancer cell specific and localizes to the cell surface, as is the case for the COA SAS1B.

SAS1B has not been detected in a variety of normal tissues, outside of growing oocytes within the ovary, but has been identified in female reproductive cancers. In a uterine tumor cell line SNU539, SAS1B was shown to be localized to the cell membrane, internalized via the endocytic pathway, and sensitive to growth arrest and cell death in the presence of an indirect antibody-saporin (drug) conjugate using a rabbit polyclonal antibody targeting SAS1B [41]. These studies position SAS1B as a viable target of an immunotoxin in cancer, with the attending advantages of limited on target/off-tumor effects on normal tissues, and support the study of ADCs for the treatment of SAS1B-positive (SAS1B^{POS}) tumors.

The following study provides evidence that SAS1B is expressed in a majority of pancreatic cancers, is localized to the cell surface, and that pancreatic cancer cells are killed when treated with an anti-SAS1B ADC, validating SAS1B as a target for further pre-clinical development.

RESULTS

SAS1B is expressed in a majority of pancreatic cancers and is not detected in normal pancreas ductal epithelium by IHC

Given the expression of *ASTL* (gene) / SAS1B (protein) in uterine cancer [41], we hypothesized that *ASTL*/SAS1B may be expressed in PDAC. Immunohistochemistry using an anti-SAS1B monoclonal antibody (mAb) (6B1; shown to largely recognize cytoplasmic SAS1B; Supplemental Figure 2.1) was performed on a TMA containing primary and metastatic pancreatic cancer samples, pancreatic intraepithelial neoplasia (PanIN; precursor lesions), and normal duct from both benign and malignant pancreas. TMA staining results were read in a blinded manner and scored by a pathologist on a 0 (negative) to 3+ positivity scale. SAS1B staining was not detected in untransformed ductal epithelium present in either benign or malignant pancreas (n=10) (Figure 2.1A-B). Low-grade PanINs were also SAS1B negative (n=8). SAS1B staining was observed in one out of six high grade PanINs. In some cases, stromal cells adjacent to ducts in normal and low grade tumors showed weak cytoplasmic reactivity (Figure 2.1A-B).

In contrast to the limited staining in low grade tumors, the majority of PDACs were SAS1B^{pos} (68%, n= 21/31), (Figure 2.1C-E). Both primary (n=13/16) and metastatic (n=8/15) tumors were SAS1B^{pos}. Most cancers exhibited 1+ or 2+ SAS1B staining intensity. When 6B1 mAb was pre-incubated with recombinant SAS1B (rSAS1B) protein

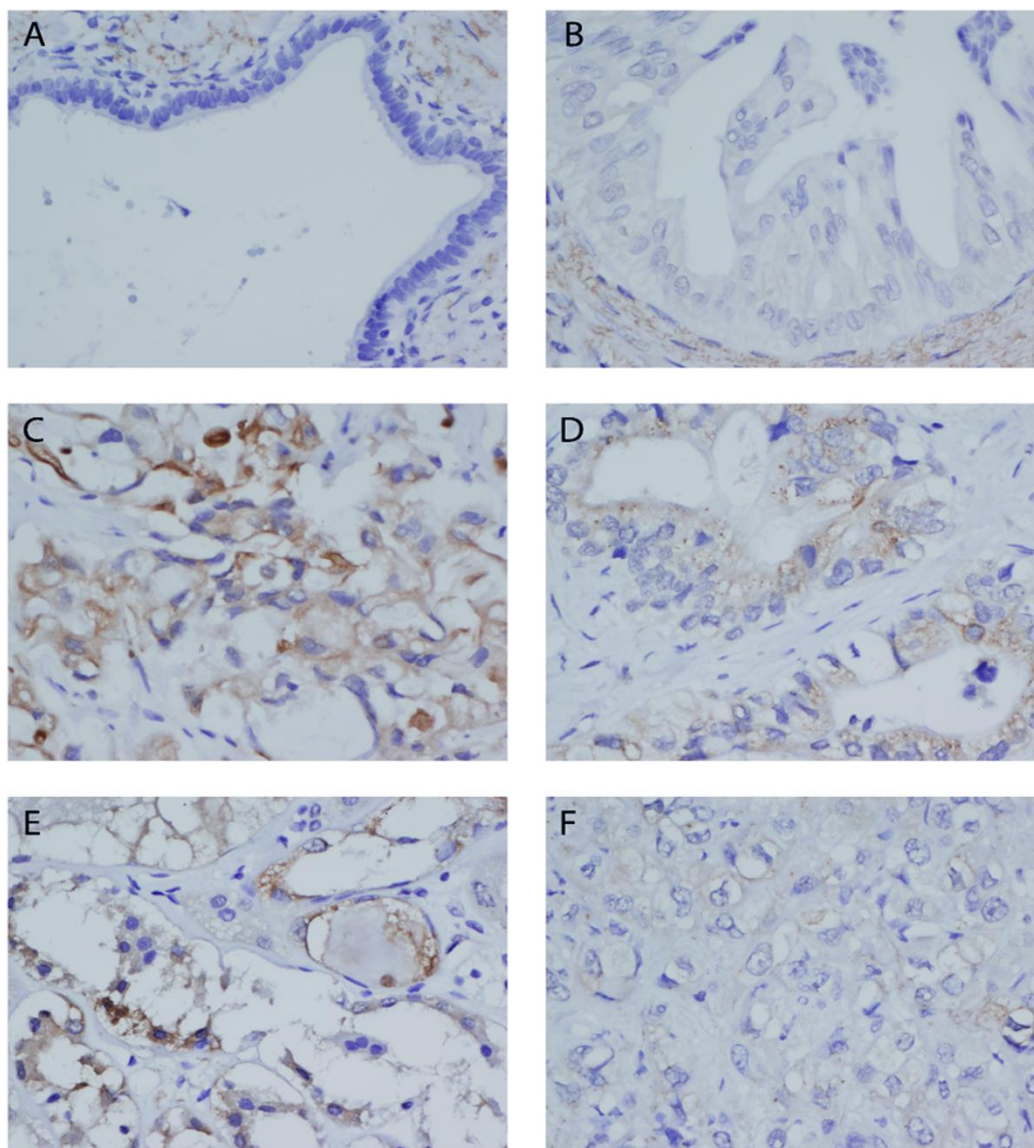
and then added to histology sections, no staining was detected (Figure 2.2). Staining of PDACs was cytoplasmic in all cases while membranous localization was also observed in a few cases. Positive staining could be characterized across a range from strong, diffuse staining that included some ill-defined membranous staining (Figure 2.1C) to focal, exclusively cytoplasmic staining (Figure 2.1D-E). Within individual tumors, SAS1B positivity ranged from about 10% to greater than 90% of cancerous cells staining. Approximately 20% of PDACs had no detectable SAS1B or showed only trace staining (Figure 2.1F). Importantly, expression of SAS1B was found both in primary tumors and in metastatic tumors from the lymph node and distal peripheral sites (Figure 2.1G). One of six high-grade PanIN samples were SAS1B^{pos}, suggesting that SAS1B expression may first appear in advanced precursor lesions during carcinogenesis. These data demonstrate SAS1B is expressed in a majority of pancreatic cancers evaluated and is not detected in normal human pancreatic ductal epithelium, providing rationale for further investigation of SAS1B as a therapeutic target for the treatment of PDAC.

***ASTL/SAS1B* is expressed in pancreatic cancer patient derived xenografts**

With the intent of identifying potential *in vivo* models that could be used to develop and to assess SAS1B-specific targets for therapeutic and diagnostic approaches, we evaluated SAS1B expression in patient derived xenografts (PDX). Tumors were obtained from PDAC PDX mouse models that have been previously shown to have high genotypic and phenotypic concordance with the source patient tumor [89]. RNA was isolated from 15 tumors and 3 normal human pancreas samples and was reverse-transcribed to cDNA. PCR analysis using a primer for the c-terminus of *ASTL* set showed no detectable *ASTL*

transcript in normal pancreas; however, 67% (10/15) of PDAC tumors were positive for *ASTL* transcript (Figure 2.3A). Amplicons were cloned and sequenced, revealing 99% identity to *ASTL* reference sequence with an occasional single nucleotide polymorphism. Although not quantitative, gel electrophoresis of PCR products suggests differences in SAS1B expression levels among tumors.

Immunohistochemical staining for SAS1B expression was performed on these PDX tumor samples; 67% (10/15) were positive for SAS1B protein (Figure 2.3B), with each tumor's protein expression concordant with *ASTL* transcript data shown in Figure 2.3A. Tumors were scored by a pathologist, in a blinded manner, on a 0 (negative) to 3+ positivity staining-intensity scale. SAS1B was largely localized intracellularly with 1+ and 2+ staining intensities. Correlation of *ASTL*/SAS1B expression with patient data showed that *ASTL*/SAS1B expression occurs in tumors from both males and females, tumors of early and late stage (II to IV), as well as in primary and metastatic tumors (Figure 2.3A). These data show concordance between *ASTL* transcript and SAS1B message within all pancreatic tumors examined. The robustness of PCR bands (e.g. tumors numbered 3 & 4) correlated with stronger IHC staining intensity (2+). The 67% incidence among this cohort of 15 PDX cancer samples matches the 68% incidence identified in the human cancer samples (Figure 2.1G). These data show that SAS1B expression is maintained when primary human tumors are grafted into immunodeficient mice, highlighting the potential utility of this model for in vivo development.



G Tissue	SAS1B Staining Intensity				Percent SAS1B ^{pos}
	0	1+	2+	3+	
Normal duct	10	--	--	--	0 (0/10)
Low grade PanIN	8	--	--	--	0 (0/8)
High grade PanIN	5	--	1	--	17 (1/6)
Adenocarcinoma	3	5	8	--	81 (13/16)
Adenocarcinoma nodal metastasis	3	3	3	--	67 (6/9)
Adenocarcinoma distant metastasis	4	--	1	1	33 (2/6)
All adenocarcinomas	10	8	12	1	68 (21/31)

Figure 2.1 SAS1B was expressed in a majority of pancreatic cancers and was not detected in normal pancreas ductal epithelium by IHC

TMAAs were stained for the expression of SAS1B with 6B1 mAb. SAS1B was not detected in normal pancreatic ductal epithelium (A) and most pancreatic intraepithelial lesions (B). Some stromal cells adjacent to these ducts showed cytoplasmic reactivity, as pictured in A/B. Many ductal carcinomas showed cytoplasmic SAS1B staining (C-E). This ranged from strong, diffuse staining that also included some ill-defined membranous positivity (C) to focal, exclusively cytoplasmic staining (D-E). A minority of ductal carcinomas were negative or showed only trace non-specific staining (F). Images are 400x magnification. SAS1B staining was scored on a 0 (negative) to 3+ positivity scale for each tissue type and result are summarized in the table (G). Percent of samples that were SAS1B positive, for each tissue type, is quantified in the last column (total number of SAS1B positive samples / total number of samples) (G).

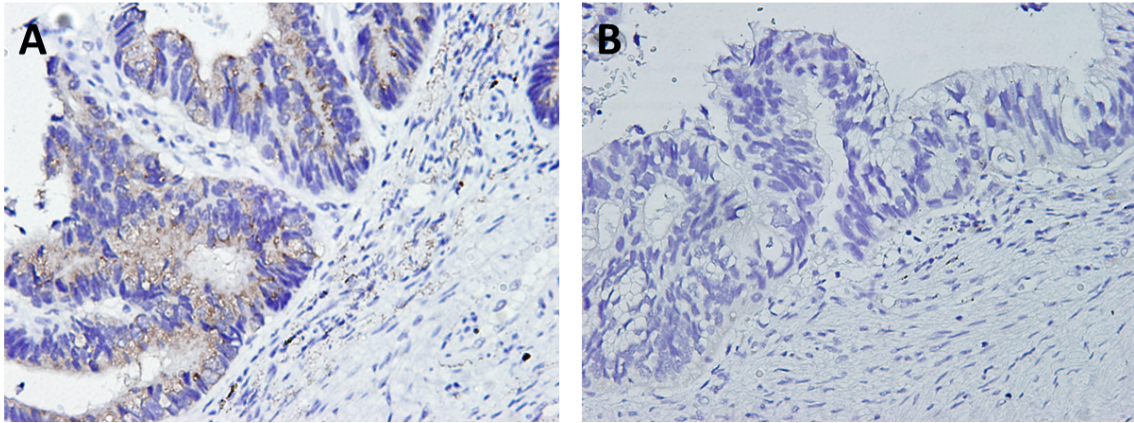


Figure 2.2 SAS1B signal in pancreatic cancer tissue was blocked by pre-incubating anti-SAS1B mAb, 6B1, with rSAS1B

[A] Human primary PDAC tumor stained with anti-SAS1B mAb, 6B1, showed robust cytoplasmic signal in the tumor and trace staining in adjacent stromal cells. [B] SAS1B signal in tumor and stroma was blocked when anti-SAS1B mAb 6B1 was pre-incubated with 40x excess rSAS1B protein for one hour before addition to the tissue section. B is a serial section of A. Images are 400x magnification.

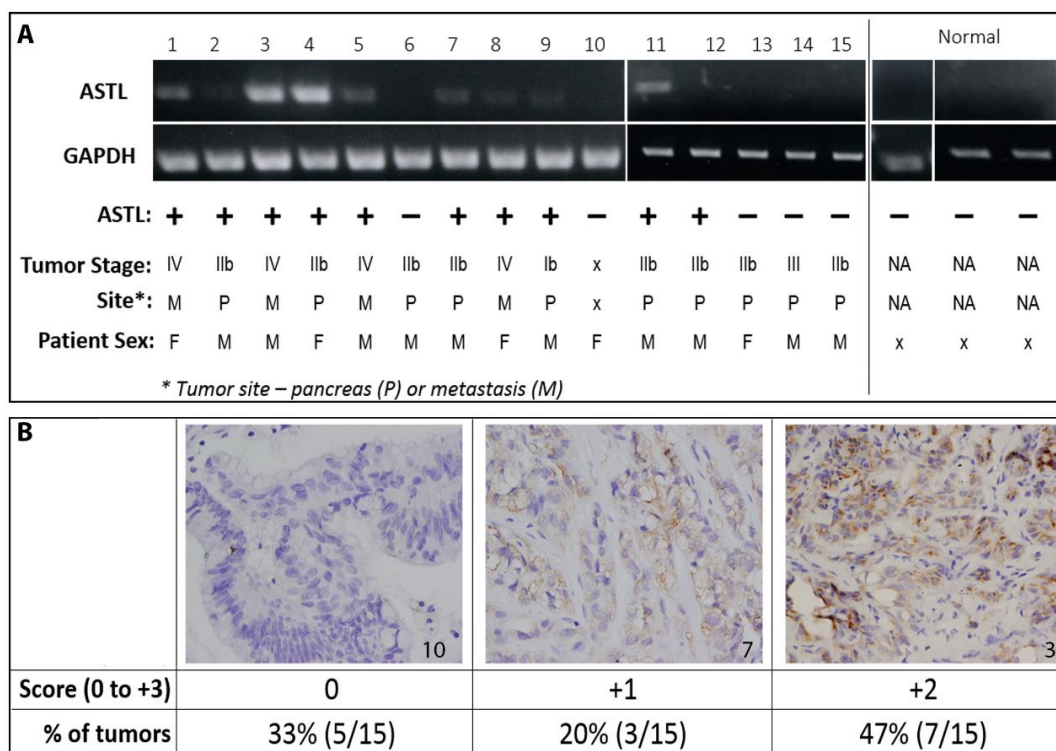


Figure 2.3 ASTL/SAS1B expression in pancreatic cancer patient derived xenografts

[A] RT-PCR analyses of 15 PDAC (1-15) PDX tumors and 3 normal human pancreas (normal) samples using a c-terminus ASTL specific primer set showed a 309bp amplicon in 10/15 PDAC samples. Tumors from both males and females, early and late stage disease, as well as primary and metastatic tumors were ASTL^{POS} (table). GAPDH was used as a housekeeping control for PCR. [B] Immunohistochemical localization of SAS1B, on representative examples from the same set of 15 PDAC tumors used in panel A, labeled with anti-SAS1B mAb, 6B1. Tumor number indicated in bottom right corner of image. Images are 400x magnification. Tumors were scored on a 0 (negative) to 3+ positivity scale; total number of tumors in each group quantified in the table.

SAS1B localizes to the cytoplasm and to the cell surface of pancreatic cancer cell lines

The IHC analyses raise the possibility that SAS1B may be expressed at the cell surface of some pancreatic cancer cells, but routine IHC is not sufficient to confirm cell surface expression. SAS1B has a putative transmembrane sequence; thus, we hypothesized that cell-surface expression of SAS1B may be sufficient to support therapeutic approaches with ADCs and/or CAR-T cells. To obtain preclinical data to address this question, three pancreatic cancer cell lines (mPanc96, 366, 608) were further evaluated *in vitro* with confocal analysis. Cell lines 366 and 608 were derived from PDX PDAC samples and are numbered 3 and 5, respectively, in the samples shown in Figure 2.3. mPanc96 is a cell line that has been substantially characterized in a variety of pancreatic cancer studies. Confocal analysis of indirect immunofluorescence (IIF) of fixed and permeabilized pancreatic cancer cells, using anti-SAS1B mAb SB2, showed that SAS1B is abundant in the cytoplasm (Figure 2.4A-C). No signal was detected with non-specific mouse IgG antibody (data not shown). These IIF data using SB2 mAb are in agreement with the IHC data indicating a prominent cytoplasmic localization of SAS1B (Figures 2.1 & 2.3). IIF on live, non-permeabilized cells was performed to determine if SAS1B is also expressed at the cell surface. IIF on live pancreatic cancer cells, using the same SB2 anti-SAS1B mAb, shows that SAS1B is present at the cell membrane in a punctate surface staining pattern (Figure 2.4E-G). No detectable SAS1B was observed in non-neoplastic keratinocytes (Figure 2.4D/H).

The majority of pancreatic cancer cells in all three cell lines express cytoplasmic and cell surface SAS1B. Cell lines 608 and 366 grow in clumps/clusters, and in these samples, the most robust live cell staining was observed at the periphery of the cell cluster.

However, when Z-stack analysis was used in confocal microscopy, punctate SAS1B signal was observed across the surface of the cells in the interior of the cell cluster (data not shown). As SAS1B expression in mPanc96, 366, and 608 cell lines can be found at the cell surface, we proceeded to test the ability of SAS1B to serve as a target for ADC-mediated killing.

Fixed/Permeabilized Live/Non-permeabilized

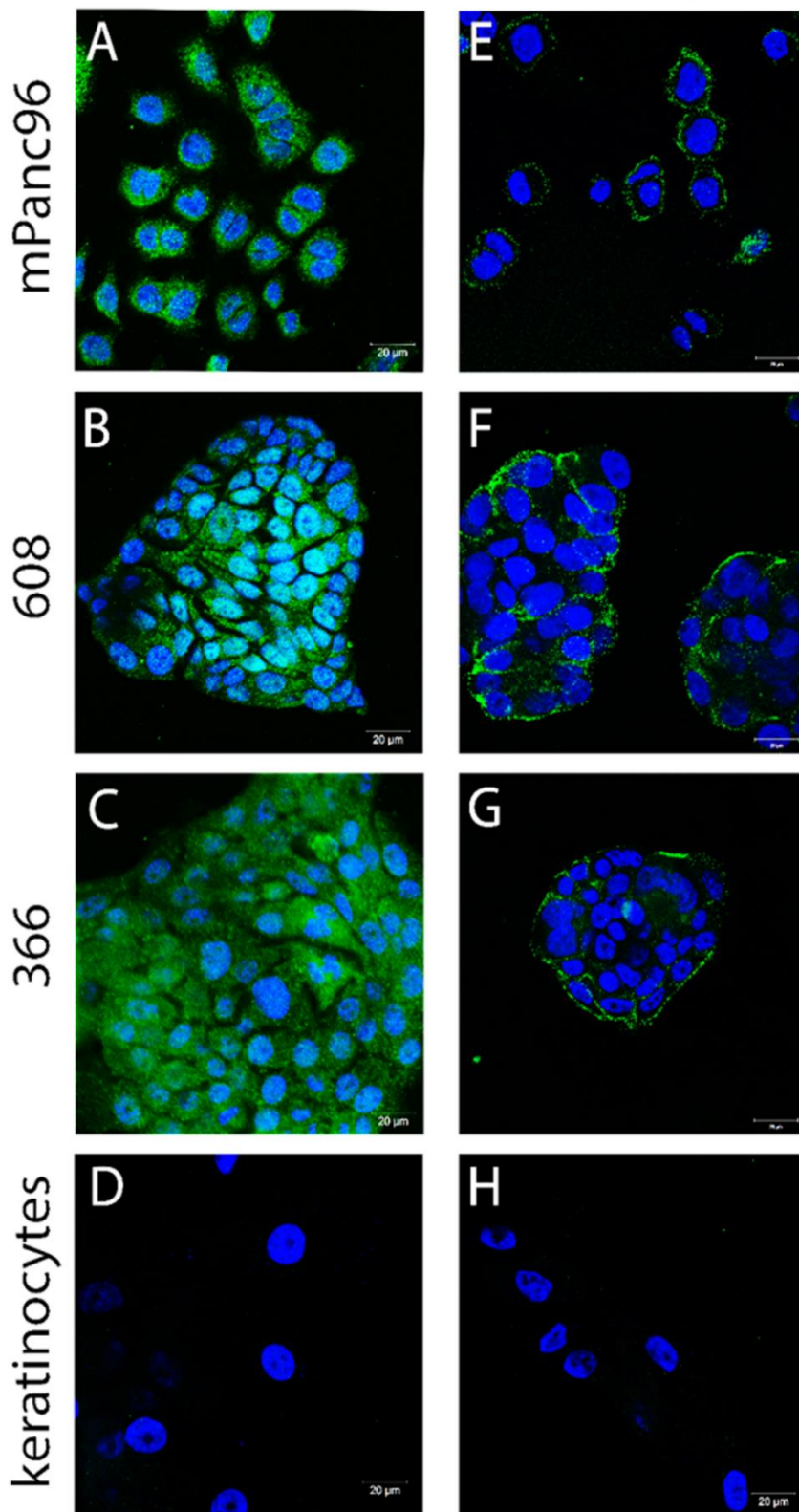


Figure 2.4 SAS1B localized to the cytoplasm and to the cell surface in pancreatic cancer cell lines

[A-D] Fixed and permeabilized indirect immunofluorescence (IIF) using anti-SAS1B mAb, SB2 showed SAS1B localized to the cytoplasm of three pancreatic cancer cell lines (mPanc96, 366, 608) compared to normal keratinocytes. [E-H] IIF on live, non-permeabilized cells using anti-SAS1B mAb, SB2, demonstrated staining of the plasma membrane of mPanc96, 366 and 608 cells but not normal keratinocytes. Data are representative of three independent experiments.

SAS1B surface expression in pancreatic cancer cell lines correlates with anti-SAS1B ADC cell killing *in vitro*

Because SAS1B localizes to the cell membrane in pancreatic cancer cells and previous data have shown that SAS1B is endocytosed [41], we hypothesized that these could be killed using an ADC targeting SAS1B, with varying degrees of cytotoxicity correlated to relative antigen level at the cell surface. To first quantify the SAS1B surface expression observed in live IIF (Figure 2.4E-H), relative amounts of cell surface SAS1B were detected by flow cytometry with SB2 performed on live pancreatic cancer cell lines (mPanc96, 366, 608) and normal keratinocytes (Figure 2.5A). Examination of relative proportions of SAS1B^{POS} cells revealed mPanc96 had the highest proportion of cells expressing SAS1B and the highest per cell SAS1B expression. 608 had intermediate expression, and 366 showed the weakest expression of SAS1B. Surprisingly, given the previous IIF data, keratinocytes also had a population of SAS1B^{POS} cells. No immunoreactivity was observed when SB2 mAb was pre-incubated with rSAS1B protein for one hour before adding to cells (Figure 2.6).

To evaluate the SAS1B antibody SB2 as a candidate targeting immunotherapeutic drug, an *in vitro* cytotoxicity assay was performed, in which cells were incubated with SB2 complexed with a secondary antibody conjugated to the DNA-alkylating agent duocarmycin DM via a pH sensitive linker (Figure 2.5B). Disruption of DNA architecture by duocarmycin results in eventual cell death. Total cellular ATP was measured using CellTiter Glo in a luminometer to determine percent viability of cells. No cytotoxicity was observed when cells were treated with secondary-drug conjugate alone as compared to cells without treatment (media only; data not shown). Significant cell death was observed in

mPanc96 and 608 cells treated with sub-nanomolar concentrations (0.01 nM, equivalent to 0.0016 $\mu\text{g}/\text{mL}$) and in 366 treated with nanomolar concentrations (1 nM, equivalent to 0.016 $\mu\text{g}/\text{mL}$) of anti-SAS1B mAb SB2 complexed with drug conjugate, as compared to the negative control ADC. At 0.016 $\mu\text{g}/\text{mL}$ SB2, a statistically significant difference in cytotoxicity was observed when comparing keratinocytes to each of the three PDAC cell lines (mPanc96, 608, 366) independently (t-test p-value <0.0001 ; ANOVA p-value <0.0001). The LD50 values for mPanc96 were 0.0055 ± 0.002 , 608 were 0.0088 ± 0.006 , and 366 were 0.011 ± 0.005 $\mu\text{g}/\text{mL}$ SB2 mAb. Although mPanc96 trended toward being more effectively killed, there were no significant differences in the LD50 between the three cancer cell lines (n=3 assays; non-linear regression analysis). Lack of significance may be due to inadequate statistical power or may be due to complications with LD50 calculations for populations which never reach 100% maximum cytotoxicity. These experiments showed that a SAS1B-ADC was not cytotoxic, even at high concentrations, to at least 40% of 608 and 366 cells while in mPanc96, only approximately 20% of cells survived treatment. Because the LD50s were not statistically different, yet flow cytometry data showed relatively more surface SAS1B expression in mPanc96 as compared to 608 and 366, these results could indicate that a higher percentage of cells will ultimately be killed by a SAS1B-ADC in a population which has greater density of surface expressed SAS1B. Perhaps internalization rates differ among cell lines and with a longer ADC incubation time, greater cytotoxicity would be achieved in 608 and 366.

Similar results, in terms of general pattern of killing, were found with additional SAS1B-specific mAbs in mPanc96 cell line. However, SB2 induced significant cell death at a concentration one log lower than SB4 and SB5 (Figure 2.7). Epitope mapping showed

that the SB mAbs match the N-terminal, pro-peptide region of SAS1B (A. Mandal et. al, manuscript in preparation). SB2, SB4, and SB5 mAbs are different clones from the same parent; differences in affinities are likely attributed to variations in mAb structure.

In the absence of drug-conjugate, anti-SAS1B mAb SB2 alone was not cytotoxic to cells (Figure 2.8), warranting the need for a cytotoxic agent since prior heat inactivation of serum in complete media prevented complement mediated cell death. The drug-conjugate, in the absence of SB2, also showed no cytotoxic effects (data not shown). SB2 mAb killing specificity was confirmed by the lack of cytotoxicity with antibody that had been pre-incubated with SAS1B blocking peptide while no effect on cytotoxicity was observed when using an SAS1B peptide which is not recognized by SB2 (Figure 2.9). Keratinocytes did not stain for the target by IIF, and despite observation of some SAS1B signal in flow cytometry, no *in vitro* cytotoxicity using anti-SAS1B-ADC was observed in these cells. Similar cytotoxic effects were observed among all three pancreatic cancer cell lines using a positive control ADC targeting epithelial cell adhesion molecule (EpCAM) (Figure 2.5B). This demonstrates that the differential cytotoxic responses observed with anti-SAS1B ADC are as a result of properties of the target rather than inherent differences in how these cells process an ADC or differential resistance to apoptosis.

Notably, mPanc96 and 366 cells had the highest and lowest SAS1B surface expression by flow cytometry and most and least ADC mediated cell killing as a proportion of the treated population, respectively. Thus, the difference in absolute killing apparent in Figure 2.5 reflects the amount of protein expressed at the cell surface. These data suggest potential utility of stratifying patients based on the level of SAS1B surface expression with regard to treatment with anti-SAS1B therapies. These results demonstrate SAS1B is a

surface target in pancreatic cancer cells capable of binding monoclonal antibodies, internalization, and delivering cytotoxic drug payloads which effectively kill cancer cells.

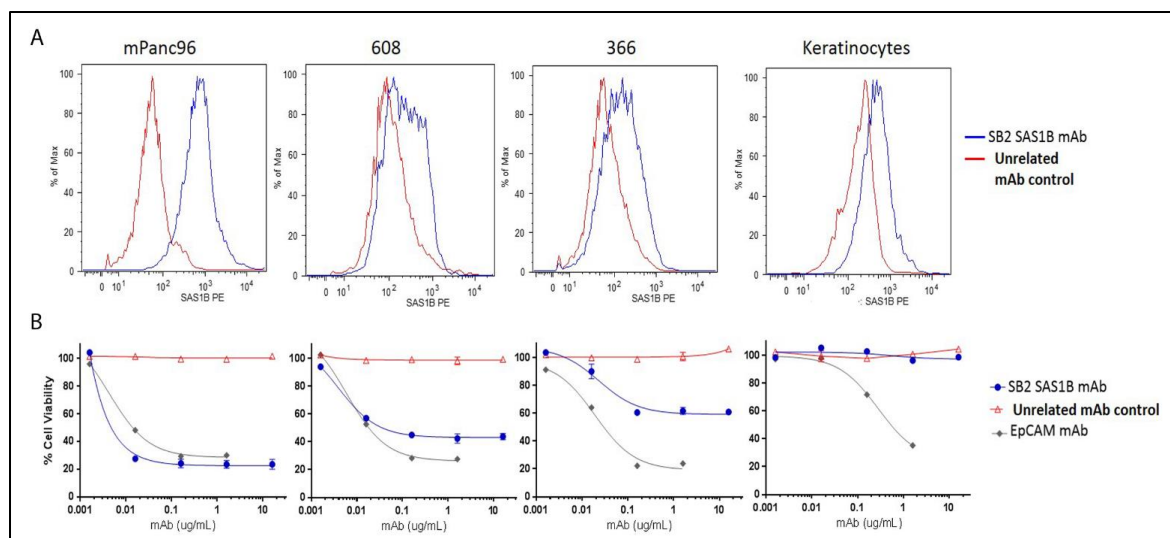


Figure 2.5 SAS1B surface expression in pancreatic cancer cell lines correlated to anti-SAS1B ADC cell killing *in vitro*

[A] Median fluorescent intensity of cell surface SAS1B detected by live cell flow cytometry with SB2 monoclonal antibody (blue line) or unrelated control antibody (red line) on PDAC cell lines mPanc96 (left), 608 (left middle), and 366 (right middle) and keratinocytes (right). **[B]** Cytotoxicity by anti-SAS1B ADC (mAb SB2) titration shown below each flow-cytometric plot for corresponding cell line. SB2- mAb-Duocarmycin immune complexes were generated (ADC) then incubated with cells for 72 hours. Relative cell viability was measured using CellTiter-Glo. Data represent averages of three independent replicates, with 3 technical replicates in each data point.

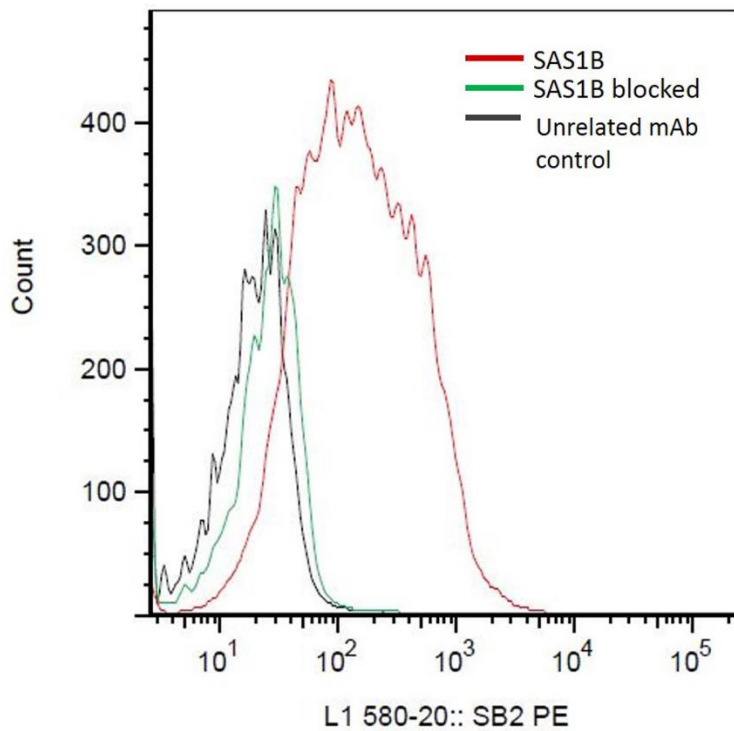


Figure 2.6 Anti-SAS1B mAb, SB2, signal in live mPanc96 cells was blocked when pre-incubated with rSAS1B protein

Cell surface SAS1B detected by live cell flow cytometry in mPanc96 cells using anti-SAS1B mAb, SB2 (red line) as compared to unrelated mAb control (black line). When SB2 was pre-incubated with 40x excess rSAS1B protein, then added to cells, SAS1B signal was effectively blocked (green line).

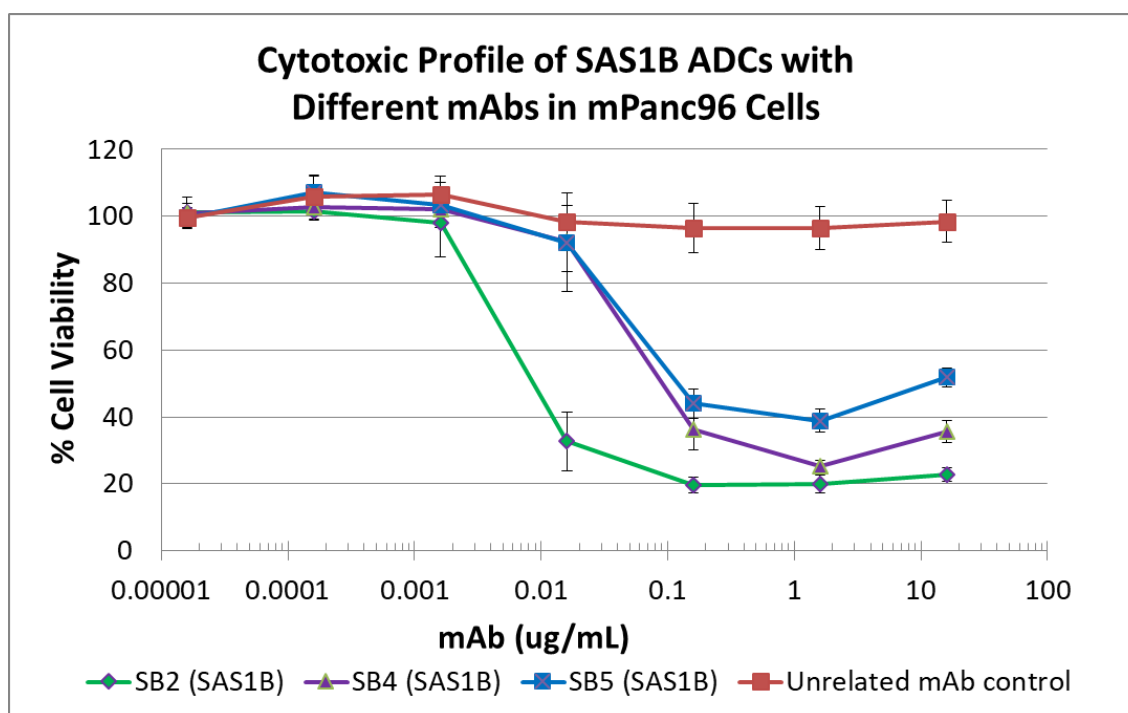


Figure 2.7 ADCs with different anti-SAS1B mAbs are also cytotoxic to mPanc96 cells

Cytotoxicity by anti-SAS1B ADCs using mAb SB2 (green line), SB4 (purple line), or SB5 (blue line). Similar cytotoxic patterns observed for each of the three anti-SAS1B mAbs however SB2 ADC cytotoxic effects observed one log lower than effects seen with SB4 and SB2. Unrelated mAb control (red line) used as negative ADC control. mAb-Duocarmycin immune complexes were generated (ADC) then incubated with cells for 72 hours. Relative cell viability was measured using CellTiter-Glo. Data represent averages of three independent replicates, with 3 technical replicates in each data point.

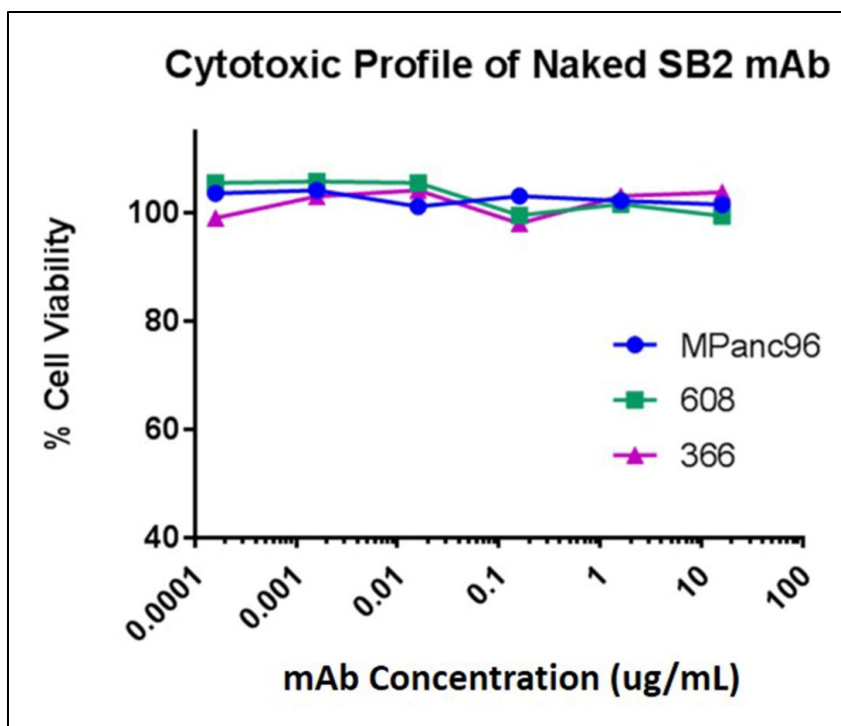


Figure 2.8 Anti-SAS1B mAb, SB2, alone was not cytotoxic to pancreatic cancer cell lines

No cytotoxic effects were observed in pancreatic cancer cell lines mPanc96, 608, and 366 when anti-SAS1B mAb, SB2, alone (no drug-conjugate) was added to cells. SAS1B mAb incubated with cells for 72 hours. Relative cell viability measured using CellTiter-Glo.

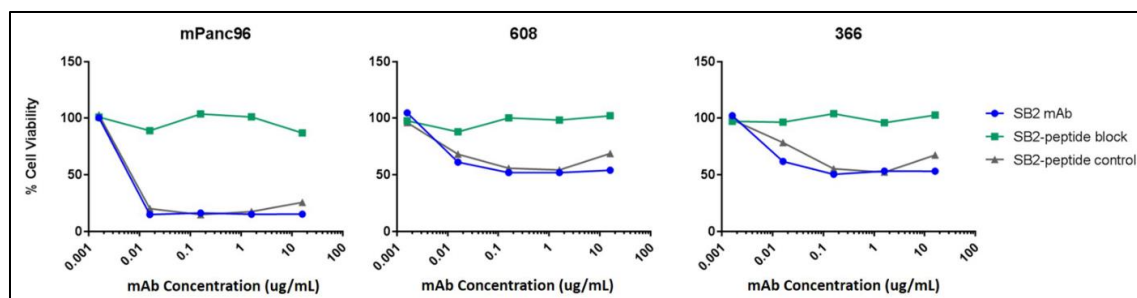


Figure 2.9 Cytotoxicity of an anti-SAS1B ADC was blocked in pancreatic cancer cell lines when SB2 mAb was pre-incubated with a SAS1B peptide

Cytotoxicity induced by anti-SAS1B ADC (SB2 mAb) (blue line) is blocked when SB2 mAb is immunoabsorbed with SAS1B peptide (green line) in pancreatic cancer cell lines mPanc96 [left], 608 [middle] and 366 [right]. Cytotoxicity is not blocked when SB2 is immunoabsorbed with a negative control peptide (grey line) consisting of an irrelevant SAS1B sequence. SAS1B ADC incubated with cells for 72 hours. Relative cell viability measured using CellTiter-Glo.

DISCUSSION

SAS1B is a newly identified cancer-oocyte antigen in pancreatic cancer

SAS1B is expressed in a majority of both patient PDACs and PDX PDAC samples. We find that SAS1B localizes to both the cytoplasm and the cell surface in PDAC cell lines. Further, we validated SAS1B as a therapeutic target by determining that co-incubation of pancreatic cancer cell lines with anti-SAS1B ADC results in cytotoxicity *in vitro*, indicating that SAS1B has characteristics of a bone fide targetable antigen for pancreatic cancer.

Among a cohort of 31 pancreas cancer samples, 68% were SAS1B^{pos} by IHC; SAS1B expression was observed in primary tumors and expression was sustained in metastatic disease (Figure 2.1). Increased staining intensity was observed with advanced disease indicative of increased SAS1B molecule density, however, the sample size was small. Further studies with increased sample size would help statistically correlate SAS1B expression intensity and frequency with disease characteristics. These data do suggest a relatively high penetrance of expression but a heterogeneity in both the overall frequency of expression and proportion of tumor cells that express SAS1B, indicating that careful pathological assessment will need to be performed prior to therapy selection. Moreover, while Pires et al. showed SAS1B expression in cancers from the female reproductive tract (precisely uterine tumors) [41], this is first report of SAS1B^{pos} cancers from males, which is notable since, in untransformed tissue, SAS1B is localized to ovaries in females [41]. The expression of SAS1B in male tumors, but not in male normal tissue, may mean that immune tolerance to SAS1B is not well established in males, making it an even more attractive target. However, this conclusion is dependent upon the verification of the low

level of expression observed in tumor stroma, and whether stromal expression is constrained to the tumor microenvironment and is absent from true normal pancreas.

SAS1B is expressed in the cytoplasm of pancreatic cancer cells by IHC (Figures 2.1 & 2.3), indirect immunofluorescence (Figure 2.4A-C), and intracellular flow cytometry (data not shown). A population of SAS1B traffics to the plasma membrane and is accessible on the cell surface of pancreatic cancer cells (Figures 2.4 & 2.5). The punctate staining pattern observed at the cell surface suggests that SAS1B may be associated with lipid rafts or sites of exocytosis. The cycling rates and half-life of SAS1B at the plasma membrane are currently unknown but the data presented here suggest that there is a greater pool of SAS1B in the cytoplasm and that a fraction of the total translated SAS1B traffics to the cell surface. How SAS1B expression relates to tumor biology and disease prognosis is unknown and requires additional studies.

Potential diagnostic and imaging applications of SAS1B

SAS1B has been shown to be exocytosed from oocyte cortical granules after fertilization and to cleave zona pellucida protein 2 (ZP2) rendering the ZP unable to support further sperm binding [38, 39], but it is unknown whether SAS1B^{POS} cancer cells secrete SAS1B. Given these data, additional studies are warranted to determine whether shed SAS1B may be able to serve as a potential diagnostic marker in circulation for early detection of pancreatic cancer. Early detection of PDAC precursor lesions and of early stage disease could increase therapeutic opportunities and outcomes for patients. Further, this is the first study to report SAS1B expression in a precursor cancer lesion (Figure 2.1G); whether or not additional PanINs harbor SAS1B expression and if SAS1B contributes to

carcinogenesis has yet to be determined. PanINs are understood to be noninvasive ductal precursor lesions to PDAC [90]. Within this study, all low grade PanINs were SAS1B^{neg} but one of six high grade PanINs was SAS1B^{pos}. High-grade PanINs are also referred to as “carcinoma in situ” and many of the genes altered in invasive pancreatic cancer are also altered in PanINs [90, 91]. Although this study suggests SAS1B may not be prevalent among precursor lesions and the sample size was small, over 80% of primary adenocarcinomas were SAS1B^{pos}. Thus, there is potential for early detection of PDAC through screening of individuals with family history of pancreatic cancer using SAS1B as a biomarker, if SAS1B is shed at sufficient levels from cancer cells. Further, as SAS1B is expressed at the cell surface of tumor cells and rarely in normal tissue, there is the potential to develop cancer imaging applications with fluorescently or radio-labeled nanoparticles [92, 93]. A SAS1B targeted imaging approach has the potential to also serve as a way to stratify patients who would be most likely to respond to SAS1B therapies. However, high shed rates could also complicate the use of SAS1B for ADC targeting or imaging, as shed SAS1B could serve as an antibody sink.

Evaluation of the therapeutic potential of SAS1B as a target for pancreatic cancer

SAS1B was shown to be internalized via the endocytic pathway in uterine tumor cells after antibody binding using a rabbit polyclonal antibody [41]. When pancreatic cancer cells were treated with complexes of SAS1B primary antibodies bound to secondary antibodies linked with the toxin duocarmycin DM, cell death was observed (Figure 2.5). This study shows that an ADC targeting SAS1B is internalized resulting in cytotoxicity of pancreatic cancer cells, thus supporting SAS1B as a candidate for ADC therapy.

The extent of anti-SAS1B ADC cell death observed correlates with the relative amount of surface-associated SAS1B within a given population of cells. mPanc96 and 366 cells were the highest and lowest SAS1B expressers by flow cytometry, respectively, and also showed the greatest and least amount of cell death (Figure 2.5). The equivalent cytotoxicity found between all three pancreatic cancer lines using a control ADC targeting EpCAM (Figure 2.5B) demonstrates that the differences observed among the cell lines with the anti-SAS1B ADC are due to target density differences rather than inherent differences in how each cell line processes and responds to an ADC. The flow cytometry data coupled with the cytotoxicity data shown in Figure 2.5 suggests that a limited pool of cell surface-associated SAS1B may be sufficient to induce cell death when SAS1B^{POS} pancreatic cancer cells are targeted with an anti-SAS1B ADC. Our data suggest that pancreatic cancer cells that have the highest density of SAS1B on the cell surface combined with the highest percentage of total cells being SAS1B^{POS} would be most likely to benefit the greatest from SAS1B targeted ADC therapy. However, in pancreatic cancer cell populations where less SAS1B is expressed, some cytotoxicity is still observed. Further studies are warranted to define the rate and regulation of SAS1B cycling to the plasma membrane to determine whether this influences the threshold of SAS1B expression needed to induce cancer cell death. This information could help guide the manipulation of surface SAS1B, and determine whether surface or intracellular expression needs to be assessed for the stratification of patients who would most likely respond to a SAS1B targeted ADC therapy.

Non-neoplastic keratinocytes showed a population of SAS1B^{POS} cells by live cell flow cytometry but were not affected by the anti-SAS1B ADC (Figure 2.5) suggesting that SAS1B-ADC complexes were not internalized in these cells as they were in PDAC cells

(Figure 2.5). The discrepancy between the IIF data showing keratinocytes were SAS1B^{neg} (Figure 2.4D/H) and the flow cytometry data showing these cells were SAS1B^{pos} (Figure 2.5A), suggests that flow cytometry may be more sensitive than the IIF assay for SAS1B detection in keratinocytes. Another explanation may be that the process of cell dissociation and handling during flow cytometry staining results in a stress-induced expression of SAS1B that is not observed in IIF, as in this setting cells remain attached to coverslips in a stress-free environment. When and how SAS1B expression is induced under varying conditions, such as stress, remains unknown, and will be important to determine as it could be exploited to enhance SAS1B expression in cancer cells, or limit on-target/off-tumor targeting of normal tissue. Alternatively, keratinocytes may express a different SAS1B isoform which is not internalized via the endocytic pathway; additional studies are required to determine whether or not this is the case.

Some stromal cells, from both normal and malignant pancreas, appeared to express SAS1B at a low level, localized to the cytoplasm, by IHC (Figure 2.1; Figure 2.2). However, *ASTL* was not detected by RT-PCR in normal pancreas (Figure 2.3A). This discordance may be because the stromal component of the normal pancreas sections analyzed in Figure 2.3A may not have been great enough to allow for detection by PCR or that stromal cells associated with transformed tissue may be induced to express SAS1B. The latter explanation may further support targeting SAS1B as elimination of tumor stroma has been shown to be critical for the prevention of tumor recurrence. This population of SAS1B^{pos} stromal cells requires further investigation to determine: 1) if staining is truly SAS1B or is a cross-reactive epitope of another protein, 2) whether or not SAS1B is on the surface of these cells, 3) what percentage of stromal cells potentially express surface-

associated SAS1B, 4) if an anti-SAS1B ADC treatment would result in stromal cell death, and 5) if the stromal cell death would be significant enough to result in negative patient outcomes, or alternatively enhance the degradation of the tumor. Given that non-neoplastic keratinocytes were shown to express SAS1B at the cell surface by flow cytometry but showed no cell death when treated with an anti-SAS1B ADC (Figure 2.5), we hypothesize that non-cancerous SAS1B^{pos} cells will not be affected by an anti-SAS1B ADC. However, surface expression without internalization would not protect stromal cells from CAR-T reactivity, or T cells that are elicited by a SAS1B vaccination approach. Future studies using PDX xenografts will be necessary to ascertain the impact of stromal expression on the optimization of SAS1B-specific immunotherapeutic options.

The heterogeneity and mosaicism of SAS1B expression observed in PDAC has implications for immunotherapy selection. ADCs are an attractive option for SAS1B^{pos} PDACs because, based on the data presented, an anti-SAS1B ADC is cytotoxic to cancerous cells but not to non-neoplastic cells which is hypothesized to be related to differences in internalization. A cancer vaccine using SAS1B as a target is an additional immunotherapeutic option that warrants exploration. However, given that heterogeneity of SAS1B expression was observed, there may be a subpopulation of SAS1B^{neg} PDAC cells which are not targeted by a vaccine. It is likely that, even with a potential anti-SAS1B ADC therapy for the treatment of PDAC, combination with one or more additional therapies would provide the maximum anti-cancer benefit to patients.

Additional studies are warranted to further evaluate SAS1B as an ADC therapeutic target for the treatment of PDAC. The PDAC PDX mouse models examined in this study, where patient tumors are affixed directly into the mouse pancreas [89], may represent a

suitable system for studying effects of anti-SAS1B therapies *in vivo*, along with assessment of SAS1B expression in the current murine genetic models of pancreatic cancers. The data presented in this study strongly suggest that SAS1B directed immunotherapies have the potential to provide a novel axis of therapy for the pancreatic cancer population.

MATERIALS AND METHODS

Antibodies & Reagents

Mouse anti-SAS1B mAb 6B1 was selected from a hybridoma technology campaign to be able to screen for SAS1B^{POS} samples by IHC. For 6B1 [Pires et al., In Submission], a truncated human SAS1B immunogen [38] was used to inject mice and mAbs were generated by the Antibody Engineering and Technology (AbET) Core (University of Virginia (UVA)). For SB2, truncated SAS1B, lacking only the signal peptide, was expressed as described earlier [37] and was used as the immunogen to generate mouse anti-human SAS1B mAbs. Mouse anti-SAS1B mAb SB2 was selected from a hybridoma campaign based on a screen for SAS1B^{POS} live cancer cells. The mAbs were generated by the AbET Core (UVA). Unrelated anti-human CABYR 3A4 mAb used as a negative control antibody for flow cytometry and cytotoxicity assays, was developed in mouse using an immunogen as described earlier [94]. Non-specific mouse IgGs were used as a negative antibody control for IHC and IIF (Cell Signaling Technology, Danvers, MA). EpCAM (CD326) antibody (Miltenyi Biotec, San Diego, CA) was used as a positive antibody control for the cytotoxicity assays.

Fab'-specific peroxidase labeled secondary antibodies (Jackson ImmunoResearch, West Grove, PA), raised in goat to recognize mouse, were used for IHC (GtαMs HRP). Goat anti-mouse Alexa Fluor 488 (GtαMs Alexa488; Molecular Probes, Eugene, OR) was used to label primary antibodies in IIF. Goat anti-mouse R-phycoerythrin (GtαMs R-PE; Molecular Probes, Eugene, OR) was used as a secondary antibody for the flow cytometry assay. Fab-anti-mouse IgG Fc region-duocarmycin DM antibody with a cleavable linker

(Fab-CL-DMDM; Moradec, San Diego, CA) was used as the secondary antibody-drug conjugate in the cytotoxicity assays.

Nickel-NTA agarose purified recombinant human SAS1B protein as described by Pires et al. [38] was used to immunoabsorb both 6B1 and SB2 mAbs in the IHC and flow cytometry assays. A SAS1B N-terminal peptide was used to immunoabsorb SB2 mAb in the cytotoxicity assay and a SAS1B peptide matching the C-terminus, not recognized by SB2, was used as a negative control peptide. SAS1B peptides were purified greater than 95% by analytic HPLC (Atlantic Peptides, Lewisburg, PA). SAS1B N-terminal peptide sequence was APLASSCAGACGTSFPDGL and the C-terminal peptide sequence was GAPGVAQEQSWLAGV.

Cell Lines and Culture Conditions

mPanc96 cells were obtained from the American Type Culture Collection (ATCC; Manassas, VA) while 608 and 366 fresh patient-derived cell lines were obtained as described previously [95, 96]. Primary keratinocytes, isolated from neonatal foreskin following a previously described protocol, were kindly provided by Dr. S.B. Vande Pol (University of Virginia, Department of Pathology,) [97, 98]. Pancreatic cancer cells were cultured in RPMI (Invitrogen, Carlsbad, CA) containing 10% heat inactivated fetal bovine serum (FBS; ThermoFisher Scientific, Waltham, MA) and 1% penicillin-streptomycin (Invitrogen, Carlsbad, CA). Keratinocytes were cultured in keratinocyte serum free medium (KSFM; Invitrogen, Carlsbad, CA) containing 1% penicillin-streptomycin. Cells were cultured in a humidified incubator (37°C, 5% CO₂). mPanc96 cells were authenticated before purchase by the ATCC with cytochrome *c* oxidase subunit 1 analysis,

DNA profiling, cytogenetic analysis, flow cytometry, and immunocytochemistry. Cell lines 608 and 366 were authenticated in 2010 and 2011 by the University of Virginia Biomolecular Research Facility with DNA profiling, cytogenetic analysis, flow cytometry, and immunocytochemistry.

Human Tissue Microarray and IHC

The pancreatic progression TMA was provided by the Cooperative Human Tissue Network, funded by the National Cancer Institute (NCI) (available at: <http://chtn.sites.virginia.edu/tissue-microarrays>). Other investigators may have received specimens from the same subjects.

IHC was performed using the protocol as described previously [41], with some modifications. Histology sections were deparaffinized by melting and clearing in xylene followed by rehydration in descending grades of alcohol. Antigen retrieval with citrate buffer was performed by microwaving for 20 minutes followed by blocking with 5% non-fat dry milk (NFDM) containing 5% normal goat serum (NGS; Sigma, St. Louis, MO) in PBS for one hour at room temperature. Anti-SAS1B mAb, 6B1, or mouse IgG's were applied to slides overnight at 4°C at 10 µg /mL. For the immunoabsorption assay, 6B1 mAb was pre-incubated with forty-times excess of rSAS1B protein for one hour prior to addition to the tissue and then sections were otherwise treated in the same manner. Slides were washed, quenched in methanol-hydrogen peroxide, incubated with 1:500 dilution of GαM HRP for one hour at room temperature, and then washed. Development of brown reaction product was then performed using 3, 3-diaminobenzidine (Sigma, St. Louis, MO). Hematoxylin was used as a counterstain then slides were dehydrated in increasing grades

of alcohol. Slides were air-dried, mounted, and then imaged with an Olympus BX51 (Center Valley, VA). A board-certified pathologist (AMM) reviewed and scored all slides.

Tissue Processing for RNA and Protein

Cell lysis was performed on flash frozen PDX PDAC tumor samples and normal pancreas using the SuperFastPrep-1 with lysing Matrix D tubes (MP Biomedicals, Santa Ana, CA) in a 4°C cold room. RNA was then purified with the RNeasy kit (Qiagen, Germantown, MD) and reverse transcribed to cDNA as described previously [41]. PDX PDAC samples used for IHC were fixed and embedded as detailed earlier [89].

Primers and RT-PCR

Primers designed to amplify the C-terminus of SAS1B, or GAPDH as a control, were used in a PCR assay, both previously described [41]. PCR products were run on a 1% agarose gel containing ethidium bromide and bands of the correct size were excised. cDNA was gel purified (QIAquick PCR Purification Kit, Qiagen, Germantown, MD) and sub-cloned using TOPO-TA cloning kit (Invitrogen, Carlsbad, CA). Plasmid DNA was purified (QIAprep Spin Miniprep Kit, Qiagen, Germantown, MD). DNA was sequenced and then searched with BLAST (NCBI) to confirm *ASTL/SAS1B* identity.

Indirect Immunofluorescence (IIF)

Fixed and Permeabilized IIF

Cells were grown for 30-40 hours on coverslips which were first pre-incubated with fibronectin (Sigma, St. Louis, MO) at a 1:2000 dilution. Cells were then fixed with 4%

paraformaldehyde (PFA) in DPBS for 15 minutes at room temperature. After washes with DPBS, cells were blocked and permeabilized with 5% heat-inactivated NGS in DPBS containing 0.1% Triton X100 for 30 minutes at 37°C. Anti-SAS1B mAb, SB2, or mouse IgGs were added to coverslips at a concentration of 6 µg /mL and incubated at room temperature for 1.5 hours. Following washes, a 1:500 dilution of GtαMs Alexa488 secondary antibody plus a 1:1000 dilution of DAPI was added to coverslips for one hour in the dark. Coverslips were washed, mounted with ProLong Gold Antifade (Invitrogen, Carlsbad, CA), dried, and imaged using a LSM 700 laser scanning confocal microscope (Zeiss, Oberkochen, Germany).

Live & Non-permeabilized IIF

Cells were grown on fibronectin coated coverslips for 30-40 hours and then blocked with 5% heat-inactivated NGS in media for 30 minutes at room temperature. Coverslips were then incubated with media containing 0.1% sodium azide (NaN₃) for 30 minutes on ice. SAS1B mAb, SB2, or mouse IgGs were added to coverslips at a concentration of 10 µg/mL and incubated on ice for 1.5 hours and then washed. A 1:500 dilution of GtαMs Alexa488 secondary antibody was added to coverslips for one hour in the dark. Coverslips were washed, fixed with 4% PFA-DPBS at room temperature for 15 minutes, washed again, then stained with a 1:1000 dilution of DAPI. Following additional washes, coverslips were processed as described in fixed IIF.

Flow Cytometry

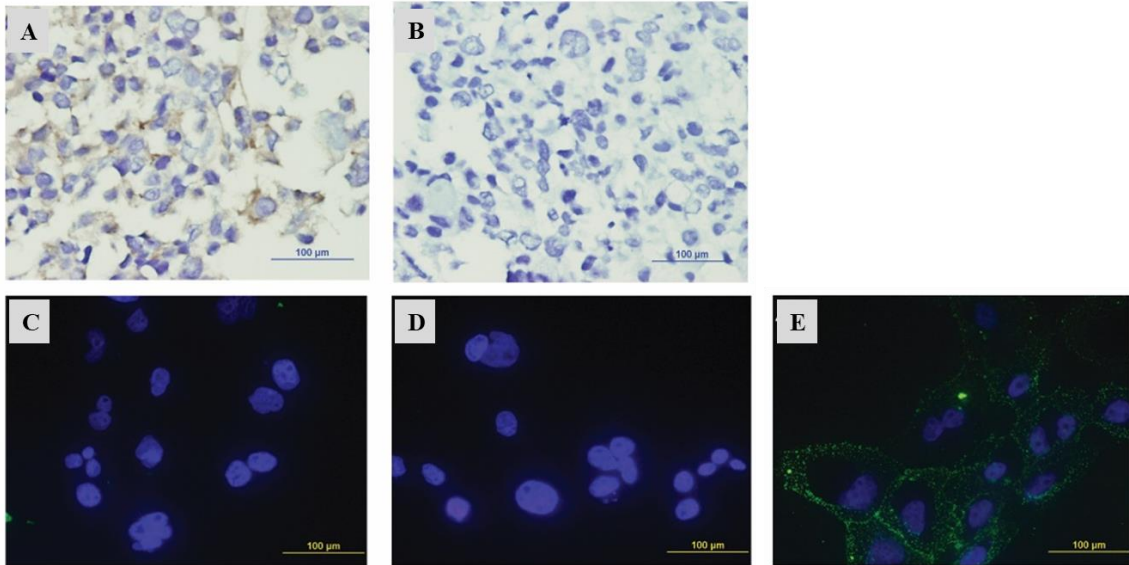
Cells were grown to 80% confluency then dissociated with StemPro Accutase (Invitrogen, Carlsbad, CA). Cells were resuspended in media and allowed to recover at

37°C, 5% CO₂ for two hours, with intermittent shaking of the tubes. Cells were blocked with media containing 0.1% NaN₃ and 5% heat-inactivated NGS (referred to as “blocking media”) for 30 minutes on ice. SAS1B mAb, SB2, or unrelated, negative control mAb, 3A4, were added to cells at a concentration of 10 µg/mL made in blocking media and incubated on ice for two hours. For the immunoabsorbed sample, SB2 was pre-incubated with forty-times excess rSAS1B protein at room temperature for one hour prior to addition to cells. EpCAM was used as a positive control antibody at a concentration of 1.0 µg/mL. Following washes, a 1:500 dilution of GtαMs R-PE made in blocking media was added to cells and incubated on ice, in the dark, for one hour. After washing, cells were resuspended in DPBS containing 1:1000 DAPI to distinguish live from dead cells. Acquisition and analysis were performed in the UVA Flow Cytometry Core Facility using a FACS Calibur flow cytometer (BD Biosciences, San Jose, CA) and FlowJo software, version 9.8.2 (FlowJo, Ashland, OR).

Cell Line Cytotoxicity

Cells were grown to 80% confluency, dissociated with Accutase, then plated in a 96 well plate and incubated overnight. Fab-CL-DMDM was pre-incubated with primary antibodies SB2, 3A4, or EpCAM made in cell media, in 1:10 serial dilutions, to allow primary antibodies to complex with secondary-drug conjugates for one hour at room temperature. For the immunoabsorption assay, SB2 mAb was pre-incubated with five-times excess SAS1B peptide, either blocking peptide or negative control peptide made of an irrelevant SAS1B sequence, overnight at 4°C before mixing with secondary-drug conjugate. Final concentration of Fab-CL-DMDM added to cells was 15 nM and

concentrations of primary antibodies ranged from 0.0016 $\mu\text{g}/\text{mL}$ (0.01 nM) to 16 $\mu\text{g}/\text{mL}$ (100 nM). Cells were incubated with ADCs for 72 hours. Following incubation, media was removed from each well and 1X CellTiter-Glo 2.0 (Promega, Madison, WI) reagent in PBS was added and then incubated at room temperature for 10 minutes. ATP level of live cells was measured at room temperature using the BioTek Cytation3 luminometer. Percent cell viability was calculated by dividing luminescence values of ADC treated cells by the baseline luminescence value obtained from averaging cells which received only Fab-CL-DMDM. Triplicate experiments were performed independently, each with 3 technical repeats. The LD50s were calculated for each cell line and analyzed for statistical significant using non-linear regression (p-value <0.05). An ANOVA, Student t-test was used to determine if the difference in cytotoxicity between pancreatic cancer cell lines and keratinocytes was statistically significant (p-value <0.05).



Supplemental Figure 2.1 SAS1B mAb 6B1 preferentially recognizes cytoplasmic SAS1B

[A] Uterine cancer cell line SNU539 showed moderate 2+ staining intensity for SAS1B using 6B1 mAb by IHC. [B] No signal was observed when probed with normal mouse IgG negative control. [C] 6B1 mAb failed to show immunoreactivity on live SNU539 uterine cancer cells by IIF. [D] Negative control normal mouse IgG negative control also showed no staining. [E] Positive control anti-integrin mAb showed surface staining in live SNU539 cells. DAPI was used to counterstain the cells (blue stain in panels C-E). Experiments performed by Eusebio Pires.

FUNDING

This work was supported by a Cancer Research Institute Clinical Team Grant: “Immunotherapeutic targeting cell surface neoantigen SAS1B” to JCH/CLS. Funding was also received from the Center for Innovative Technology (CIT): “mAbs to target surface metalloprotease” ER14S-003-LS awarded to ESP/JCH. Additional funds were provided by the University of Virginia Vice President for Research. This research was also supported by the UVA Cancer Center through the NCI Cancer Center Support P30 CA44579 awarded to TWB, with support from the Commonwealth of Virginia.

Chapter 3

ASTL/SAS1B: Expression in normal cells and additional cancers

INTRODUCTION

SAS1B has emerged as an exciting potential therapeutic target for the treatment of various cancers due to limited localization among normal tissues combined with neoplastic cell surface localization. A crucial characteristic of SAS1B as an effective target for ADC or CAR-T therapy is that SAS1B localizes to the cell surface of cancer cells but has limited or no cell surface expression in non-neoplastic cells. Two observations, previously published by our group, suggest no ASTL/SAS1B expression among panels of normal tissue: 1) no ASTL expressed sequence tags provided in the Unigene database from normal tissues and 2) IHC performed on an array of normal human tissues using the SAS1B rabbit pAb showed no expression of SAS1B in any of the tissues examined (adrenal cortex, adrenal medulla, alveoli, bladder, breast epithelium, cartilage, cerebral cortex, fallopian tube, heart aorta, heart myocardium, kidney cortex, liver, lymph node, pancreas, parathyroid, peripheral nerve, placenta villi, prostate, salivary glands, small intestine mucosa, testes, thymus, thyroid, and tonsil) [41]. Additionally, IHC on a panel of 16 normal mouse tissues showed no SAS1B expression [38] and no ASTL transcript was detected in 15 normal mouse tissues by Northern blot [37]. Development of effective anti-SAS1B therapies for the treatment of SAS1B^{POS} cancers depends on solid data regarding SAS1B expression in normal tissues. For example, a SAS1B-ADC will potentially be cytotoxic to any cells expressing and internalizing an adequate amount of cell surface SAS1B. To be used clinically, the expression profile of SAS1B in various cancers will need to be determined and it will need to be shown exhaustively that there are limited, if any, on-target, off-tumor effects of the SAS1B targeted therapy *in vivo*.

Given SAS1B that expression was observed in female reproductive cancers [41] and pancreatic cancers [Knapp et. al, Manuscript Submitted], and that SAS1B is a COA, we hypothesized that SAS1B was expressed in other cancer indications. To test this, we broadened the scope of analysis to include solid cancers from the head and neck region as well as hematologic malignancies. Interrogation of additional cancer indications will provide insight into the range of cancers that may potentially benefit from a targeted therapy to SAS1B.

Head and Neck Cancer

Worldwide, head and neck cancer is the fifth most common cancer diagnosis and the eighth most common cause of cancer death [99]. Cancers of the head and neck are heterogeneous and include cancers of the oral cavity, oropharynx, hypopharynx, larynx, lip, nose, and paranasal sinuses. Over 90% of head and neck cancers are squamous cell carcinomas (HNSCC) [100]. For approximately one-third of patients, diagnosis is at an early stage of the disease and treatment is surgery or radiotherapy with a favorable prognosis. However, two-thirds of patients present with advanced-stage cancers involving lymph node metastases for which the standard of care is surgery combined with adjuvant radiation therapy and/or chemotherapy [101]. Five-year survival rates are 40-50% highlighting inadequacies in current treatment regimens [100]. Chemotherapy resistance is high, locoregional recurrence develops in the majority of patients, and distant metastases occur in 20-30% of HNSCCs, emphasizing the need for better therapeutics [102-104]. Generally, the standard of care for treating HNSCC patients is limited based on the lack of tumor-cell targeted treatments and because of unacceptable toxicity to the patient.

Treatment strategies aimed at organ and function preservation include: concomitant chemoradiotherapy, intensity-modulated radiation therapy, and molecular-targeted biological agents [101, 105]. New and promising therapeutics include targeted therapies which discriminate cancer cells from normal cells such as ADCs [101].

Currently, two monoclonal antibodies used in the treatment of HNSCC are cetuximab and bevacizumab. Cetuximab, an anti-epidermal growth factor receptor (EGFR) monoclonal antibody, was approved in combination with radiotherapy for recurrent/metastatic HNSCC. Although cetuximab has been shown to improve survival, skin toxicity is common [106, 107]. Less promising, bevacizumab, an anti-vascular endothelial growth factor (VEGF) monoclonal antibody, is likely to provide benefit only in recurrent/metastatic settings in combination with chemotherapy, and has associated vascular complications [101]. Clinical use of cetuximab and bevacizumab demonstrates feasibility of using monoclonal antibody based strategies in the treatment of head and neck cancers.

Leukemia

Leukemia is the ninth most common cancer in the US with 62,130 predicted new cases in 2017 and 24,500 estimated deaths in 2017. Although leukemia is among the most common childhood cancers, it most often occurs in older adults. Leukemia develops in blood-forming tissues, such as bone marrow, which results in production of abnormal white blood cells. The four main types of leukemia are acute lymphoblastic leukemia (ALL), acute myelogenous leukemia (AML), chronic lymphocytic leukemia (CLL) and chronic myelogenous leukemia (CML) [108]. Treatment is based largely on the type of leukemia

and stage of disease. Common treatments include chemotherapy, biological therapy, targeted therapy, radiation, and stem cell transplant [109]. The introduction of the tyrosine kinase inhibitor, imatinib (Gleevec) resulted in significant overall 5-year survival rate improvements for patients with CML from 30% before Gleevec to 89% [110]. Leukemia researchers continue to work towards developing novel therapeutics which target cancer cells exclusively to achieve higher selectivity and treatment efficacy.

The importance of studying SAS1B incidence in a variety of cancers is to gain insight into the range of cancer patients who may benefit from a potential therapeutic targeted against SAS1B. Initial studies will examine small cohorts of samples from various tumors and if SAS1B expression is indicated, our group suggests larger scale SAS1B expression profiling. Studying the pattern of SAS1B expression, with regard to protein isoform cellular localization and level of cell surface expression, will aid in identification of candidate patient subpopulations who are eligible for an anti-SAS1B therapy. However, to develop SAS1B theranostics (therapy plus companion diagnostic), we need to first understand the repertoire and expression patterns of SAS1B protein isoforms, encoded by ASTL splice variants, present in cancer cells. As an example of the potential value of such studies, determining which protein isoforms localize to the cancer cell surface will guide mAb generation, against surface-exposed SAS1B epitopes, to be used in SAS1B-ADC therapy; congruently, these studies may aid in development of a companion diagnostic test to identify candidate patients.

Alternative splicing

Alternative splicing of mRNAs is regarded as a crucial mechanism for gene regulation and generating transcriptome and proteome complexity [111-113]. High throughput sequencing technology has recently been used to approximate that nearly 95% of multi-exon human genes are involved in alternative splicing [114]. Defects or alterations in alternative splicing have been shown to be involved in various diseases including cancer [113, 115, 116]. Patterns of alternative splicing can be tissue, stimulus, or disease specific [117]; examining variants in different tumor types as well is imperative for distinguishing predominant variants in different tissue and disease states. Splice variant protein isoforms may be structurally and physiologically different from each other and as compared to the wild-type protein [117], and can have very significant functional impacts in cancer biology [116]. Some splice variants may encode secreted proteins while other variants may encode membrane proteins [118, 119]. The nature and number of splice variants of human SAS1B, and whether these transcripts are translated into proteins, is currently unknown.

Encoded by a single copy gene, mouse oocyte SAS1B is alternatively spliced into six unique variants, each of which encodes translated proteins. This results in SAS1B protein micro-heterogeneity. All mouse variants contain a characteristic zinc-binding active site motif and a putative transmembrane domain, while three variants also contain a putative signal sequence upstream of an N-terminal cleavage sequence to produce the fully processed form. Mouse SAS1B is 67% homologous to human SAS1B and it is conserved among mammals [37].

The human SAS1B gene is divided into 9 exons. Although the coding region has been sequenced in humans, splice variants, isoforms, and protein expression still needs to

be elucidated in order to characterize SAS1B expression and function in cancer tissues. SAS1B has been shown to localize to both the cytoplasm and the cell membrane in cancer cells [41] and to be exocytosed from oocyte cortical granules [39]; thus, we hypothesize that there are at least three different isoforms of SAS1B. Physiological and structural differences of SAS1B protein isoforms may result in differential cellular localization and function. Specific SAS1B splice variant protein isoforms may be preferentially expressed or upregulated in a particular cancer type [120]. Determination of the main SAS1B isoforms and whether they are membrane-associated in tumors will aid in development of targeted diagnostic and therapeutic treatments against SAS1B.

RESULTS

ASTL/SAS1B expression in normal tissues

While early studies reported no detection of SAS1B in normal mouse and human tissues, [37, 38, 41], recent development of more sensitive assays suggests potential expression of ASTL/SAS1B in limited normal tissues. Understanding the complete expression profile of SAS1B not only in cancer indications but also in normal tissues will help guide development and implementation of anti-SAS1B therapies. The Genotype-Tissue Expression (GTEx) database (Broad Institute), which collects human tissues from genotyped donors, was interrogated for ASTL hits. Expression values are shown in reads per kilobase of transcript per million mapped reads (RPKM). While most tissues had no or negligible ASTL expression, presence of ASTL transcript in some normal tissues, notably whole blood, spleen, and bladder, was observed (Figure 3.1). EBV transformed lymphocytes also showed ASTL expression, keeping with the observation that transformed cells in culture express the COA, ASTL/SAS1B. Additionally, both sun-exposed and non-sun exposed skin samples expressed ASTL transcript, which is consistent with our findings that human keratinocytes were ASTL/SAS1B^{POS} (Chapter 2, Results). Some ASTL expression was also observed in bladder. It remains to be seen whether SAS1B localizes to the cytoplasm and/or the cell membrane in bladder cells, what percentage of bladder cells are SAS1B^{POS} and whether SAS1B expression is restricted to a specific subpopulation of bladder cells. Ovary did not show appreciable ASTL signal, which is reasonable given that only a few oocytes within the ovary will express ASTL at any given time leading to overall low transcript level. Additionally, tissues may have been from post-menopausal women. The GTEx data does not indicate whether protein translation occurs in these

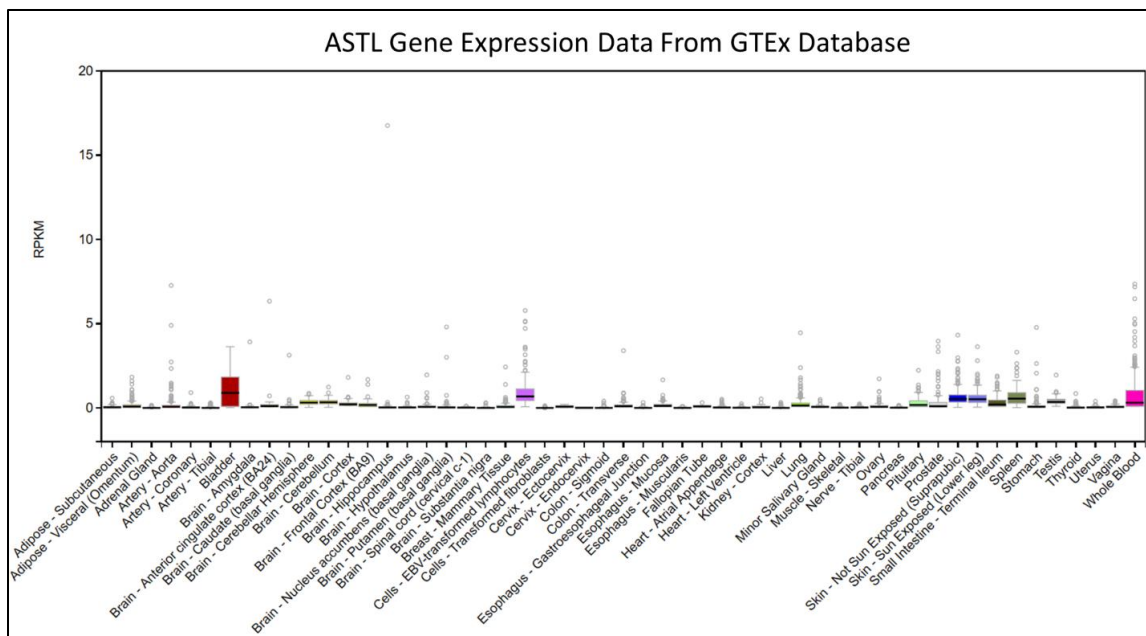


[Figure 3.1] ASTL gene expression data from GTEx database

ASTL gene expression from GTEx database showing no or minimal ASTL expression in a variety of normal tissues. Expression values are shown in reads per kilobase of transcript per million mapped reads (RPKM). Box plots include median and 25th and 75th percentiles with outliers ± 1.5 times the interquartile range shown as points. Majority of tissues have no or negligible ASTL transcript expression; whole blood and bladder have the highest ASTL hits.

tissues, which sub-population(s) and proportion of cells from a given tissue are ASTL^{POS}, or any information about splice variant/protein isoform expression and cellular localization. Addressing these issues in the ASTL^{POS} tissues identified by GTEx will inform development of anti-SAS1B therapeutics. For example, a SAS1B-ADC could still be useful if normal cells identified as ASTL^{POS} by GTEx database either lack SAS1B protein translation or do not express SAS1B at the cell surface.

Given the RNA sequencing data from GTEx which showed ASTL transcript in whole blood, human peripheral blood mononuclear cells (PBMCs) isolated from whole blood, were examined for SAS1B expression by flow cytometry. PBMCs consist of lymphocytes (T cells, B cells, NK cells) and monocytes (which can differentiate into macrophages and dendritic cells). PBMCs were either fixed and permeabilized to observe intracellular signal or were live, non-permeabilized cells to visualize cell surface proteins; SAS1B protein was detected using the SB2 mAb. In this pilot study of one patient sample, a small fraction, 3.1%, of PBMCs showed cytoplasmic expression of SAS1B by flow cytometry (Figure 3.2, row two/left column; experiments performed by Walter Olson). Of the 3.1% of positive cells, approximately 44% were monocytes and 66% were lymphocytes. Myeloid derived cells appear in the upper two quadrants (y-axis high) while lymphoid derived cells appear in the lower two quadrants (y-axis low) (Figure 3.2). SAS1B^{POS} monocytes cells account for approximately 6.02% ($(1.36/(21.3+1.36))$) of the total population of myeloid derived cells while SAS1B^{POS} lymphocytes make up a smaller portion of total lymphoid derived cells, 2.25% ($(1.74/75.6+1.74)$) (Figure 3.2 row two/left column). Antibody specificity for SAS1B was shown by immunoabsorbing the SB2 mAb with a SAS1B blocking peptide as compared to no immunoabsorption observed when a

SAS1B control peptide, which is not recognized by SB2, was used (Figure 3.2, rows three and four/left column). A very small percent of lymphocytes, 0.51% ($(0.43/(0.43+83.3))$) were identified as expressing cell surface SAS1B while monocytes did not show cell surface localization of SAS1B (Figure 3.2, row two/right column). Because this small population of cell surface SAS1B^{pos} lymphocytes remained when SB2 was immunoabsorbed with the SAS1B blocking peptide (Figure 3.2, row three/right column), it likely represents non-specific antibody binding rather than a true population of cells expressing cell surface SAS1B. This suggestion is supported by the high level of noise observed when live, non-permeabilized PBMCs were incubated with isotype control (Figure 3.2, row one/right column). A similar experiment using a three additional buffy coat samples showed similar results ranging from less than 1% to 2% of PBMCs expressing intracellular, but not surface localized, SAS1B. These preliminary results suggest SAS1B may be expressed intracellularly in a very small population of PBMCs but does not localize to the cell surface. Despite the SAS1B^{pos} fraction of PBMCs is small, it remains a definitive, albeit undefined, population in the peripheral blood. Additional flow cytometry experiments using PBMCs co-stained with cell type specific markers plus SAS1B will provide validation of SAS1B expression in PBMCs as well as insight into which sub-population(s) of PBMCs are SAS1B^{pos}.

With the intention of validating preliminary results suggesting some human PBMCs express cytoplasmic SAS1B and to determine which sub-population(s) of leukocytes in blood express SAS1B, mouse splenocytes were analyzed. The results generated in mouse indicating which leukocyte cell type(s) are SAS1B^{pos} will guide subsequent similar experiments using human samples. Splenocytes were isolated from

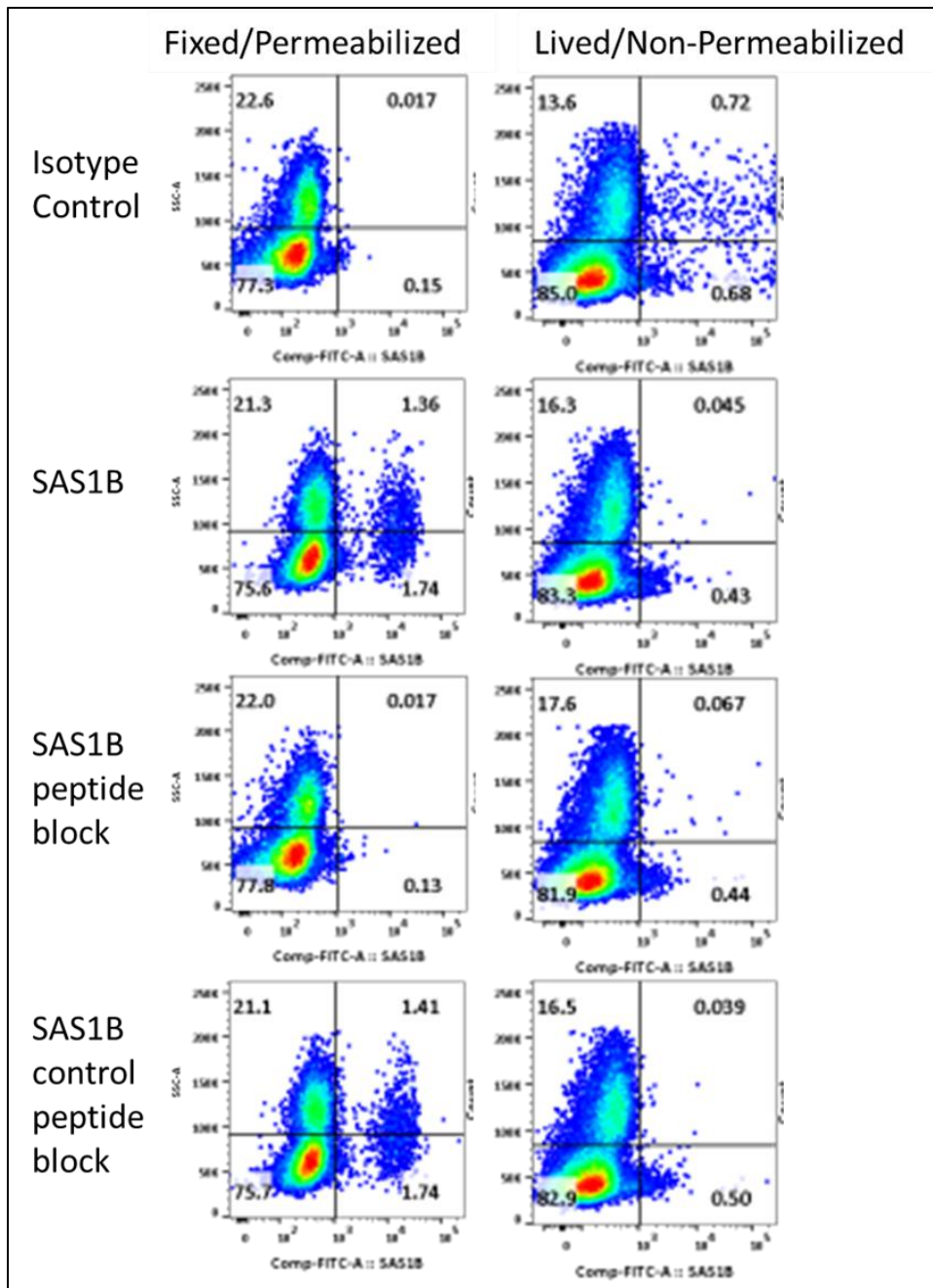


[Figure 3.2] SAS1B localizes to the cytoplasm, but not to the cell surface, in a small population of human PBMCs

PBMCs from a healthy, human donor were either fixed and permeabilized (left column) or were live and non-permeabilized (right column) and then stained with anti-SAS1B mAb, SB2 (second row). Lymphoid derived cells were concentrated in the lower half while

myeloid cells appeared in the upper half of the grids on scatter plots. Approximately 2% and 6% of lymphoid (y-axis low) and myeloid (y-axis high) derived cells, respectively, were positive for intracellular SAS1B (left column, row 2). No cell surface SAS1B signal was observed on live cells (right column, row 2). SB2 isotype control was used as a negative antibody control. When SB2 was immunoabsorbed with a blocking peptide, intracellular PBMC signal was blocked (left column, row 3). Intracellular SAS1B signal was not blocked when SB2 was pre-incubated with a SAS1B control peptide which is not recognized by SB2 (left column, row 4). Results indicate intracellular, but not cell surface, localization of SAS1B in a small portion of PBMCs. (Experiments performed by Walter Olson.)

mouse and stained with serum from guinea pig immunized against mouse SAS1B or pre-immune control serum. Total mouse splenocytes were permeabilized and stained for intracellular SAS1B which showed 2.3% of all splenocytes were SAS1B^{pos} (Figure 3.3A; experiments performed by Aaron Stevens). All negative controls – no secondary antibody, no primary antibody, and pre-immune sera – showed no signal. Given the low percentage of SAS1B^{pos} cells, specific sub-populations of immune cells were gated based on cell surface markers and then assessed for SAS1B positivity. Cytotoxic T cells were gated based on CD8^{pos}, helper T cells on CD4^{pos}, natural killer cells on NK1.1^{pos}, B cells on B220^{pos}, and dendritic cells on CD11c high plus MHCII^{pos}. Most immune cell sub-populations were SAS1B^{neg} while 39.5% of dendritic cells were SAS1B^{pos}. We then asked what proportion of immune cell sub-population(s) make up the total pool of intracellular SAS1B^{pos} splenocytes identified in the far right plot of Figure 3.3A (2.3% SAS1B^{pos}). Less than 3% of SAS1B^{pos} cells were either helper T Cells (CD4), cytotoxic T cells (CD8), or natural killer cells (NK1.1). About half of SAS1B^{pos} cells were dendritic cells and 25% were B cells. While dendritic cells were shown to express intracellular SAS1B, when live, non-permeabilized total splenocytes were probed for cell surface SAS1B, only 0.15% of cells were SAS1B^{pos} (Figure 3.3D). To confirm SAS1B expression, these experiments need to be repeated with an additional group of splenocytes that are incubated with SB2 which has been immunoabsorbed with the SAS1B blocking peptide. This population of SAS1B^{pos} live, non-permeabilized splenocytes may represent non-specific antibody binding as suggested for a similar population in human PBMCs (Figure 3.3). If the SAS1B^{pos} population is confirmed by the immunoabsorption assay, additional experiments are required to statistically assess whether the SAS1B signal is higher than the negative

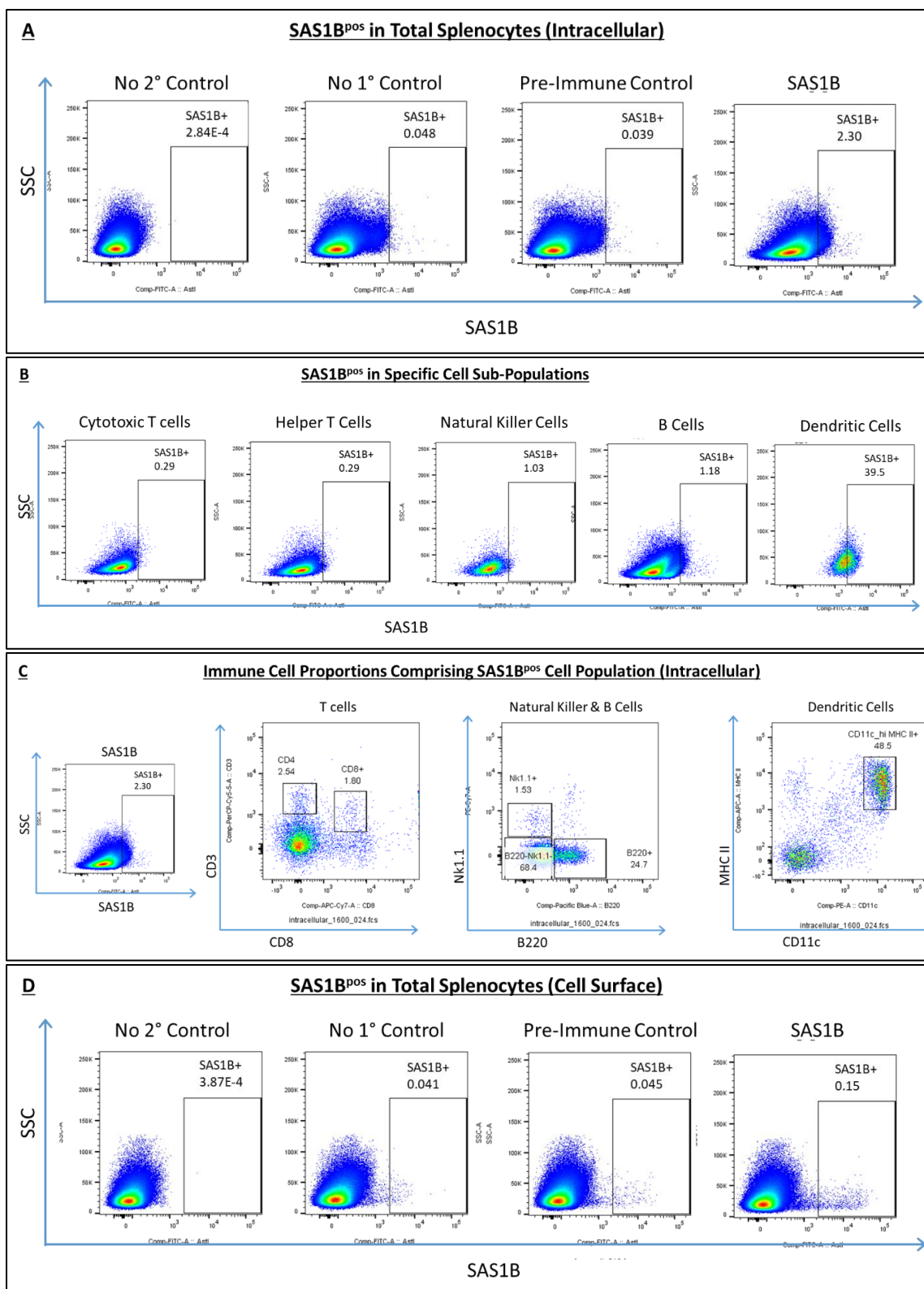


[Figure 3.3] Mouse SAS1B was expressed intracellularly in dendritic cells and B-cells

SAS1B expression was examined in mouse splenocytes using serum from guinea pigs immunized with mouse SAS1B by flow cytometry. [A] Of total mouse splenocytes probed for intracellular SAS1B expression, 2.3% were SAS1B^{pos}. All negative controls, no secondary antibody control, no primary antibody control, and pre-immune guinea pig serum, showed no signal. [B] Intracellular SAS1B staining of splenocyte sub-populations. Cytotoxic T cells were gated based on CD8^{pos}, helper T cells on CD4^{pos}, natural killer cells on NK1.1^{pos}, B cells on B220^{pos}, and dendritic cells on CD11c high plus MHCII^{pos}. Most immune cell sub-populations were SAS1B^{neg} while 39.5% of dendritic cells were SAS1B^{pos}. [C] Proportion of immune cell populations comprising the pool of intracellular SAS1B^{pos} cells identified in Panel A. The far left plot (taken from Panel A) shows the gating strategy used to identify SAS1B^{pos} cells; the specific cell types comprising this population were subsequently analyzed. Less than 3% of SAS1B^{pos} cells were either helper T Cells (CD4), cytotoxic T cells (CD8), or natural killer cells (NK1.1). About half of SAS1B^{pos} cells were dendritic cells and 25% were B cells. [D] Only 0.15% of total splenocytes were positive for cell surface SAS1B expression. Negative controls had no signal. Experiment repeated twice; representative results shown. (Experiments performed by Aaron Stevens.)

controls. These data show that mouse SAS1B was expressed intracellularly, but not at the cell surface, in the dendritic cell sub-population of total mouse splenocytes.

An additional population of B cells were also positive for intracellular SAS1B; however, for both B cells and dendritic cells, only a fraction of cells expressed SAS1B. Whether there is a population of secreted SAS1B remains to be determined; one potential approach is to use a sandwich ELISA to capture circulating SAS1B from healthy patient serum samples. Although why only a fraction of dendritic and B cells express SAS1B remains unknown, SAS1B expression may be related to the cell cycle. Flow cytometry co-staining with cell cycle markers will clarify if SAS1B expression is related to cell cycling in these cell types. SAS1B may also be preferentially expressed in certain subtypes of dendritic cells and B cells; to determine if this is the case, cells can be co-stained with additional markers to identify specific dendritic and B cell subtypes.

Three lines of preliminary evidence (Figures 3.1, 3.2, and 3.3) suggest SAS1B is expressed in a subset of leukocytes and validate further exploration of SAS1B incidence in certain whole blood cell populations. Importantly, the data presented in Figures 3.2 and 3.3 represent small sample sizes and must be repeated in additional subjects to validate preliminary results. More experiments are necessary to define SAS1B expression in normal tissues, which is a critical component guiding anti-SAS1B therapeutic development for the treatment of SAS1B^{POS} cancers. Additionally, *in vivo* studies using a SAS1B-ADC will be needed to assess the impact of expression on mouse health and immunity.

ASTL/SAS1B was expressed in a high percentage of HNSCCs and localized to the cell surface in vitro

RNA was isolated from 24 HNSCC patient samples and was reverse-transcribed to cDNA. PCR amplification of the unique c-terminus region of ASTL showed 100% (24/24) of HNSCC tumors were ASTL positive (Figure 3.4A). Amplicons were cloned and sequenced, revealing 99% identity to ASTL reference sequence. Although not quantitative, PCR band intensity suggests differences in levels of ASTL between tumors. Western blot analysis, using a rabbit polyclonal antibody (pAb) generated to recombinant SAS1B [41], showed that SAS1B was expressed in 8/8 tumors (Figure 3.4B). There is 100% concordance between ASTL message and SAS1B protein in the cohort of 8 tumors. No immunoreaction was observed when tumors were probed with pre-immune antibodies (Figure 3.4B). The predicted molecular weight (primary sequence) of SAS1B is 46 kDa; however, two predicted SAS1B isoforms of higher molecular weight at ~48 kDa and ~65 kDa were also routinely observed using this pAb [41]. Protein extracts from pancreatic cancer cell lines (mPanc96, 608, 366) as well as a uterine cancer line (SNU539) show a similar banding pattern on Western blot when probed with the Rb pAb (data not shown). These results are limited by the absence of normal head and neck tissue to use as SAS1B^{neg} controls in PCR and Western blot assays. However, preliminary screening results warrant further exploration into SAS1B expression in head and neck tumors and additional normal tissues.

Given that patient HNSCC tumors express SAS1B, cell lines were examined to establish an *in vitro* system which could be used to evaluate SAS1B as a potential therapeutic target in HNSCC. Eight HNSCC cell lines were examined for ASTL transcript presence by PCR and for SAS1B protein by Western blot (Figure 3.5). All cell lines are

squamous cell carcinomas with different origins: Cal27, SCC-9, SCC-25, SCC-61, and OSC-19 are from the tongue, FaDu is from the pharynx, while UNC-7 and UNC-10 are derived from lymph nodes. ASTL transcript was detected in 8/8 cell lines by PCR (Figure 3.5A) with varying gel band intensities suggesting differences in ASTL transcript levels among cell lines. When immunoblotted with the SAS1B rabbit pAb, total cellular protein from 8/8 cell lines showed a major band ~65 kDa which is consistent with observations from patient tumors in Figure 3.4B. The predicted molecular weight of SAS1B at 46 kDa was present in 6/8 cell lines with 2/8 cell lines also having an additional band at ~48 kDa as well. Additional studies, described below, are necessary to determine which immunoreactive bands correspond to which protein isoform and to concretely show each band is in fact SAS1B.

We hypothesized that SAS1B may be glycosylated and that this may explain immunoreactive bands at larger-than-expected molecular sizes regularly observed (50 and 65 kDa) in cell lines from multiple cancer indications (HNSCC, PDAC, uterine). An initial screen using three glycosylation prediction algorithms support our hypothesis that SAS1B is glycosylated (Figure 3.6). All three algorithms predicted an N-glycosylation site at amino acid 265 in the proteinase domain. Two additional N-linked sites in the proteinase domain were also predicted by one algorithm. Analysis from the three algorithms predicted 19 to 49 O-linked glycosylation sites, with the majority concentrated in SAS1B's unique C-terminal region (Figure 3.6). SAS1B was predicted not to have any C-linked glycosylation sites. Subsequent studies (described in Chapter 3, Discussion) comparing glycosidase treated and untreated samples are necessary to experimentally determine SAS1B's glycosylation pattern and inform observed immunoassay results.

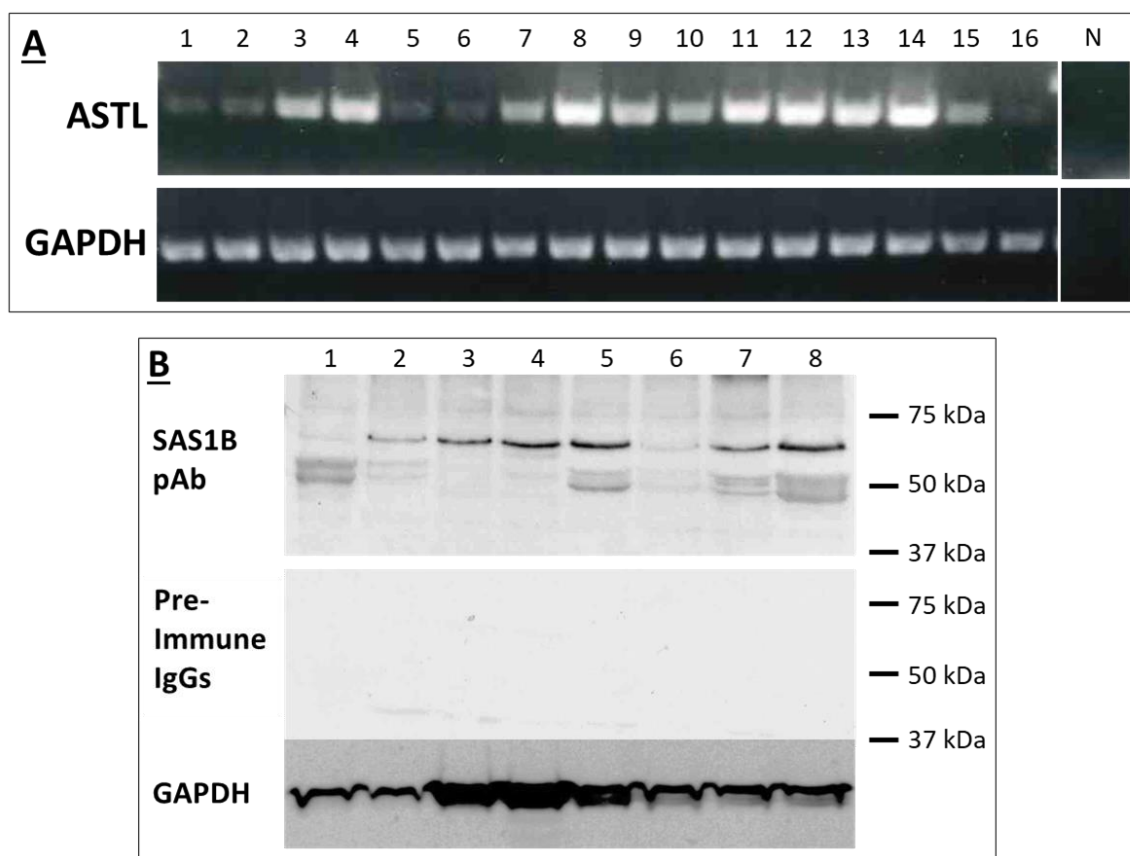


Figure 3.4 ASTL/SAS1B was expressed in a high percentage of patient HNSCCs

[A] RT-PCR analyses of 16 HNSCC (1-16) tumors using a c-terminus ASTL specific primer set showed a 309bp amplicon in 16/16 tumors. GAPDH was used as a housekeeping control for PCR. A total of 24 tumors were examined; 24/24 were positive for ASTL mRNA, 16 of which are shown here. [B] Western blot analyses of 8 HNSCC tumors (1-8), corresponding to the same tumors examined in [A], immunoblotted with either anti-SAS1B pAb or pre-immune IgGs. GAPDH used as a loading control. Predicted molecular weight of SAS1B is 46 kDa; higher bands predicted to be glycosylated forms and/or protein isoforms.

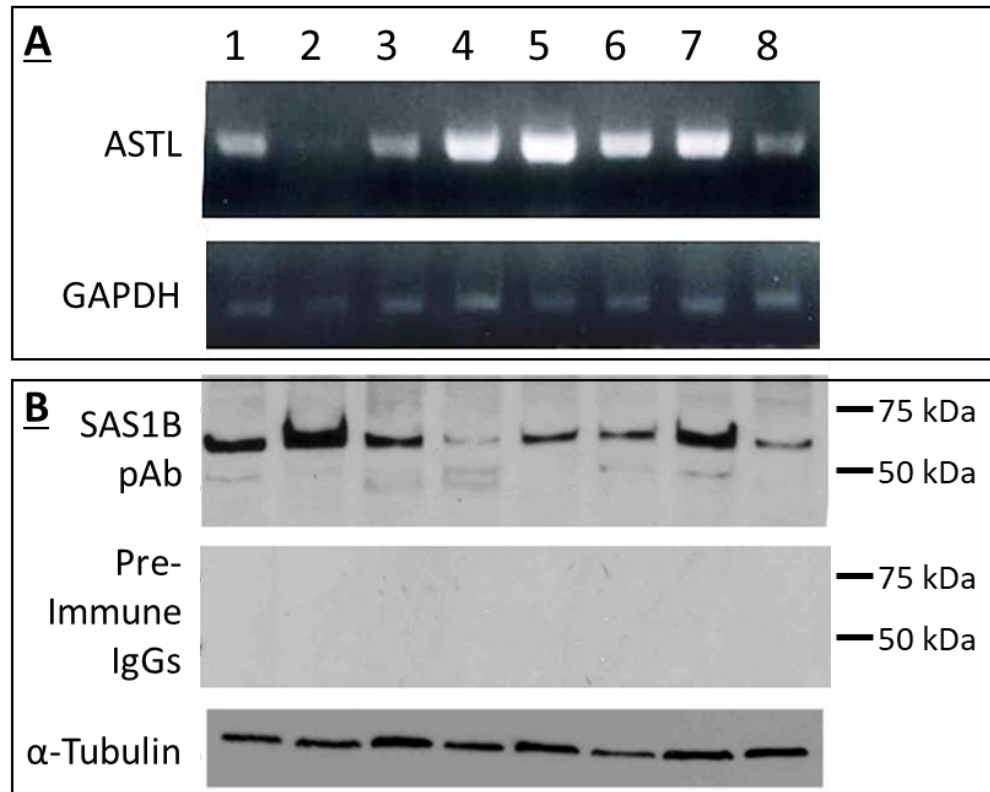


Figure 3.5 HNSCC cell lines expressed ASTL/SAS1B

[A] RT-PCR analyses of HNSCC cell lines using a c-terminus ASTL specific primer set showed a 309bp amplicon in 8/8 cell lines. GAPDH was used as a housekeeping control for PCR. Numbers correspond to the following cell lines: 1) Cal27, 2) FaDu, 3) SCC-9, 4) SCC-25, 5) SCC-61, 6) UNC-7, 7) OSC-19, 8) UNC-10. [B] Western blot analyses of 8 HNSCC cell lines immunoblotted with either anti-SAS1B pAb or pre-immune IgGs. α -Tubulin used as a loading control. Predicted molecular weight of SAS1B is 46 kDa; higher bands predicted to be glycosylated forms and/or protein isoforms.



KEY

SAS1B protein domains:

Signal peptide (orange)

Propeptide (fuchsia)

Proteinase domain (blue)

Unique C-terminal region (green)

O-glycosylation sites predicted by:

★ Hirst Group (U. Nottingham)

● NetOGlyc (Tech. U. Denmark)

▲ GlycoEP (Microbial Tech., India)

N-glycosylation sites predicted by:

⋯ Hirst Group

□ Hirst Group, NetNGlyc, & GlycoEP

[Figure 3.6] SAS1B is predicted to be heavily O-glycosylated

N-linked and O-linked glycosylation status of SAS1B amino acid residues as predicted by three bioinformatics algorithms (Hirst Group, NetOGlyc or NetNGlyc, and GlycoEP). SAS1B is predicted to be heavily O-glycosylated, with a concentration in the unique C-terminal region; stars (Hirst Group), circles (NetOGly), and triangles (GlycoEP) shown represent predicted O-linked residues. One N-linked glycosylation site is predicted by all

three algorithms (solid rectangle) and two additional sites (dotted rectangles) are predicted by the Hirst Group algorithm. Amino acid residue positions listed about every 20 residues and protein domains are distinguished by color (signal peptide – orange, propeptide – fuchsia, proteinase domain – blue, and unique C-terminal region – green).

If one or both of the larger immunoreactive protein bands observed in Western blot of HNSCC samples is not due to glycosylation, other methods will be used to determine if the bands are due to antibody cross-reactivity. In an unbiased approach, immunoprecipitation of SAS1B from cancer cell lines using SAS1B antibodies followed by 2-D gel electrophoresis and liquid chromatography tandem mass spectrometry (LC/MS-MS) analysis will confirm presence of SAS1B peptides, or other potential protein peptides, at a given molecular weight. A second approach would be to knock-out or knock-down SAS1B in a given cell line; immunoreactive bands representing SAS1B should be absent or display reduced intensity, demonstrating antibody specificity. Nonetheless, these preliminary studies suggest several HNSCC cell lines express ASTL/SAS1B, including potential glycosylated forms of SAS1B and/or protein isoforms, and should be used for further *in vitro* studies including assessment of an ADC targeting SAS1B in HNSCC.

To confirm the presence of SAS1B protein, the cell line OSC-19 was further characterized by IIF using a different SAS1B mAb, SB2. SAS1B was shown to localize to the cytoplasm in the vast majority of OSC-19 cells when cells were fixed, permeabilized, and then stained with SB2 (Figure 3.7B); no signal detected when cells were probed with normal mouse IgG as a negative control (Figure 3.7A). Cytoplasmic SAS1B expression appears to be concentrated in the peri-nuclear region with suspected endoplasmic reticulum (ER) and Golgi apparatus association. This observation is consistent with the presence of a N-terminal signal peptide which is predicted to result in translocation of SAS1B into the ER membrane where translation continues (known as cotranslational transport).

Live, non-permeabilized OSC-19 cells were then examined by IIF to determine if SAS1B localizes to the cell membrane and may thus be a potential ADC target. Figure

3.7D showed SAS1B cell surface localization when stained with SB2 mAb and no detectable signal when OSC-19 cells were probed with normal mouse IgGs (Figure 3.7C). A punctate pattern of SAS1B expression was observed over the majority of the cell surface of most cells (Figure 3.7D) and was consistent with the staining pattern observed in pancreatic cancer cells (Figure 2.4E-G). As hypothesized earlier, the punctate pattern of expression may indicate SAS1B is associated with lipids rafts and/or exocytosed and associated with other cell membrane protein(s). These data support future studies testing an anti-SAS1B ADC in HNSCC cell lines to further evaluate SAS1B as a viable therapeutic target for the treatment of HNSCC.

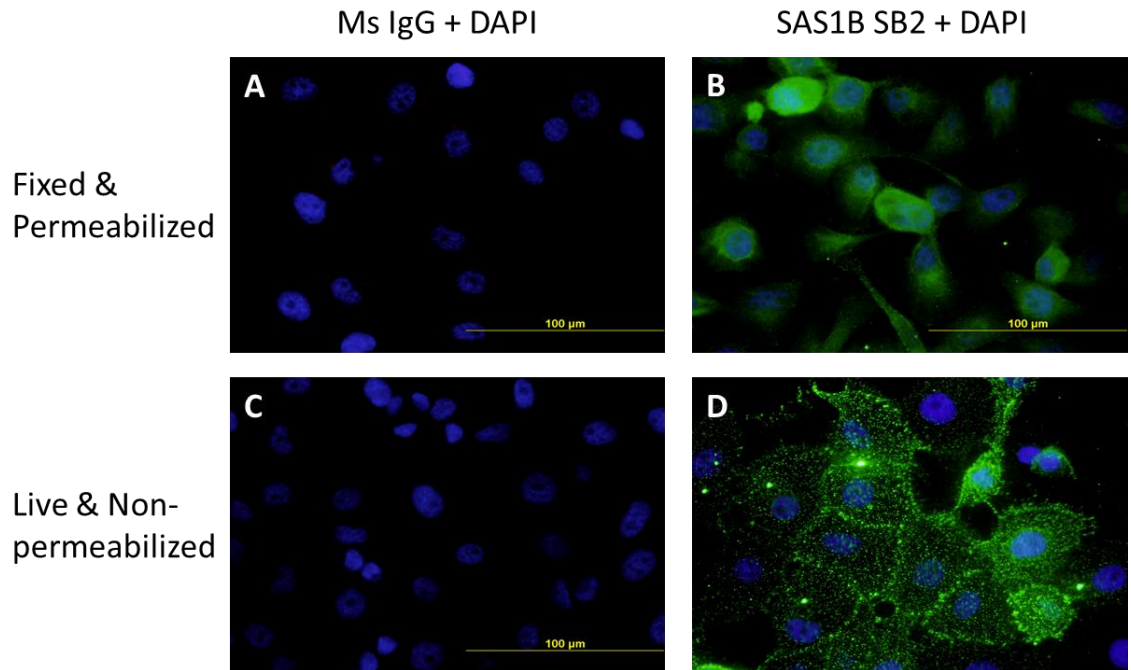


Figure 3.7 SAS1B localized to the cytoplasm and to the cell surface in OSC-19

[A-B] Fixed and permeabilized IIF on the HNSCC cell line OSC-19. SAS1B (green) revealed cytoplasmic localization using SB2 mAb [B]. Cell nuclei stained with DAPI (blue). No signal detected when OSC-19 cells were probed with normal mouse IgG control [A]. [C-D] IIF on live, non-permeabilized OSC-19 cells. SAS1B detected at the plasma membrane using SB2 mAb [D]; no signal observed when cells were stained with normal mouse IgG control.

ASTL/SAS1B was expressed in about 30% of leukemia samples

ASTL/SAS1B has been previously shown to be expressed in solid tumors from uterus, pancreas, and head and neck but has not been studied in liquid cancers, more commonly referred to as hematological malignancies. To assess whether SAS1B is present in liquid tumors, primary patient leukemia samples and leukemia cell lines were analyzed. RNA obtained from AML and LGL (large granular lymphocytic) patient samples was reverse transcribed to cDNA then amplified by PCR. Total ASTL transcript incidence among both types of leukemia was 32% (9/28) while type specific incidences were similar with 38% (5/13) AML samples and 27% (4/15) LGL samples ASTL^{POS} (Figure 3.8A). Although not quantitative, differences in band intensities are suggestive of ASTL transcript level variation among patients; if this correlates to protein differences remains to be seen.

Leukemia cell lines were then examined to establish an *in vitro* system to be used to study effects of anti-SAS1B therapeutic options for leukemia. Total protein from six AML cell lines (HL60, Kasumi-1, KG-1, OCI-AML3, MOLM-13, MOLM-14) and two LGL cell lines (NKL, TLG1) examined all showed an immunoreactive band at the predicted molecular weight of SAS1B at ~46 kDa by Western blot analysis (Figure 3.8B). No immunoreactivity was observed when probed with pre-immune IgGs. GAPDH was used as a protein loading control. Band intensities are similar between cell lines suggesting relatively comparable SAS1B expression levels. Western blot analysis revealed one immunoreactive band at 46 kDa in leukemia which differs from previous data in HNSCCs showing a major band at 65 kDa and a doublet at ~46/50 kDa (Figures 3.8B and 3.5B). SAS1B expression data from patient samples and from cell lines supports further evaluation of SAS1B as a potential therapeutic target for the treatment of leukemia.

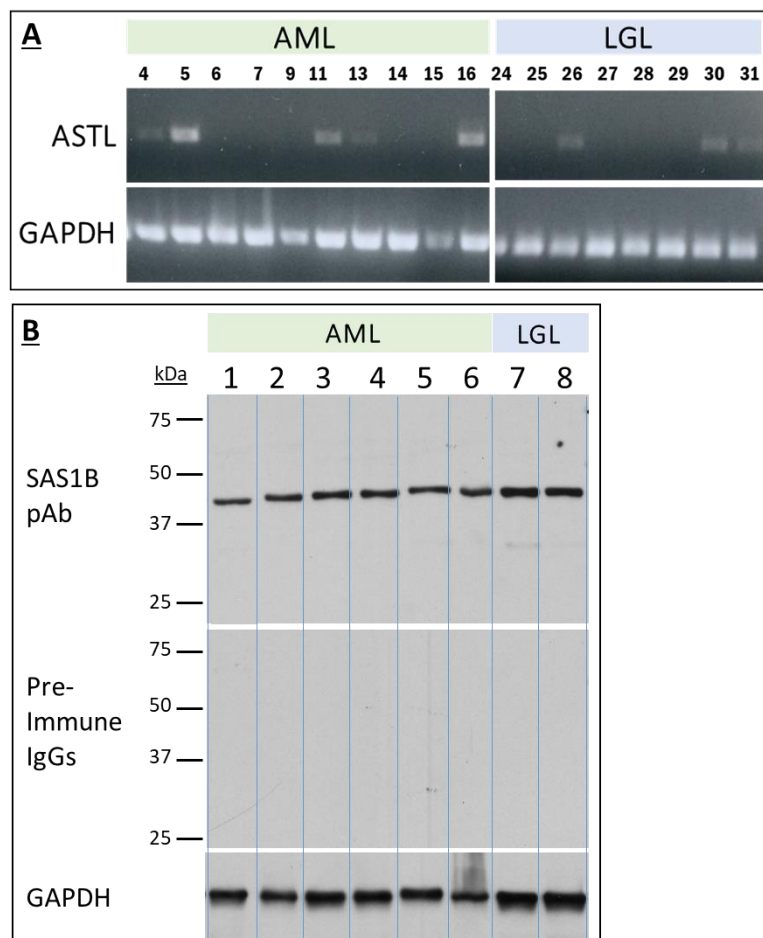


Figure 3.8 ASTL/SAS1B was expressed in leukemia patient samples and cell lines

[A] Representative RT-PCR analyses of leukemia samples from patients using a c-terminus ASTL specific primer set showed a 309bp amplicon in 32% (9/28) of leukemia samples. Of AML samples, 38% (5/13) were ASTL^{pos} while 27% (4/15) of LGL samples were ASTL^{pos}. GAPDH was used as a housekeeping control for PCR. [B] AML (# 1-6) and LGL (# 7-8) cell lines, analyzed by Western blot, all showed a 46 kDa immunoreactive band when probed with SAS1B pAb and no reactivity was seen when probed with pre-immune IgGs. GAPDH used as a loading control. Numbers correspond to the following cell lines: 1) HL60, 2) Kasumi-1, 3) KG-1, 4) OCI-AML2, 5) MOLM-13, 6) NKL, 7) TLG1.

Efficient ASTL amplification by PCR is hindered by ASTL RNA secondary structure

The faint bands observed in the PCR amplification of several leukemia samples (Figure 3.8A) prompted additional optimization to improve RT-PCR assay sensitivity. ASTL secondary structure predictions implicated RNA secondary structure as a barrier to efficient reverse transcription. Previous RT-PCRs for ASTL transcript in HNSCC and leukemia used a conventional reverse transcription approach. To improve sensitivity, 3' ASTL gene specific primers (GSPs) were used instead of oligodTs in the reverse transcription reaction and primer-RNA binding was enhanced by pre-incubating RNA with primer at 65°C to melt RNA secondary structure followed by cooling at a rate of 0.1°C/second to prevent secondary structure from snapping back before primers could bind. The effect of using GSPs or oligodTs on PCR amplification of ASTL was compared in three cell lines, SNU539, Cal27, and Panc366; a representative experiment using SNU539 is shown in Figure 3.9. RNA was reverse transcribed using one of two ASTL gene specific primers (GSP), a GAPDH GSP, or oligodTs. cDNA was qPCR amplified using three different primer sets: ASTL exons 2-3 (pink), ASTL exons 5-6 (blue), or GAPDH housekeeping control (orange); reverse primer is the same as used for reverse transcription reaction (Figure 3.9A). As indicated by the lower PCR C_q values (crossing point; cycle at which the relative fluorescent unit (RFU) crosses the threshold) for both ASTL primer sets using ASTL GSPs in the reverse transcription reaction as compared to oligodTs, ASTL PCR amplification was improved using GSPs. Using a GSP for GAPDH reverse transcription had no effect on the qPCR C_q value suggesting RNA secondary structure does not affect reverse transcription of GAPDH. These results indicate that ASTL RNA secondary structure prevents efficient reverse transcription, resulting in lower PCR

yield, and can be overcome using gene specific priming and enhancing primer-RNA binding by first melting RNA secondary structure.

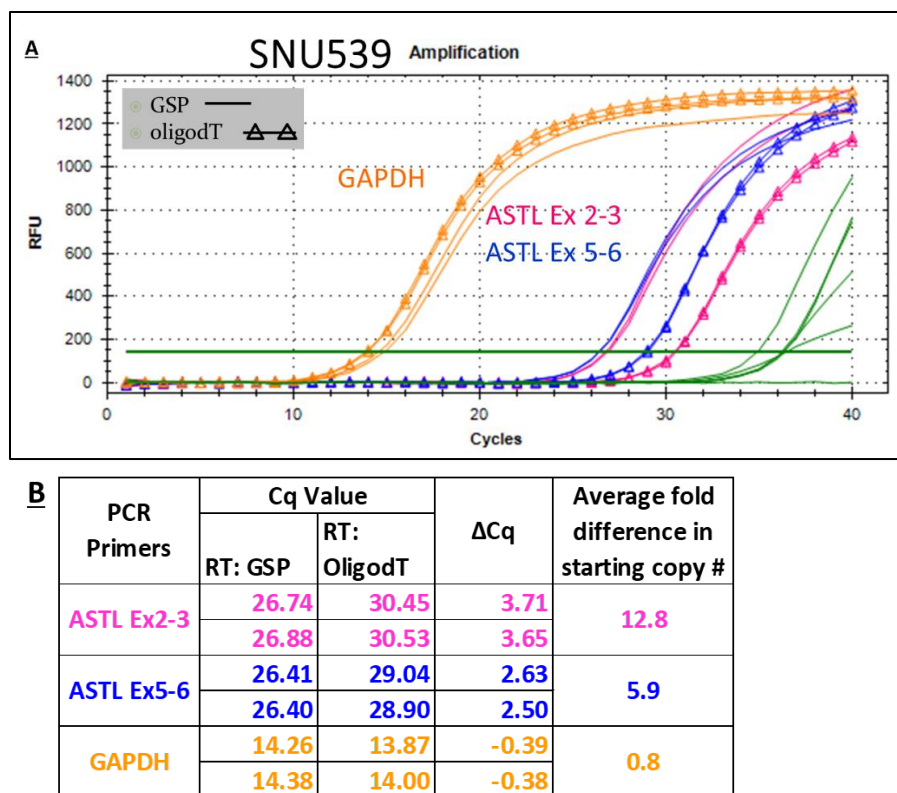


Figure 3.9 Improved RT-PCR amplification of ASTL

RNA from SNU539 cells was reverse transcribed to cDNA using either an ASTL gene specific primer or oligodTs; cDNA was then PCR amplified. [A] Semi quantitative RT-PCR amplification plot of ASTL exons 2-3 amplicon (pink), ASTL exons 5-6 amplicon (blue), housekeeping control GAPDH (orange), or no template negative control (green). PCR run in duplicates. Reverse transcription performed with either ASTL gene specific primers (GSP; straight line) or oligodTs (line with triangles). [B] Table reporting Cq values (crossing point; cycle at which the relative fluorescent unit (RFU) crosses the threshold) obtained from plot in A. Change in Cq values (oligodT – GSP) listed. Average fold difference in starting copy number indicate ASTL gene specific primed reverse transcription reaction resulted in more copies of ASTL cDNA in starting material for qPCR as compared to oligodTs.

Alternative splicing of ASTL results in at least six putative splice variants in cancer

ASTL/SAS1B expression has been demonstrated in several cancer types. Locational differences of SAS1B – cytoplasm and cell membrane – suggest alternative splicing of ASTL. We hypothesize that alternative splice variants of human ASTL/SAS1B are present in SAS1B^{pos} tumors and that the repertoire and/or levels of individual variants may differ between cancer types. Determining which isoforms are present at the cell surface will aid in development of targeted diagnostics and therapeutics such as production of cell surface SAS1B specific mAbs to be used in ADCs.

In a pilot experiment, PCR primers were designed to amplify full length SAS1B with the intent of discovering any additional splice variants such as insertion/deletion mutants which would be amplified with this primer set. An additional forward primer was designed based on an EST sequence, deposited into the NCBI's Unigene Database, from a uterine tumor which suggested a novel 5' translation start site within intron 1 for ASTL [42]. Two cell lines were analyzed: a HNSCC line, Cal27, and a malignant mixed Mullerian tumor (MMMT) line, SNU539. The Herr lab's initial studies into SAS1B and cancer were done with SNU539 as an *in vitro* model which has been characterized in [41]. Cytoplasmic RNA, representing the pool of mature mRNAs, was isolated from cell lines and was reverse transcribed to cDNA. PCR was performed using two primer sets: 1) forward primer spanning ASTL exon 1-2 (E1-2 For) + reverse primer located at the very 3' end of exon 9 (E9 Rev), and 2) forward primer beginning at novel ATG start site in intron 1 (I1 For) + E9 Rev. Products were run on a 1% agarose gel; bands were excised, purified, and amplicons were subcloned. Clones were nucleotide sequenced, blasted, and then compared to the ASTL reference sequence.

Five novel ASTL splice variants (SV-B to SV-F) were identified from the PCR screen; ASTL reference sequence was labeled as splice variant A (SV-A). SV-B, SV-E, and SV-F were identified using primer set 1 (E1-2 For + E9 Rev) while SV-C and SV-D were amplified using primer set 2 (I1 For + E9 Rev). A schematic representation of the exon structure of all splice variants is shown in Figure 3.10A. SV-A is a 9 exon, 431 amino acid protein with a predicted molecular weight of 46 kDa. SV-B is identical to SV-A except for a 54 basepair (bp) (18 amino acid) in-frame deletion from the 5' end of exon 8 – part of the proteinase domain. SV-E encodes a truncated version of SAS1B, predicted to produce a 12 kDa protein, which is lacking the majority of the proteinase domain, including the catalytic site, and the unique C-terminus. In SV-E, a 421bp sequence from intron 4 is not spliced resulting in new in-frame stop codon at the second codon in intron 4. Like SV-E, SV-F has the same 5' end as SV-A; however, exon 8 is deleted in SV-F causing a frameshift mutation resulting in an in-frame stop codon at amino acid position 8 in exon 9. SV-F is predicted to encode a 248 amino acid, 27 kDa protein. SV-C differs from SV-A at the 5' end. SV-C is missing exon 1 and has a novel start site within intron 1 resulting in addition of 21 amino acids from intron 1 added to exon 2, as compared to the reference sequence. The inserted intron 1 sequence gives SV-C/D a unique 21 amino acid N-terminus that differs from that found in SV-A/B/E/F. The new N-terminal sequence in SV-C/D is hydrophobic overall and amino acids 10-24 are predicted to encode an α -helical transmembrane domain. SV-C does not have the signal peptide found at the N-terminus in SV-A; SV-C also lacks a scission sequence typical of signal peptides and as seen in SV-A. SV-D has an identical 5' end as SV-C but contains the 85bp intron 7. An in-frame stop codon is present at the beginning of intron 8 thus the putative protein encoded by SV-D is

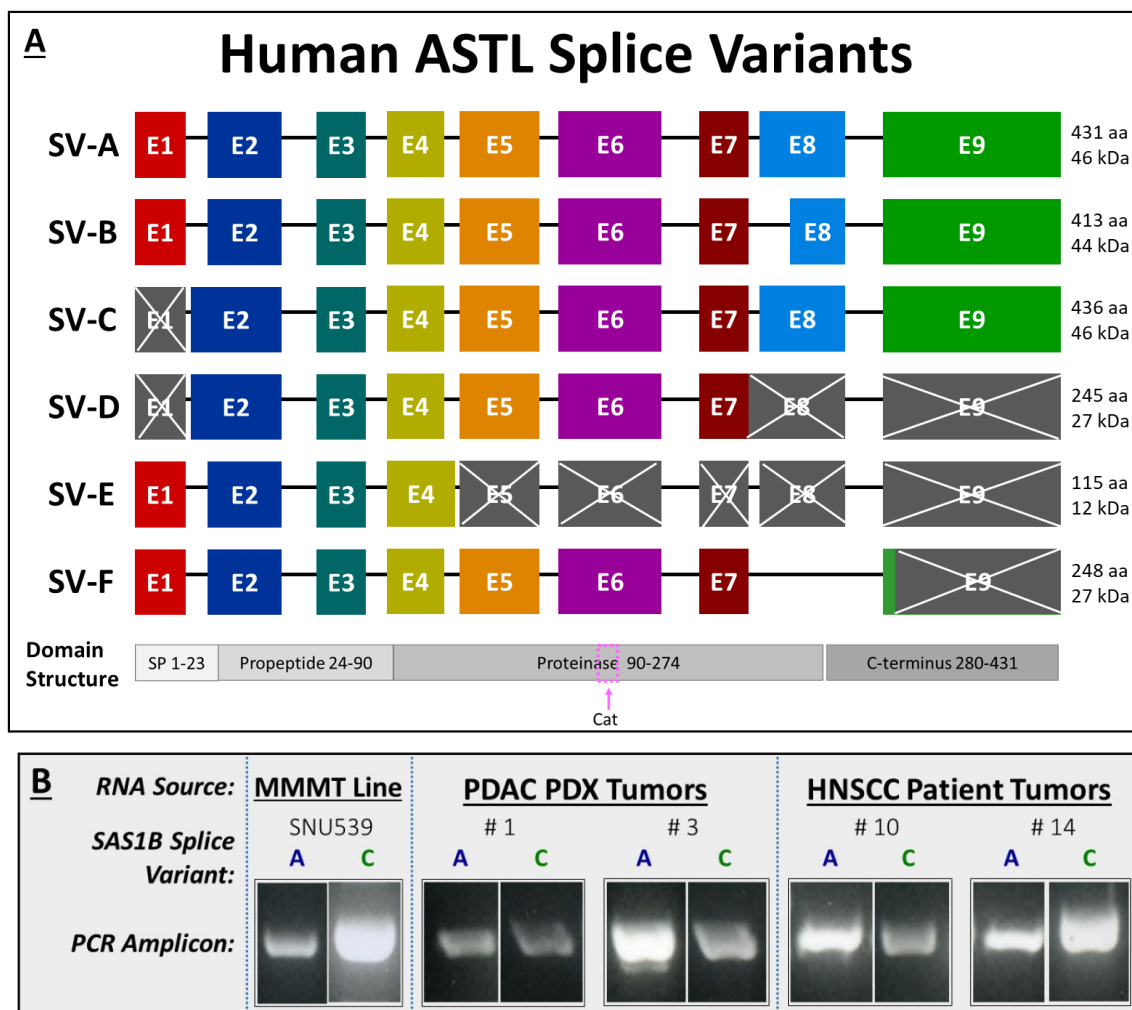


Figure 3.10 ASTL splice variants identified in cancer cells

[A] Exon structure schematic of ASTL splice variants known as SV-A to SV-F. Total number of amino acids and predicted molecular weight shown for each variant. Gray boxes with white X indicate regions which are not translated. For reference, SAS1B SB2 mAb, used extensively in our work, maps to amino acids 32-40 of the propeptide region. [B] Representative RT-PCR amplification of ASTL SV-A and SV-C, using variant specific primers, from a uterine cancer cell line (malignant mixed Mullerian tumor, MMT; SNU539), PDAC PDX tumors, and HNSCC tumors from patients. SAS1B domain

structure shown below variants with amino acid numbers listed for each domain; SP = signal peptide, Cat = catalytic site (pink box).

245 amino acids and 27 kDa. Of the known splice variants, SV-A and SV-C are predicted to be the major forms because 1) SV-A is the known reference sequence, 2) an EST of SV-C in uterine cancer was deposited into Unigene, and 3) SV-A and SV-C sequences were recovered with greater frequency than the others in our pilot PCR screen.

A preliminary PCR screen for SV-A and SV-C mRNA was done in PDAC PDX tumors and HNSCC patient tumors to confirm existence of variants in tumors in addition to previous data in cancer cell lines. ASTL SV-A and SV-C were both present in 2/2 PDAC PDX tumors and in 2/2 HNSCC patient tumors (Figure 3.10B). PCR gel bands were excised, purified, subcloned and then DNA sequenced. Clones matching SV-A and SV-C sequences were obtained from each respective PCR; SV-B sequences were also revealed from the SV-A PCR of PDAC PDX #3. Only a few clones were selected for sequencing thus reducing the likelihood of identifying the less-common variants in the selected tumors. Although not quantitative, intensity variation of PCR bands in Figure 3.10B suggest tumor specific differences in SV-A and SV-C transcript level. These preliminary screens suggest ASTL splice variants exist in cancers and there may be tumor specific transcript level variation among tumors.

To determine if the predominant ASTL variants, SV-A and SV-C, were translated into SAS1B protein isoforms, human SAS1B SV-A and SV-C constructs were transfected in an *in vitro* mammalian expression system using human embryonic kidney 293T cells (293T) (Figure 3.11; Experiments performed by Jagathalpa Shetty). Two SAS1B expression constructs were generated: 1) hSAS1B SV-A¹⁻⁴³¹ and 2) hSAS1B SV-C¹⁻⁴³⁶ (Figure 3.11A). DNA inserts were generated from PCR amplification of hSAS1B SV-A and SV-C from plasmids and were fused in-frame with pcDNA 3.1/V5-His TOPO TA

plasmid by topo-cloning. The vector carried a V5 epitope followed by a polyhistidine (6xHis) tag. The constructs were confirmed by PCR and DNA sequencing. Plasmids containing SV-A, SV-C, or no inserted DNA (mock/control) were transiently transfected into 293T cells. Total protein extracted from transfected cells was resolved on SDS-PAGE gels and Western blotted to confirm SAS1B protein translation (Figure 3.11B). Immunoblotting with anti-His antibody confirmed SV-A and SV-C protein translation occurred in transfected 293T cells as evidenced by immunoreactive bands at the predicted molecular weight (~52 kDa for SV-A and ~53 kDa for SV-C). Total protein from mock transfected 293T cells (control) was used as a negative control. No staining with control antibodies – normal mouse IgGs (Ms IgG) or mouse secondary antibody alone (Ms 2° only). SAS1B N-terminus mAbs (SB2, SB4, and SB5) recognized a band of the predicted molecular weight in both SV-A (~52 kDa) and SV-C (~53 kDa) transfected cell lysates, matching the staining pattern seen with anti-His. The anti-SAS1B pAb raised in rabbit (Rb pAb), previously discussed [38], also recognized the expected protein size for SV-A and SV-C. The Rb pAb recognized an additional protein band at ~42kDa which is hypothesized to be a recombinant protein breakdown product resulting from autoprolysis, which is known to occur in meprins and astacin [44]. These immunoblot results indicate that ASTL SV-A and SV-C mRNAs were translated into recombinant SAS1B proteins *in vitro* and demonstrate that the SAS1B antibodies, Rb pAb, SB2, SB4, and SB5 recognize recombinant SAS1B SV-A and SV-C proteins.

Indirect immunofluorescence was performed on 293T cells transfected with SV-A, SV-C or no DNA plasmid (mock/control) to determine cellular localization of SV-A and SV-C proteins (Figure 3.11C). SAS1B^{POS} cells were localized using the anti-V5 tag

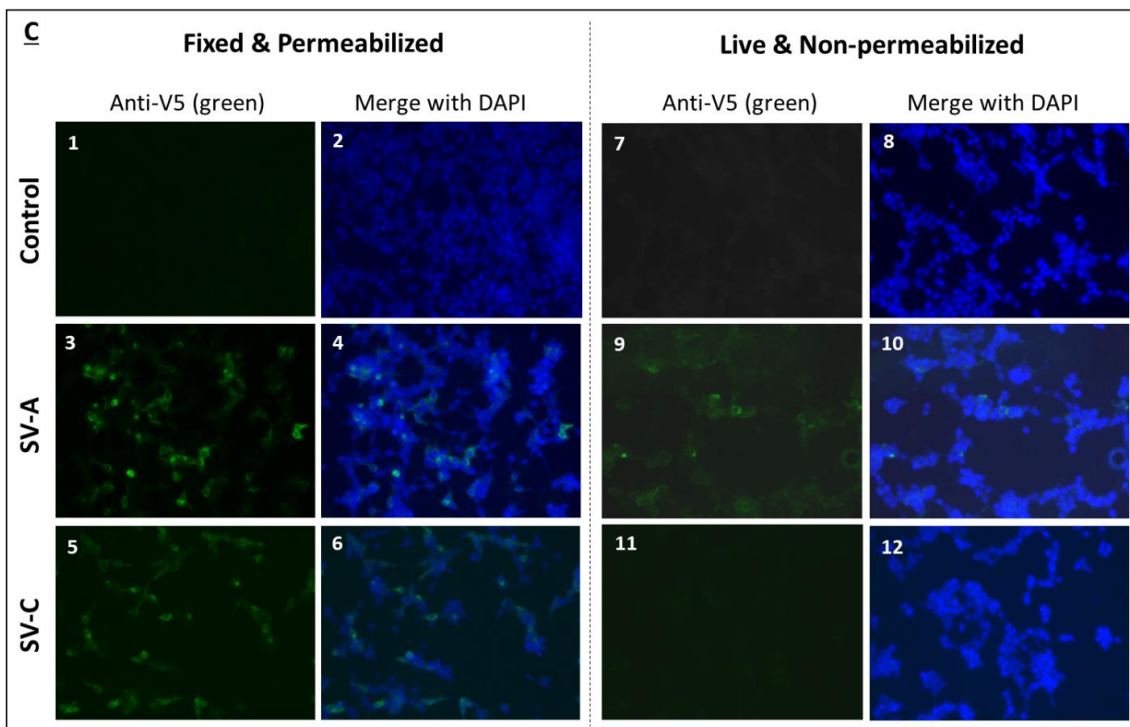
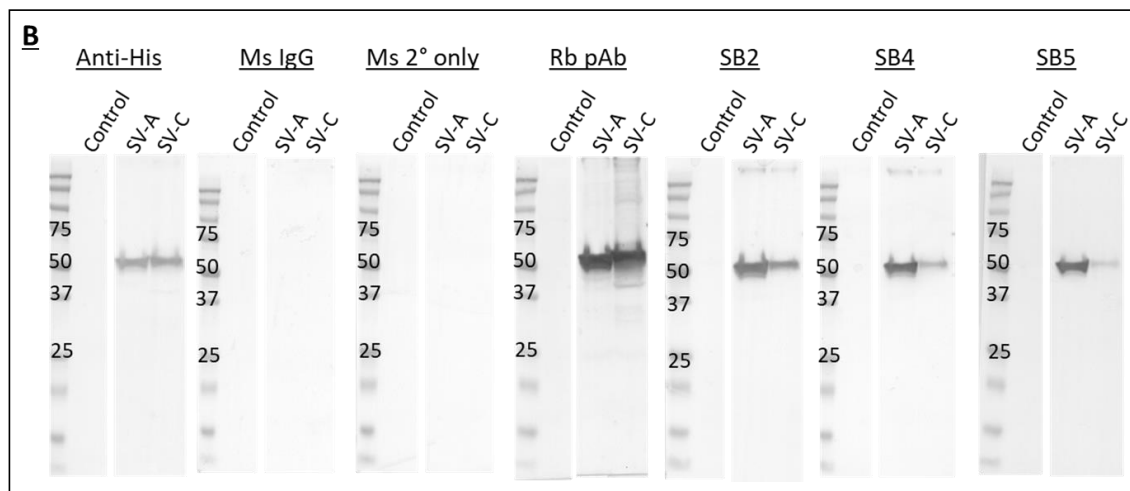
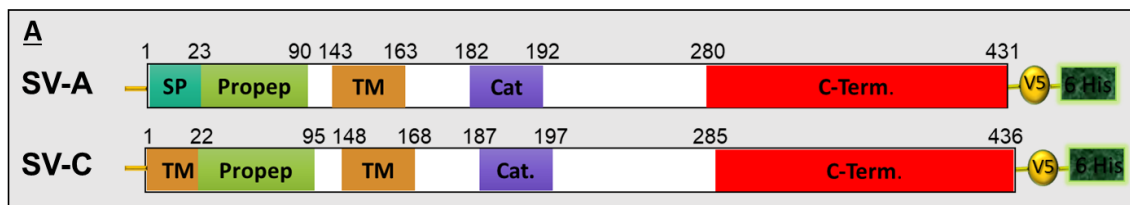


Figure 3.11 Transfection of 293T cells with ASTL SV-A and SV-C mammalian expression constructs resulted in expression of SAS1B proteins

[A] Structure of the protein domains for ASTL/SAS1B SV-A and SV-C plasmid DNA constructs used for transfection into 293T cells. [B] Total protein from transfected 293T cells were run on an SDS-PAGE gel and Western blotted using the following antibodies: anti-His, normal mouse IgGs (Ms IgG), secondary antibody only (Ms 2° only), SAS1B pAb raised in rabbit (Rb pAb), and SAS1B N-terminus mAb (SB2, SB4, SB5). Total protein from mock transfected 293T cells used as negative control cell population (control). Transfected SV-A and SV-C proteins migrated at the predicted molecular weight (~52 kDa) as seen when probed with anti-His; SAS1B antibodies (Rb pAb, SB2, SB4, and SB5) also recognized the same molecular weight band. Molecular weight markers listed in far left lane for each blot (kDa). [C] IIF on 293T cells transfected with SV-A construct, SV-C construct, or mock transfection plasmid (control). Cells probed with anti-V5 tag antibody (green) and DAPI nuclear stain (blue). SV-A and SV-C proteins localized to the cytoplasm in fixed and permeabilized IIF (Panels 3-4 and 5-6, respectively). SV-A localized to the plasma cell membrane in live and non-permeabilized IIF (Panels 9-10) while SV-C was not detected (Panels 11-12). No signal observed in mock transfected cells (Panels 1-2, 7-8). Images are 10x magnification. (Experiments performed by Jagathalpa Shetty)

antibody (green); nuclei were stained with DAPI (blue). SV-A and SV-C proteins localized to the cytoplasm of 293T cells in fixed and permeabilized IIF (Figure 3.11C panels 3-4 and 5-6, respectively). SV-A localized to the plasma cell membrane in live and non-permeabilized IIF (Figure 3.11C panels 9-10) while SV-C was not detected using the V5 tag antibody (Figure 3.11C panels 11-12). Lack of live cell signal in SV-C transfected cells may be because: 1) SV-C is not trafficked to the cell membrane, 2) SV-C is located at the cell membrane but the C-terminus, which contains the V5 tag, is located intracellularly or 3) SV-C localizes to the cell membrane with an extracellular C-terminus which is not accessible for antibody binding due to protein folding. No immunoreactivity was observed in mock transfected cells (Figure 3.11C, panels 1-2, 7-8). These results show that SAS1B SV-A and SV-C protein isoforms both localized to the cytoplasm while only SV-A was detected at the cell membrane. Taken together, preliminary results indicate ASTL is alternatively spliced and at least some splice variants are translated into SAS1B protein isoforms which appear to differ in cellular localization.

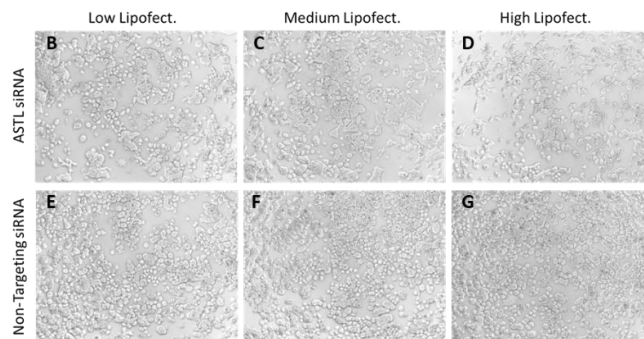
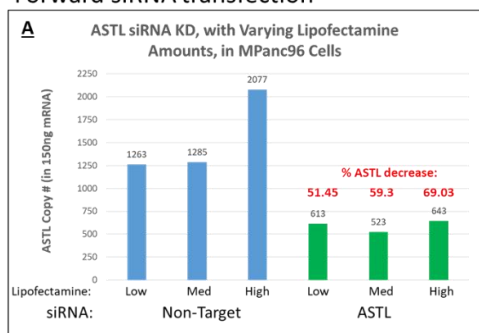
siASTL knock-down in mPanc96 cells appears to reduce total cell number

With the intention of creating an ASTL/SAS1B knock-down cancer cell line to use as an important negative control for a variety of assays including Western blot, IIF, and cytotoxicity, small interfering RNA (siRNA) targeting ASTL was transiently transfected into the mPanc96 cell line. siRNA is a type of RNA interference (RNAi) which selectively targets a particular mRNA for degradation, essentially blocking further protein expression [121]. In an attempt to optimize the protocol, three different concentrations of the transfection reagent, lipofectamine, were used (low, medium, and high as according to the

manufacturer's suggestions) and forward or reverse transfection was performed (Figure 3.12). In forward transfection, mPanc96 cells were plated on day 0 and transfection occurred on day 1 whereas in reverse transfection, transfection occurred at the time of cell plating (day 1). In both cases, cells were harvested after 72 hours of transfection. RT-qPCR was performed on RNA harvested from transfected mPanc96 cells; ASTL copy number was ascertained using a standard curve generated from qPCR of serial dilutions of an ASTL plasmid. Percent ASTL decrease was determined by comparing ASTL copy number in cells that received siASTL to cells which received siNon-targeting (Figure 3.12 A/H). Bright field images were captured prior to RNA harvest (Figure 3.12 B-G, I-N). Lipofectamine concentration did not appear to affect efficiency of transfection or ASTL copy number (Figure 3.12 A/H). Forward or reverse siASTL transfection produced similar ASTL knockdown effects – a 60% ASTL decrease for forward transfection and 48% ASTL decrease in reverse transfected cells (Figure 3.12 A/H). Qualitatively, a slight reduction in cell number was observed when mPanc96 cells were forward transfected with siASTL as compared to the siNon-targeting control (Figure 3.12 B-D vs. E-G). A more pronounced reduction of cell number was observed when cells were reverse transfected with siASTL (Figure 3.12 I-K vs. L-N). Reverse siASTL transfected cells also appeared different morphologically with elongated cell bodies and less cell clustering (Figure 3.12 I-K). These initial observations suggest siASTL transfection may be cytotoxic to mPanc96 cells since cytotoxic effects were not observed in the siNon-targeting control. Cytotoxic effects of siASTL appear to be more pronounced when siRNA is added to cells at the time of plating rather than allowing cells to spread for 1 day before transfection. Importantly, additional experiments with all proper controls are necessary to determine whether the

observed cytotoxic effects are true or are a result of lack of proper experimental optimization. If subsequent experiments prove SAS1B knock-out is lethal to cancer cells, we may speculate that, and further investigate if, SAS1B is involved in signaling pathways that regulate and/or contribute to cell viability and/or cell death.

Forward siRNA transfection



Reverse siRNA transfection

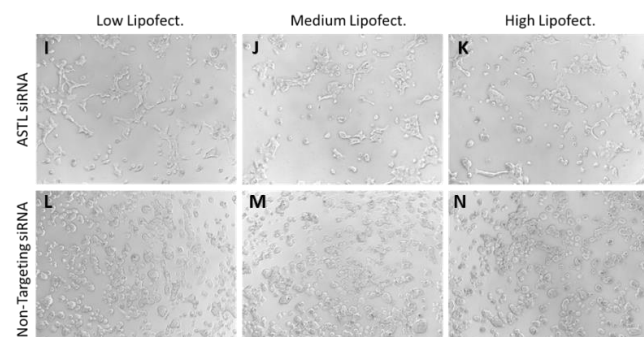
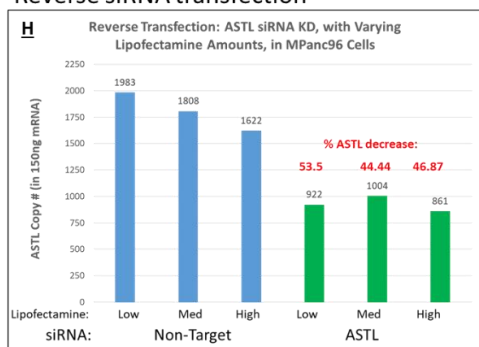


Figure 3.12 siASTL knock-down in mPanc96 cells reduced total cell number

mPanc96 cells transfected with siASTL or siNon-targeting with varying concentrations of transfection reagent (Lipofectamine) for 72 hours. [A-G] Forward transfection: cells plated on day 0 and transfected on day 1. [A] Quantification of ASTL copy number by qPCR; siASTL decreased ASTL copy number by an average of 60% as compared to the non-targeting siRNA group. [B-G] Total cell number appears to be slightly reduced across all lipofectamine concentrations as compared to non-targeting siRNA in [E-G]. [H-N] Reverse transfection: transfection at time of cell plating (day 1). [H] siASTL decreased ASTL copy number by an average of 48% as compared to non-targeting siRNA group. [I-K] Total cell number appears to be reduced across all lipofectamine concentrations as compared to control in [L-N]. Morphology of siASTL treated cells appears different than control siRNA treated cells – cells appear elongated and more likely to grow as single cells in siASTL. Brightfield images: 10x magnification.

DISCUSSION

Some non-neoplastic cells may express SAS1B: Implications for SAS1B Targeted Immunotherapies

Although several lines of evidence indicate SAS1B is undetectable in panels of normal tissues from both mouse and human [37, 38, 41], some recent contradictory data has emerged suggesting expression of ASTL/SAS1B in non-neoplastic cells. Understanding the complete expression profile of ASTL/SAS1B among normal human tissues is essential for development of clinically useful SAS1B targeted therapies. RNA sequencing data from the GTEx database indicates ASTL transcript in a few normal cell types including bladder, whole blood, skin, and spleen (Figure 3.1). Presence of ASTL transcript in normal cells only becomes a potential problem for SAS1B targeted therapies like ADCs, CAR-T, or cancer vaccination if protein translation occurs. Intracellular staining of human PBMCs from whole blood, with a SAS1B mAb, confirms ASTL translation occurs in one of the tissues identified as ASTL^{POS} by GTEx. A pilot experiment assessing SAS1B expression in human PBMCs by flow cytometry showed a small but consistent population of SAS1B^{POS} cells (Figure 3.2). However, SAS1B expression was only detected in fixed and permeabilized PBMCs, indicating intracellular SAS1B localization, but was not detected in live, non-permeabilized cells, suggesting no cell surface SAS1B expression.

Because this small SAS1B^{POS} population of PBMCs existed in a majority of samples analyzed (n=4), we reasoned that SAS1B expression is specific to a small subset of leukocytes. Dendritic cells were suggested as a potential source of SAS1B^{POS} PBMCs as they account for only 1-2 % of PBMCs [122]. Readily available mouse splenocytes, which

were then used to analyze leukocyte subpopulation(s), showed similar results – about 2% of splenocytes expressed intracellular SAS1B with no detectable cell surface SAS1B expression (Figure 3.3 A/D). As predicted, cytoplasmic SAS1B expression was observed in 40% of murine dendritic cells by flow cytometry (Figure 3.3 B). Additionally, while only 1% of B cells were SAS1B^{POS}, of the total 2% SAS1B^{POS} splenocyte population, 25% were B cells (Figure 3.3 B-C). Similar experiments need to be repeated in human samples. Analysis of SAS1B expression in various specific leukocyte sub-types from multiple human PBMC samples by flow cytometry will provide a validated and more thorough understanding of SAS1B expression among PBMCs.

In addition to SAS1B expression in human PBMCs from normal donors, keratinocytes showed both cytoplasmic and cell surface SAS1B expression by flow cytometry (Figure 2.5A) and pancreas stromal cells also showed some cytoplasmic SAS1B expression by IHC (Figure 2.2). Despite cell surface SAS1B expression, a SAS1B-ADC was not cytotoxic to keratinocytes (Figure 2.5 B) suggesting non-neoplastic, SAS1B^{POS} cells are not sensitive to a SAS1B-ADC. As previously discussed (Chapter 2, Discussion), lack of SAS1B-ADC cytotoxicity in keratinocytes may be due lack of internalization and/or differences in isoform expression. Whether stromal cells express cell surface SAS1B remains unknown; but, even if non-neoplastic stromal cells do express surface SAS1B, they may also be insensitive to a SAS1B-ADC. Analysis of stroma from other malignancies is needed to determine if SAS1B^{POS} stroma is associated with additional cancer types or if it is specific to the pancreas. Despite these preliminary results contradicting previous reports showing no SAS1B detection in normal tissues, clinical utility of a SAS1B ADC or CAR-T has not yet been disqualified.

While the success of both ADCs and CAR-Ts depend on target specificity, ADC targets must be internalized into the cell while CAR-T cytotoxicity is independent of target internalization. SAS1B^{POS} cells which do not internalize cell surface SAS1B theoretically will not take up an ADC and will therefore remain insensitive to the cytotoxic effects of an ADC. Because CAR-T therapy does not depend on target internalization therefore on-target, off-tumor cytotoxicity may occur in the skin of patients treated with a SAS1B CAR-T. However, a more thorough assessment of SAS1B expression in keratinocytes, as well as other potential SAS1B^{POS} normal cells, is first necessary. The keratinocytes used in our work were from newborn foreskin from one individual; we suggest screening a larger cohort including adults for cell surface localization of SAS1B by flow cytometry. Of interest, for CAR-T development, will be the percent of cells expressing SAS1B; potential toxicity would theoretically be worse if 95% of cells expressed the target as opposed to only 10%. There may be a threshold off-tumor skin cytotoxicity that patients can endure so the observation of cell surface SAS1B expression in keratinocytes still does not preclude this theoretical therapy from use. For ADC treatment, it will be critical to determine whether lack of endocytosis is the reason for no observed cytotoxicity in SAS1B-ADC treated keratinocytes; this can be accomplished by live cell immunofluorescence using the SAS1B mAb, SB2. Keratinocytes co-stained SAS1B and endosomal pathway markers (e.g. with green and red fluorescent label, respectively) and monitored over time by video microscopy. If SAS1B is endocytosed, a yellow color produced from green and red overlap, will be evident; if SAS1B is not endocytosed, no green signal will be observed intracellularly. Normal cells which express cell surface SAS1B pose a potential problem for CAR-Ts and also to ADCs if they are internalized. Whether or not potential on-target,

off-tumor cytotoxic effects could be countered by additional treatment or if toxicity would be intolerable in patients remains to be seen.

Multiple approaches should be employed to confirm SAS1B expression and cellular localization in potentially SAS1B^{POS} normal cell types. In addition to flow cytometry, another approach to determine if SAS1B localizes to the cell surface would be to use the biotin-avidin system to biotinylated cell surface proteins. Proteins are recovered using avidin and subsequently analyzed by Western blot. Subcellular, or phase, partitioning of cell lysates followed by immunoblotting may also yield information about cellular localization of SAS1B as cytoplasmic and membrane forms will be present in separate fractions. Once we understand which specific populations of normal cells express SAS1B, we can consider ways to treat any potential off-tumor, on-target toxicity that may be associated with an ADC or CAR-T. Ultimately, administering potential SAS1B ADCs or CAR-Ts in murine models *in vivo* will be of great benefit to see how well SAS1B targeted immunotherapies are tolerated and to what extent off-tumor toxicity occurs.

Normal cells that express only cytoplasmic forms of SAS1B pose much less of a challenge to development of SAS1B based ADCs and CAR-Ts. Lack of cell surface antigen will, in theory, prevent both ADCs and CAR-Ts from binding to the surface of cells which express only cytoplasmic forms of SAS1B, such as dendritic cells or B cells. However, if follow-up experiments determine that a SAS1B cell surface population exists in some leukocytes, there still may be ways in which ADCs and/or CAR-Ts can still be useful, depending on the pattern of SAS1B expression. For example, as discussed in Chapter 1, CD19 is targeted by CAR-T for the treatment of CD19^{POS} lymphoma/leukemia but is also expressed by non-neoplastic B cells. Cytotoxicity to B cells is countered by

giving patients immunoglobulin (IgG) infusions concurrent with treatment. IgG treatment may also benefit patients treated with a SAS1B CAR-T therapy as a small subset of B cells has been shown to express SAS1B. Follow up studies using flow cytometry to analyze human PBMCs with B cell subpopulation markers will help identify the specific type of B cells that may express SAS1B. Preliminary studies suggest a very small portion of B cells express SAS1B, only about 1% (Figure 3.3B); cytotoxicity to this small population may be tolerated by patients. On the other hand, a much higher proportion, 40%, of dendritic cells were SAS1B^{pos} (Figure 3.3B). If subsequent studies with more samples confirm these initial findings and show that there is a population of cell surface SAS1B in dendritic cells, we may consider ways to increase dendritic cell population in SAS1B-immunotherapy treated patients.

Dendritic cells are professional antigen presenting cells which play an essential role in both innate and acquired immunity and are thus vital to proper immune system functioning [123]. Multiple studies have shown that autologous dendritic cells can be cultured *ex vivo* and transferred back to a patient [124-126]. One potential way to counter side effects of dendritic cell cytotoxicity, which would likely cause serious immunodeficiency, associated with SAS1B targeted ADC or CAR-T therapy may be to propagate SAS1B^{neg} autologous dendritic cells *ex vivo* then administer back to patients. While our current data suggests only intracellular SAS1B localization in dendritic and B cells, which theoretically shouldn't be a problem for ADCs or CAR-Ts targeting SAS1B, potential cytotoxicity of these cell populations may be countered by administration of SAS1B^{neg} dendritic cells and immunoglobulin. A more thorough understanding of SAS1B expression in immune cells, as well as in keratinocytes, bladder, and any other potential

SAS1B^{POS} tissues, is critical to development of SAS1B immunotherapies to be used in the treatment of SAS1B^{POS} cancers.

Multiple cancer types express ASTL/SAS1B

To expand the potential impact of therapies targeting SAS1B, it is crucial to understand which cancer types are SAS1B^{POS} and the SAS1B expression patterns within each cancer type. In addition to female reproductive and pancreatic cancers, ASTL/SAS1B was detected in 100% of HNSCCs (Figure 3.4) and 32% of leukemia samples (AML and LGL specifically) (Figure 3.8A) from patients. SAS1B expression in leukemia indicates that SAS1B expression is neither specific to solid tumors nor is it specific to cancers of epithelial origin (carcinomas), as leukemia arises from hematopoietic cells.

All HNSCC (n=8) and leukemia (n=8) cell lines surveyed expressed SAS1B (Figures 3.5 and 3.8B, respectively), providing a way to study cellular localization of SAS1B and effects of anti-SAS1B therapeutics *in vitro*. IIF on the HNSCC cell line, OSC-19, showed that SAS1B localized to the cytoplasm and to the plasma membrane (Figure 3.7) providing rationale for the hypothesis that a SAS1B-ADC will be cytotoxic to SAS1B^{POS} HNSCC cells. SAS1B expression appeared to be concentrated in the perinuclear region on OSC-19 cells (Figure 3.7B), likely to be due to association with the ER and Golgi. In contrast, the pattern of SAS1B expression in live OSC-19 cells was punctate across the entire cell surface (Figure 3.7D). The vast majority of OSC-19 cells were SAS1B^{POS} by both fixed/permeabilized and live/non-permeabilized IIF. While the pattern of SAS1B expression by IIF in OSC-19 cells, using SB2 mAb, was similar to the pattern

observed in PDAC cell lines (Figures 3.7 and 2.4), qualitatively, the cell surface SAS1B signal intensity appeared relatively stronger in OSC-19 cells (Figure 2.4E-G vs. Figure 3.7D). Based on this observation, we predict the anti-SAS1B SB2-ADC may induce *in vitro* cytotoxic effects at a lower LD₅₀ and/or in a great proportion of HNSCC cells, as compared to PDAC cells. Reasons for potential quantitative differences in SAS1B expression among cancer types have yet to be determined but may be related to the functional role of SAS1B or transcription/translation regulation differences. These results validate additional studies in HNSCC and leukemia to assess the cytotoxic potential of anti-SAS1B therapies, such as using a SAS1B-ADC as previously described in a PDAC *in vitro* system (Figure 2.5).

Although most patients diagnosed with AML are past reproductive age, some AML diagnoses are made in children and teens. We suspect other types of leukemia to be SAS1B^{POS} as well based on the observation of SAS1B expression in AML and LGL leukemia as well as in a fraction of normal dendritic and B cells, of myeloid and lymphoid lineages, respectively. This includes the most common form of childhood leukemia, acute lymphocytic leukemia (ALL); the observation of SAS1B^{POS} B cells (derived from lymphocytes) supports the prediction that at least some ALL samples will be SAS1B^{POS}. SAS1B-ADC therapy would be particularly advantageous for female patients who are at or below reproductive age. Common cancer therapeutics (e.g. chemo- and radio-therapy) can be particularly harmful to children in terms of future reproductive potential. A SAS1B-ADC therapy may result in on-target/off-tumor effects on the population of growing oocytes within the ovary but would not harm the pool of primordial follicles; thus, fertility could be restored in female cancer patients after cessation of treatment. An important next

step will be to screen various other types of childhood cancers (e.g. neuroblastoma and lymphoma) in addition to cancers typically arising in patients past reproductive years.

Although results are preliminary and need to be confirmed, PCR and Western blot analyses from small cohorts suggest ASTL/SAS1B may be expressed in additional cancers including renal clear cell carcinoma, breast cancer, and melanoma (data not shown). Because PCR (Figure 3.9) and IHC assays have been optimized to detect ASTL/SAS1B with greater sensitivity since some of the preliminary screening experiments were performed, we expect that some initial incidence results to increase (e.g. leukemia) if re-screened with newer, more sensitive assay protocols. We also predict that more cancer types are SAS1B^{POS} and suggest a larger effort focused on understanding the incidence and expression of SAS1B in larger cohorts of many tumor types; this will be vital to determine which patients may benefit from a targeted therapy to SAS1B. One approach to efficiently screen larger cohorts of tumors is to stain TMAs for SAS1B by IHC. However, this approach is currently limited by the SAS1B mAb, 6B1, used for screening as this mAb preferentially recognizes cytoplasmic SAS1B as compared to cell surface SAS1B (Supplemental Figure 2.1; experiment performed by Eusebio Pires); data generated would not indicate which patients may respond to a SAS1B-ADC. Epitope mapping of the 6B1 mAb could offer clues into SAS1B isoform localization. If we consider ASTL SV-A (predicted cell surface form) and SV-C (predicted cytoplasmic form), while 6B1 may map to the unique N-terminal region of SV-C, it may also map to a shared, inaccessible epitope in SV-A as a result of potential conformational differences of SV-A and SV-C. Regardless, additional methods and/or molecular tools (e.g. antibodies) are necessary for screening larger cohorts of patients for cell surface SAS1B expression.

Western blotting could potentially be used as a SAS1B/cancer screening method after additional studies are performed to determine precisely which immunoreactive bands are SAS1B. Preliminary SAS1B Western blot screens in HNSCC (Figures 3.4B and 3.5B) and leukemia (Figure 3.8B) were done using the anti-SAS1B rabbit polyclonal antibody (Rb pAb). Although this antibody has been previously validated by mass spectrometry as recognizing SAS1B [41], it remains unclear which immunoreactive bands are SAS1B; a major band is observed at ~65 kDa and a doublet at ~46/48 kDa. The predicted molecular weight of SAS1B is 46 kDa, however, that does not factor any post translational modifications that may increase the molecular weight of the protein. The higher molecular weight bands observed in HNSCC samples (Figures 3.4B and 3.5B) and in renal clear cell carcinoma (same pattern as HNSCC; data not shown) could be: 1) unidentified protein isoforms, 2) cross-reactive protein(s), or 3) a result of post translational modifications. A comprehensive study of the ASTL splice variants and SAS1B isoforms, as described below, will indicate if any variants exist with higher predicted molecular weights. Specificity of the antibody can be determined by making a SAS1B knock-out/down in a cancer cell line then doing the Western blot to compare wild type vs. knock down cells; bands which are truly SAS1B should disappear when SAS1B is knocked-out *in vitro*. Post translational modifications may also result in increased protein molecular weight.

Glycosylation, the attachment of saccharide moieties to proteins, is a common post-translational modification which can add significant molecular weight to a molecule. Most plasma membrane and secretory proteins contain one or more carbohydrate chains whereas cytosolic and nuclear proteins are usually not glycosylated. Oligosaccharides attached to glycoproteins may have a variety of functions including assisting in proper protein folding,

protection from proteolysis, cell-cell adhesion, and signal transduction [127, 128]. Meprins, the closest astacin family member to SAS1B, are extensively glycosylated with ~25% of the total molecular mass attributed to carbohydrate [129, 130]. N-linked and O-linked are the two most common forms of glycosylation [128], both of which are present in meprins. N-linked glycoproteins can have large and extensively branched glycans whereas O-linked glycans usually have simpler oligosaccharide structures. N-linked glycosylation is important for proper folding, processing, and secretion of proteins from the ER and the Golgi [128]. Multiple glycosylation prediction algorithms predict one to three potential N-linked glycosylation sites in SAS1B within the proteinase domain. SAS1B is also predicted to be heavily O-glycosylated with, 19 to 38 predicted glycosylation sites based on analysis from three different glycosylation prediction programs. The majority of the predicted glycosylation sites reside the unique C-terminal region which distinguishes SAS1B from all other human metalloproteases. Given the extensive roles that glycans are known to play, it is reasonable to suggest that these glycans may be contributing to the unique activity of SAS1B.

It is also likely that SAS1B protein isoforms with different cellular localization and/or functions may be differently glycosylated. For example, meprin- β , which is an integral membrane form, is heavily O-glycosylated whereas the secreted meprin- α does not have O-linked oligosaccharides [130]. Different glycans also confer distinct functional differences in meprins; N-linked oligosaccharides in meprin- α is important for secretion and enzymatic activity whereas O-linked glycans in meprin- β offer protection from proteolytic cleavage [129, 130]. Based on the predicted glycosylation status of SAS1B and meprins being heavily glycosylated, we hypothesize that addition of sugar moieties to

SAS1B may account for the observed immunoreactive bands on Western blot which run at a higher molecular weight than predicted based on the amino acid sequence.

Additional studies are required to determine if SAS1B is glycosylated and if so, how glycosylation affects molecular weight and potential SAS1B protein localization and functional differences. Differences in SAS1B glycosylation may exist between neoplastic and normal (e.g. oocytes) SAS1B^{POS} cells given that aberrant glycosylation is considered a hallmark of cancer and is thought to have an important role in neoplastic progression [131]. Furthermore, protein glycosylation may vary between cancer types. Because glycans can significantly impact the molecular composition of a glycoprotein, changes in glycosylation can cause functional modifications as a result of differences in charge and conformation of a protein [131]. To test whether SAS1B has N-linked and/or O-linked glycosylations as predicted, cell protein lysates can be treated with specific glycosidases to remove glycans. Protein separation by SDS-PAGE gel electrophoresis followed by detection by western blot using SAS1B mAbs is used to observe potential molecular size changes between glycosidase treated and untreated cells. A glycoproteomic approach could also be employed where glycoproteins which have and have not received glycosidase treatment are analyzed by liquid chromatography and tandem mass spectrometry (LC-MS/MS) and compared. Results from these studies will also have implications for theranostic SAS1B antibody production as alterations to glycans, which reside on the protein surface, may impact antibody binding and should thus be considered. Potential SAS1B glycosylation differences between normal and cancer cells offers an additional targeting strategy given that, although challenging, antibodies can be developed which target specific glycan sequences.

Unlike Western blot analysis of HNSCCs, which shows 2 immunoreactive bands which run at higher-than-predicted molecular sizes (Figure 3.4B and 3.5B), only one main immunoreactive band at the predicted molecular weight (46 kDa) was observed in leukemia samples (Figure 3.8B). Although additional studies are needed to confirm these data, this observation suggests leukemias may have a different repertoire of SAS1B protein isoforms and/or differences in glycosylation as compared to the solid tumors analyzed thus far. If the higher immunoreactive bands observed in HNSCC Western blotting are due to glycosylation, it may be that leukemia primarily expresses non-glycosylated, cytosolic or secreted form(s) of SAS1B. Differences in SAS1B isoform expression between solid and liquid tumors may be related to the inherent metastatic differences between these groups of cancers. Leukemia, unlike solid cancers, may be considered inherently metastatic due to the characteristic cell motility of leukocytes. Conversely, carcinomas must acquire anchorage independent growth in order to intravastate into circulation and extravasate at a distant site. It may be postulated then, that the potential contribution of cell surface localized SAS1B to metastasis via degradation of the ECM in solid tumors, may not be necessary or advantageous for leukemia progression [132]. The suggestion that solid tumors, which are anchorage dependent, expresses glycosylated, cell surface localized SAS1B whereas liquid tumors, which are anchorage independent, express non-glycosylated cytoplasmic or secreted SAS1B, is supported by two observations in normal cells: 1) keratinocytes express cell surface SAS1B (Figure 2.5) and 2) dendritic and B cells express intracellular, but not surface localized SAS1B (Figure 3.3).

Although lack of membrane-associated forms of SAS1B would preclude SAS1B-ADC or CAR-T treatment for leukemia, other types of SAS1B based immunotherapies,

such as vaccination, may still be an option. However, successful vaccination relies on the target, SAS1B, being specific to cancer cells, of which a better understanding is first required. Determining the range of protein isoforms expressed in various cancers and glycosylation status of SAS1B will help direct development and utility of anti-SAS1B therapies.

Alternative splicing of ASTL results in multiple ASTL splice variants encoding unique SAS1B protein isoforms

Preliminary PCR screens, which identified five putative unique ASTL splice variants (SV-B to SV-F) in addition to the reference sequence (SV-A) in the uterine cancer cell line, SNU539 and HNSCC cell line, Cal27 (Figure 3.10A), suggest that ASTL is alternatively spliced. Variants A-D have also been identified by PCR in PDAC PDX tumors and HNSCC patient tumors (Figure 3.10B) suggesting variants were not cell line or cancer-type specific. Transfection studies in 293T studies using full length SV-A and SV-C constructs demonstrate that these variants were translated into SAS1B protein isoforms (Figure 3.11) suggesting existence of SAS1B protein heterogeneity.

Early efforts were focused on determining differences between the 2 groups of predicted isoforms, SV-A/B/E/F versus SV-C/D, which differ at the N-terminus. The SV-A group has a classical signal peptide encoded by exon 1 and contains a canonical scission sequence which is predicted to be cleaved during processing. Signal peptides, which are found in membrane-associated and secreted proteins, dictate protein translation by ribosomes that are associated with the membrane of the rough endoplasmic reticulum

(RER) and then trafficking through the secretory pathway. In most cases, proteins that do not have signal peptides are translated by ribosomes free in the cytosol and remain as cytosolic proteins [133]. In contrast to SV-A, the SV-C group N-terminal domain encoded in intron 1 does not contain the typical signal peptide with a cleavage sequence, present in SV-A, and is thus predicted to persist in each SAS1B protein encoded by SV-C/D. Although SV-C does not have a predicted typical signal peptide with cleavage site, the 21 amino acid sequence from intron 1 is generally hydrophobic and contains a predicted α -helical domain, which are features of a transmembrane domain. Bioinformatics analysis, combined with the IIF data showing cytoplasmic but not cell surface localization of SV-C in transfected 293T cells (Figure 3.11C panels 9-10), offers two possibilities: 1) the putative transmembrane-like domain at the N-terminus of SV-C acts as a non-cleaved signal peptide directing secretion of SV-C, or 2) absence of classical signal peptide or defined transmembrane domain results in cytosolic localization of SV-C. These initial studies propose multiple ASTL splice variants and SAS1B protein isoforms exist and suggest therapeutic and diagnostic value in identifying which isoforms are targetable, as described in Chapter 4.

The search for an ASTL/SAS1B negative cell line

We attempted to make an ASTL/SAS1B knock-down line after a search for an ASTL/SAS1B negative cell line to use as a negative control in various assays was unsuccessful. All immortalized and transformed cancer cell lines examined were ASTL and/or SAS1B positive depending on which assay was used for the initial assessment. Non-transformed, non-cancerous cell lines which had been immortalized were also

ASTL/SAS1B positive (e.g. HEK-293, mouse 3T3 fibroblasts, human pancreatic stellate cells, normal immortalized keratinocytes; data not shown). These observations suggest that ASTL/SAS1B expression *in vitro* may be related to immortalization and transformation; however, it is unclear if ASTL/SAS1B expression is a passenger during global mutation acquisition during immortalization or if ASTL/SAS1B confers a growth advantage to cells *in vitro*. The search for an ASTL/SAS1B negative cell line was far from exhaustive so such a line may still exist, but efforts were switched to creating a knock-down line instead.

Preliminary attempts to transiently knockdown SAS1B via siASTL in mPanc96 cells resulted in an apparent, qualitative reduction in total cell number 72 hours after reverse transfection (Figure 3.12 B-N). Morphological changes were also observed in siASTL transfected cells, suggesting prominent cellular effects when cells have reduced ASTL/SAS1B. Although intriguing, these results are preliminary and additional experimentation is required before any conclusions are made. Because siASTL is a pool of four siRNAs, the observed results may be due to off-target effects of siRNAs binding to non-ASTL transcripts. Potential ways to increase siRNA knock-down efficiency include 1) increasing concentration of siRNA, 2) transfect with individual siRNAs to identify which works the best, 3) maintain threshold of siRNA in cells by adding a second dose of siRNA on day 2, or 4) try different cell lines known to be easily transfectable. Alternatively, other methods could be utilized to achieve knock-down or knock-out including transfection with other types of RNAi (e.g. short hairpin RNA (shRNA)) or with an ASTL CRISPR/Cas9 knock-out plasmid.

These preliminary studies suggest SAS1B expression is in a far greater range of cancer indications than previously recognized. ASTL splice variants and SAS1B protein isoforms, as well as post-translational modifications, which appear to be evident in cancer cells, may play an important role in the development of SAS1B theranostics. While preliminary data suggests SAS1B to be a worthwhile cancer therapeutic target to study, many unanswered questions remain to be examined surrounding SAS1B's basic biology and clinical relevance.

METHODS

Flow cytometry: human PBMCs

Buffy coat samples, from whole blood, were obtained from healthy donors from Virginia Blood Services (Richmond, VA); peripheral blood, containing myeloid and lymphoid cells, was isolated using a ficoll gradient (Ficoll-Paque™ Plus; GE Healthcare Bio-Sciences, Pittsburgh) and cryo-preserved in liquid nitrogen. After thawing, PBMCs recovered in thaw medium (RPMI with 10% fetal calf serum and 100 Units of DNase/mL) at 37°C, 5% CO₂ incubator for one hour. PBMCs were divided into two portions for staining either intracellular or surface expression of SAS1B. For intracellular detection, PBMCs were washed in PBS, then labeled with the live/dead cell stain Aqua (Invitrogen/Molecular Probes) at 4°C for 30 minutes, followed by washing 3 times in FACS buffer (PBS+0.1% BSA+0.1% sodium azide). Cells were fixed and permeabilized for intracellular staining according to manufacturer's instructions (Cytofix/Cytoperm (perm buffer), BDBiosciences). Cells were suspended in 0.05 mL of perm buffer with 0.05 mL of SAS1B mAb, SB2, or isotype control (IgG2b, Invitrogen) antibody, for a final concentration of 10 µg/mL, in 50% perm buffer and RPMI containing 10% FCS and 0.1% sodium azide (RPMI-FACS buffer) and incubated for one hour. For the immunoabsorption assay, SB2 was pre-incubated with either the SAS1B blocking peptide or the SAS1B control peptide (sequences listed in Chapter 2, Methods) for 1-2 hours at 37°C at a 1:1 peptide:antibody ratio. Following 3 washes in perm buffer, 0.1 Ml of Fitc-conjugated sheep anti-mouse IgG (SAM-IgG-Fitc; F(ab')₂ fragment; Cappel, MP Biomedicals) diluted to 1 µg/mL in perm buffer was applied to cells for 45 minutes and washed again in perm buffer, followed by 2 washes in FACS buffer. For detection of SAS1B on the cell

surface, PBMCs were centrifuged from thaw media, washed once in RPMI-FACS buffer and cells suspended in 100 μ L of SB2 mAb with or without peptide block. After 1 hour incubation, cells were washed in cold RPMI-FACS buffer (3x) followed by incubation in 0.1 mL SAM-IgG Fitc (2 μ g/mL) for 45 minutes. After washing 3x in PBS, cells were labeled with Aqua for 30 minutes at 4C, washed in RPMI-FACS buffer, fixed in 4% paraformaldehyde for 10 minutes at room temperature. Sample acquisition and analysis was done using a Canto2 flow cytometer and FlowJo software, respectively.

Glycosylation prediction

The SAS1B reference sequence, also known as splice variant A, was analyzed using three bioinformatics glycosylation prediction algorithms: the Hirst Group at University of Nottingham in the UK, NetOGly and NetNGly at the Technical University of Denmark, and GlycoEP at Microbial Technical Institute in India). Potential N-linked, O-linked, or C-linked glycosylation sites were predicted.

Mouse splenic harvest and flow cytometry

Spleens were harvested from recently euthanized C57BL/6, homogenized, and treated with red blood cell lysis. Live/dead stain was applied to splenocytes followed by blocking with Fc receptor block and normal mouse serum. Cells were incubated with the following immune cell markers for 25 minutes: CD8 for cytotoxic T cells, CD4 for helper T cells, B220 for B cells, NK1.1 for natural killer cells, and CD11c high plus MHC-II for dendritic cells. Cells were then permeabilized for intracellular staining, and incubated with a 1:1600 dilution of serum, from a guinea pig immunized with mouse SAS1B (previously described, [37]), for 30 minutes. For live cell staining, cells were not fixed and

permeabilized. Following washes, cells were incubated with secondary goat anti-guinea pig antibody conjugated to FITC for 30 minutes and washed again before analysis. Staining controls included pre-immune serum, no primary (secondary only), and no secondary (primary only). All incubations were done at 4°C. Samples were acquired on a Canto2 flow cytometer (UVA Carter Immunology Center) and analyzed using FlowJo software.

Cell culture

HNSCC and leukemia cell lines were obtained from our collaborators, Dr. Mark Jameson and Dr. Thomas Loughran (UVA), respectively. HNSCC cell lines were grown in DMEM/F-12 containing 5% heat inactivated FBS and 1% penicillin-streptomycin. Leukemia cell lines were cultured in RPMI containing 20% FBS and 1% penicillin-streptomycin. Cells were cultured in a humidified incubator (37°C, 5% CO₂).

Tissue/Cell Line Processing for RNA and RT-PCR

Cell lysis was performed on flash frozen HNSCC tumor samples using the SuperFastPrep-1 with lysing matrix D tubes in a 4°C cold room. Cell lines were harvested by scraping the cell monolayer in lysing buffer. RNA was then purified with the RNeasy kit (Qiagen, Germantown, MD) and reverse transcribed to cDNA as described previously [41] using gene specific primers or oligodTs. Primers designed to amplify the C-terminus of SAS1B, or GAPDH as a control, were used in a PCR assay, both previously described [41]. Additional SAS1B primers used for ASTL splice variant PCRs analysis and qPCR optimization are listed in Table 3.1 below.

ASTL Primer	Sequence (5' to 3')	Location
E1-2 For (SV-A/B/E/F)	CTC TCC TTG CCA GGT GTG ATC CTA	Exons 1-2
E9 Rev	CCT ACC AGT GCT GTG GGC ATG GGA	Exon 9
I1 For (SV-C/D)	ATG TCC TGC TGT CTG GTC TCA CCG	Intron 1 – Exon 2
SV-D Rev	GCT GAA GGC AAG CCT GGA ACC CAG	Exon 7 – Intron 7
Ex2-3 For	GTA CCA GCT TCC CAG ATG GC	Exons 2-3
Ex2-3 Rev	CTC TGG GGT TTC TTC CAG GAT	Exon 3
Ex5-6 For	GAG GCT CTT GCG GAG TTT GA	Exons 5-6
Ex5-6 Rev	CAC ACT CGA GAA GCA CCC ATA	Exon 6

Table 3.1: DNA primers used for ASTL splice variant detection (top four) and qPCR optimization (bottom four).

PCR products were run on a 1% agarose gel containing ethidium bromide and bands of the correct size were excised. cDNA was gel purified (QIAquick PCR Purification Kit, Qiagen, Germantown, MD) and sub-cloned using TOPO-TA cloning kit (Invitrogen, Carlsbad, CA). Plasmid DNA was purified (QIAprep Spin Miniprep Kid, Qiagen, Germantown, MD). DNA was sequenced and then searched with BLAST (NCBI) to confirm *ASTL/SAS1B* identity. For qPCR, SYBR green master mix was utilized, samples were run using the BioRad CFX96 instrument, and data analyzed using CFX manager software. Plasmids containing SV-A were amplified in a 1:4 dilution series to obtain a standard curve to use for semi-quantification of ASTL.

Tissue/Cell Line Processing for protein plus Western blot and IIF

Flash frozen HNSCC tumor samples were lysed as described above. Cell lines were harvested by scraping cells in the dish/flask in Celis buffer, containing protease inhibitor cocktail [134], which is urea-containing total denaturing buffer expected to extract all cellular proteins. For Western blotting, 30µg total protein was loaded onto a 10% SDS gel, proteins were electrophoresed and, following transfer to a nitrocellulose membrane, were blocked with NFDN-PBS and incubated with 5 µg/mL concentration of SAS1B rabbit polyclonal antibodies (previously described, [38]) overnight at 4°C. Blots were washed with

PBST and then incubated with 1:10,000 dilution of G α Rb-HRP for 1 hour in the dark. Following washes, immunoreactive bands were detected by ECL.

Fixed/permeabilized and live/non-permeabilized IIF was performed as described previously (Chapter 2, Methods).

Transient Transfection of SAS1B in HEK-293T cells, Western blot, & IIF

HEK-293T cells were cultured in DMEM/F-12 containing 10% heat-inactivated FBS, 1% non-essential amino acids, and 1mM sodium pyruvate at 37°C in a humidified incubator with 5% CO₂. For transient transfection, 293T cells were seeded at a density of 0.5×10^6 per T75 vented culture flask one day prior to transfection. Plated cells were transfected with 20ug plasmid DNA (constructs described below) per T75 flask using TurboFect™ transfection reagent following the manufacturer's instructions. The cells were harvested 72 hours post-transfection, washed with PBS, and the cell pellets were used for preparation of protein lysates or frozen immediately at -70°C for future use.

Two SAS1B expression constructs were generated to encompass SAS1B domains of predicted major splice variants: 1) entire open reading frame of hSAS1B-SV-A¹⁻⁴³¹ or 2) whole open reading frame of hSAS1B-SV-C¹⁻⁴³⁶. The DNA fragments for each of the SAS1B inserts were generated by PCR from hSAS1B SV-A and SV-C plasmids. The SAS1B DNA fragments were fused in frame with pcDNA 3.1/V5-His-topo vector by TOPO cloning. The vector carried a C-terminal V5 epitope followed by a polyhistidine (6xHis) tag. The constructs were confirmed by PCR and DNA sequencing. The primers used for PCR amplification of the SV-A insert were F: GAT ATG GAG GGT GTA GGG GGT CTC TGG and R: ATC TTC GGA CAT CCC CTT GAA ATG ATT; primers used

for SV-C were F: GAT ATG TCC TGC TGT CTG GTC TCA CCG and R: ATC TTC GGA CAT CCC CTT GAA ATG ATT. Control cells were transfected with empty plasmid. **Western blot:** Proteins were electrophoresed and then Western blotted as described above. Blots were probed with anti-His, Ms IgGs, Ms secondary only, Rb pAb, SB2, SB4, or SB5.

IIF: SV-A or SV-C constructs described above, or empty plasmid, were transfected into 293T cells at ~50-70% confluence. Before transfection, cells were seeded on 24-well plates containing poly-d-lysine coated 12mm round coverslips and transfected with Turbofect™ for 48 hours at 37°C. Cells were fixed with 4% PFA in PBS for 12 min, washed in PBS 3x, permeabilized in 100% methanol for 15 min, washed again, and blocked in culture media contain 5% NGS for 30 minutes. Cells were incubated with SAS1B mAbs (10ug/mL) for 1 hour and/or rabbit-anti-V5 epitope tag antibody-DyLight 488 conjugated (5ug/mL). Complexes of mAbs with SAS1B were then localized with AlexaFlour-594 conjugated F(ab)₂goat anti-mouse IgG antibody (5ug/mL) for 1 hour in blocking buffer. Cover slips were mounted with SlowFade Diamond containing DAPI to stain nuclei and visualized in a Zeiss LSM 700 confocal microscope and a Zeiss axiovert 200 fluorescence microscope.

Transient siRNA Transfection in mPanc96 Cells

mPanc96 cells, cultured as described earlier (Chapter 2, Methods), were seeded at a density of 0.5×10^6 per 10 cm dish one day prior to transfection. Two siGENOME SMARTpool siRNAs were obtained from Dharmacon for transfection. ASTL siRNA pool contained the following four target sequences: GAACGTTCCACGTGCATCA, TTCATGAGCTCATGCATGT, TATGACTACTCCTCTGTGA, and

GGGGATGTCCGAAGATTAA. Non-targeting siRNA pool contained the following sequences which do not match any known human genes: UAGGCUAUGAAGAGAUAC, AUGUAUUGGCCUGUAUUAG, AUGAACGUGAAUUGCUCAA, UGGUUUACAUGUCGACUAA. 50 uM siRNA stock was mixed with Optimem serum free media, mixed with RNAiMax transfection reagent, and then added to cells in a final concentration of 50nM siRNA. RNA was harvested from cells after 72 hours.

Chapter 4

Future Directions

We have shown that ASTL/SAS1B is a cancer-oocyte antigen which is expressed within the cytoplasm and at the cell surface in various cancers including PDAC, HNSCC, and leukemia and has limited expression among normal tissues (Chapters 2 & 3). Combined with the finding that an SAS1B-ADC was cytotoxic to SAS1B^{POS} cell lines with an apparent correlation between surface exposed SAS1B and level of cytotoxicity achieved (Chapter 2), we propose that SAS1B is may represent an ideal target for development of selective tumor treatments. However, we do not yet know if a SAS1B-ADC will be effective as a tumoricidal therapy *in vivo*. We have also shown expression of ASTL splice variants in cancer cell lines suggesting potential protein microheterogeneity with regards to functional and/or localization differences. We have not yet determined the function and localization of the putative protein isoforms nor have we shown which isoform(s) are the major targetable forms for cancer therapeutics. Our work has validated the need for additional studies regarding the therapeutic potential of an SAS1B-ADC using animal studies as a next step. However, our knowledge is limited by an incomplete understanding of the role of SAS1B in cell biology as well as many of the basic biological properties of SAS1B including regulation, function, protein microheterogeneity, substrates, binding partners, and low expression in normal tissues. Although we have not yet defined potential functional roles of SAS1B in cancer, we suspect SAS1B is an active metalloprotease in cancer based on what is known about functional SAS1B expressed in the ovary. Thus, more studies are needed to address the following questions, which will greatly aid in the development of clinically effective therapeutics directed against SAS1B:

1. *What is the pattern of expression and cellular localization of ASTL splice variants and SAS1B isoforms in cancer?*

2. *What is the functional role of SAS1B in cancer?*
3. *How is SAS1B regulated in cancer?*
4. *Is SAS1B expressed in pancreatic cancer stem cells?*
5. *What is the threshold of SAS1B surface expression needed for ADC cytotoxicity in PDAC cell lines and how does this relate to potential cutoff for which patients will be treated?*
6. *Does a SAS1B-ADC effectively stop tumor growth or shrink tumors in vivo?*

1. What is the pattern of expression and cellular localization of ASTL splice variants and SAS1B isoforms in cancer?

Initial studies, which indicate that ASTL is alternatively spliced resulting in SAS1B protein heterogeneity, vindicate a comprehensive study of ASTL/SAS1B variants to determine the full repertoire of splice variants in cancer, whether variants are translated into proteins, cellular localization of protein isoforms, and if isoform expression levels differ between cancer types. One approach to capture ASTL splice variants in a largely hypothesis-independent approach, is via RNA-sequencing (RNA-seq), a powerful and emerging technology for quantitative transcriptome profiling [135, 136]. In theory, RNA-seq will capture almost all of the expressed transcripts in a sample, known and unknown. Many different types of splicing events can be identified using RNA-seq including exon-skipping, mutually exclusive exons, intron retention and alternative 5' or 3' sites [116, 137]. Novel transcriptional start sites and termination sites could also be revealed within non-coding intronic sequences. Benefits of using RNA-seq as the primary variant identification method include: low background noise, high sensitivity, minimal RNA

sample requirements, and quantitative measurements of alternatively spliced isoforms [116, 136]. Deep sequencing will be performed on fragments of polyA-selected mRNAs to obtain an inventory of mRNA isoforms. Sequenced cDNA fragments (reads) will be mapped to human genomic SAS1B and transcript variant levels will be quantified. To confirm the accuracy of RNA-seq analysis of alternative splicing, a subset of tumors will be amplified using semi-quantitative RT-PCR. Additional PCR reactions using primers designed to flank identified splice variants will be used to confirm results from RNA sequencing and to generate amplicons for subcloning. Amplicons will be subcloned and nucleotide sequences verified by DNA sequencing; sequencing will be performed at least twice.

Confirmation of SAS1B isoform expression will be performed using 1D and 2D gel electrophoresis and Western blotting with anti-SAS1B rabbit pAb and/or other SAS1B antibodies. Spots resolved on SDS-PAGE gels will be cored and sent for liquid chromatography tandem mass spectrometry (LC/MS-MS) in order to verify the presence of SAS1B peptides. Post-verification, isoforms can be cloned into mammalian expression vectors containing two different fluorescent tags on the N- and C- termini and then transfected *in vitro* to: 1) determine cellular migration and localization of each isoform (e.g. cytosolic or membrane-associated), 2) define protein orientation of membrane-associated isoforms, and 3) purify endogenous mammalian SAS1B isoforms for use in developing isoform specific mAbs. Knowledge of major isoform(s) and localization of isoforms within tumors will help determine which isoform(s) are ideal for the development of targeted diagnostic and therapeutic treatments against SAS1B, such as generating a

monoclonal antibody to the membrane-associated predominant variant in tumors to use in an antibody-drug conjugate therapeutic.

2. What is the functional role of SAS1B in cancer?

While two clear roles of human SAS1B have been described pertaining to fertilization, the potential functional role SAS1B may be playing in the context of cancer has not yet been elucidated. SAS1B was reported to be exocytosed from oocyte cortical granules and to cleave zona pellucida 2, which contributes to the structural modification (i.e. hardening) of the zona pellucida (ECM surrounding the egg) in the post-fertilization block to polyspermy [39]. Our group defined another role of SAS1B as the first reported oolemmal binding partner for a known intra-acrosomal sperm ligand, SLLP1, prior to gamete fusion [37]. Recombinant human SAS1B has been shown to hydrolyze synthetic substrates used for assaying metalloproteases, *in vitro* [43], suggesting potential functional activity in cancer cells.

The potential action of SAS1B in cancer may be better predicted by combining what is known about SAS1B in fertilization with analysis of the functional roles of SAS1B homologues. SAS1B is phylogenetically related to MMPs and ADAMs, proteases that are significantly associated with cancer and metastasis, hinting that SAS1B may have a similar association. Most closely related to SAS1B are meprins which are implicated in disease states such as inflammation, fibrosis, neurodegenerative disorders, and cancer via cleavage of a variety of substrates [52]. Meprins were shown to play a role in breast cancer cell invasion and migration, indicating a potential role in tumor progression [138]. Meprin

α , through degradation of ECM components, was proposed to contribute to colon carcinoma progression by facilitating migration, intravasation, and metastasis [51, 53]. BTPs (BMP-1/tolloid-like proteinases), other close homologues of SAS1B, are involved with morphogenesis, tissue repair, and tumor progression [57]. Downregulation of BMP-1, a BTP, in non-small cell lung cancer resulted in decreased tumor invasion *in vitro* by suppressing TGF- β activity which lead to downregulation of MMP2 and MMP2, key oncogenic genes [139].

Based on the known roles of SAS1B in fertilization, the activity of the closely-related homologues in cancer, and the presence of ASTL splice variants and putative SAS1B protein isoforms in cancer, we hypothesize that SAS1B may have at least one functional role in cancer. Oolemmal SAS1B plays a critical role in gamete fusion by binding with the sperm protein, SLLP1 during fertilization [37]. Cancer cells are known to fuse with normal cells (stromal, epithelial, macrophages) and with other cancer cells [140]. Cell fusion events can result in the formation of the highly tumorigenic and chemoresistant polyploid giant cancer cells (PGCCs) when cancer cells fuse together [141] and in metastasis initiation when cancer cells fuse with macrophages [142]. In culture, the SAS1Bpos SNU539 SAS1B localized to the cancer cell surface may play a role in cancer cell fusion through interaction with other membrane-associated proteins that are yet to be identified.

However, we believe a more likely scenario involves SAS1B playing a physiological role in cancer as an active metalloprotease. Given that SAS1B homologs (meprins, BMP-1) appear to promote cancer progression via cleavage of various substrates and that SAS1B is a metalloprotease which cleaves ZP2 during fertilization [39], we

hypothesize that SAS1B may cleave ZP-domain containing proteins potentially present in the tumor microenvironment. Thus, SAS1B may be involved in cancer metastasis via degradation of the ECM [143] or the extracellular domains of signaling molecules. The ZP domain, present in extracellular proteins, appears to function as a polymerization module. A search for ZP domain homologs using the SMART algorithm (a simple modular architecture research tool) revealed 16 non-redundant ZP domain containing proteins in humans (Table 4.1). Notable examples of human ZP-domain proteins associated with cancer include transforming growth factor- β (TGF- β) receptor type III (TGF β R3), endoglin (ENG), and deleted in malignant brain tumor 1 (DMBT-1) [143].

Deregulation of the TGF- β signaling pathway, which has multiple important physiological roles in development, cellular proliferation, synthesis of extracellular matrix, angiogenesis and immune responses, may result in tumor development. TGF β R3, as well as the structurally related protein ENG, are TGF- β co-receptors and modulators of the TGF- β response; TGF- β signaling is widely reported to be altered in cancer [144]. Furthermore, TGF β R3 has been shown to have tumor suppressor phenotype in renal cell carcinoma [145]. DMBT-1 has also been described as a putative tumor suppressor. Tissue-specific dual functionality of the DMBT-1 gene has been suggested in epithelial cancer which resolves contradictory data of DMBT-1 as a tumor suppressor gene: protection of monolayered epithelia and differentiation of multilayered epithelia, potentially due to differences in protein isoform expression [146]. Alterations in DMBT-1, usually deletions and loss of expression, have been observed in many cancers including: brain, oesophageal, gastric, colon [147], breast [148], HNSCC [149], and lung [150]. In the porcine and equine species, DMBT-1 has been implicated in fertilization via secretion into the oviduct and

localization to the ZP and oocyte cytoplasm [151]. Because alterations in DMBT-1 expression have been observed in multiple cancer types, some of which coincide with SAS1B expression (HNSCC, breast), and DMBT-1 was also shown to play a role in fertilization, we suggest that DMBT-1 is an ideal candidate substrate for SAS1B (first suggested by M. Harding). The expression of an active protease, such as SAS1B, could be a way to inactivate the tumor suppressor function of DMBT-1 or TGF β R3. In this hypothetical scenario, the genes for DMBT-1 / TGF β R3 would remain but the onset of SAS1B expression would inactivate the tumor suppressor functionality by proteolytic cleavage.

One initial approach to identifying candidate ZP domain protein substrates for SAS1B would be to look for co-expression of SAS1B and known ZP domain homologs in different cancer types. A SAS1B knock-out cancer cell line would then be compared to the untreated cancer cell line via SDS-PAGE Western blot analysis with substrate specific antibodies to detect potential molecular size changes due to cleavage. Alternatively, SAS1B binding partners may be revealed by performing co-immunoprecipitation (co-IP) with SAS1B antibodies from cancer lysates; binding partners can be detected by SDS-PAGE and Western blot analysis.

Aside from ZP-domain proteins, SAS1B may also have additional, unknown substrates in cancer. The unique C-terminal region of SAS1B, which shows no similarity to other domains present in the equivalent region of most astacins [43], is predicted to participate in the recognition of its putative substrates. Additionally, the wide range of substrates meprin cleaves, dependent on factors such as subunit expression, cell type, disease state, and glycosylation status, suggests that SAS1B may proteolyze additional

unknown proteins. An unbiased proteomics approach using PROTOMAP (protein topography and migration analysis platform; described in [152]) technology could be employed to identify differential protein expression (e.g. due to proteolysis) between a SAS1B knock-out line and control cells. Control and SAS1B knock-out cell lysates are analyzed via SDS-PAGE; gels are then cut into bands and trypsinized. Peptides are identified by LC-MS/MS and analyzed by peptographs, which plot gel migration versus sequence coverage for each protein, to show approximate site(s) and extent of cleavage. To confirm identified substrates are directly acted on by SAS1B, and not indirectly through a cascade of proteolytic activators, rSAS1B can be incubated with a potential substrate and subsequently analyzed by Western blot by which molecular size changes due to proteolysis will be evident.

Abbreviation	Protein Name/Description
CUZDI	CUB and zona pellucida-like domain-containing protein 1
DMBT1	Deleted in malignant brain tumors 1 protein
EGLN	Endoglin
GP2	Pancreatic secretory granule membrane major glycoprotein 2
OIT3	Oncoprotein-induced transcript 3 protein
POZP3	POM121 and ZP3 fusion protein
Q5DID0-2	Isoform 2 of uromodulin-like 1
TECTA	Alpha-tectorin
TGBR3	Transforming growth factor beta receptor type 3
TGR3L	Transforming growth factor beta receptor type 3-like protein
UROM	Uromodulin
ZP1	Zona pellucida sperm binding protein 1
ZP2	Zona pellucida sperm binding protein 2
ZP3	Zona pellucida sperm binding protein 3
ZP4	Zona pellucida sperm binding protein 4
ZPLD1	Zona pellucida-like domain-containing protein 1

[Table 4.1] Human ZP-domain containing proteins

The SMART (a simple modular architecture research tool) algorithm was used to search for human proteins containing ZP domain homologs. The 16 non-redundant human proteins containing a ZP domain identified from the search are listed alphabetically.

3. How is ASTL/SAS1B regulated in cancer?

While there is some available insight regarding the control and regulation of ASTL/SAS1B in the ovary, how ASTL/SAS1B is regulated in malignancies remains unknown. By analyzing available SAS1B-ovary data and closely related homologs, preliminary hypotheses can be generated concerning the regulation of ASTL/SAS1B in cancer. The precise temporal and spatial expression pattern of SAS1B in the ovary in several eutherian orders indicates tight, conserved regulation [38]. SAS1B has been suggested to be under hormonal control given that expression of SAS1B is highly induced in superovulated mice [43]. The tight control of SAS1B observed in the ovary is likely lost in the malignant process, which is a well-documented occurrence in other proteases [153-156]. Regulation can occur at the transcriptional, translational, or post-translational levels.

Many CTAs, of which SAS1B is the sole member defined so far of the partner class of COAs, have been shown to be silenced in somatic cells via CpG island promoter methylation effects on chromatin structure and transcription factor binding. CTA expression can be induced *in vitro* using targeted experimental promoter demethylation [73, 157, 158]. During gametogenesis and early embryogenesis, DNA methylation patterns are changed and chromatin is restructured which allows for CTA gene expression [159]. It is appreciated that cancers dedifferentiate and reactivate the gametogenic program normally silenced in somatic tissues [66]. Global epigenetic changes, including promoter hypomethylation, are a hallmark of cancer [160]. Given this knowledge, we propose that ASTL/SAS1B is also normally silenced in somatic cells by promoter hypermethylation and that global hypomethylation in tumorigenesis results in activation of ASTL. To test this, genomic DNA from SAS1B^{pos} cancer cells and from corresponding SAS1B^{neg} normal cells

can be treated with bisulfate; subsequent DNA sequencing will reveal which cysteines in the ASTL promoter region are methylated [161]. If the hypothesis is correct, the ASTL promoter region in SAS1B^{pos} cancer cells will be less methylated than that in ASTL/SAS1B^{neg} normal cells. A follow-up experiment in which ASTL/SAS1B^{neg} cells are treated with demethylating agents to induce ASTL/SAS1B expression will confirm hypermethylation as a silencing mechanism. It remains unclear whether ASTL/SAS1B expression correlates with tumorigenesis or is a passive bystander activated by cellular transformation. Determining whether SAS1B plays a functional role in cancer cells, as outlined in Chapter 4 Section 1, will help answer this central question.

At the level of transcription, the transcription factor newborn ovary homeobox protein (NOBOX) has been implicated in the control of ASTL expression. NOBOX, which shows preferential oocyte expression, is essential for folliculogenesis and the regulation of oocyte-specific gene expression in the mouse [162]. As such, NOBOX has been described as one of the master transcription factors regulating oogenesis. ASTL expression in NOBOX knock-out mouse ovaries was decreased 13.9-fold [163] suggesting NOBOX promotes ASTL transcription. Additionally, bioinformatics analyses show consensus NOBOX binding sites in the ASTL promoter region (M. Harding, unpublished data). It is reasonable to hypothesize that NOBOX may be regulating ASTL transcription in cancer as well. A preliminary Western blot screen could be employed to determine if NOBOX is expressed in ASTL/SAS1B^{pos} cancer cell lines. To determine whether ASTL is associated with NOBOX regulation, NOBOX could be knocked-out in ASTL^{pos} cancer cell lines. A decrease in ASTL expression by RT-qPCR in the NOBOX KO would suggest regulatory control of ASTL by NOBOX.

Initially, proteolytic activity of rSAS1B was shown to be abolished *in vitro* by inhibitors of metalloproteinases and by batimastat (BB-94), an inhibitor originally designed to target MMPs overexpressed in cancer [43]. Fetuin-B, which is decreased 7.1-fold in NOBOX KO mouse ovaries [163], has since been shown to be a selective physiological inhibitor of ovastacin [164, 165]. The liver-derived protein fetuin-B prevents premature ZP hardening by blocking prematurely released SAS1B and has been shown to be an essential component in maintaining fertility. Fetuin-B is a potent competitive inhibitor of SAS1B. Mechanistically, it has been suggested that the 55 kDa fetuin-B can diffuse through the ZP to block prematurely released ovastacin. Post-fertilization, the fetuin-B level within the ovary, which is in steady state with plasma-fetuin-B, cannot sustain inhibition of the high level of ovastacin secreted from the cortical granula; no fetuin-B is produced in the ovary but rather comes from the liver [165]. Furthermore, tumor suppressor activity of fetuin-B was implicated in an overexpression study in skin squamous carcinoma cells which resulted in tumor growth prevention in mice [166]. In line with these findings, fetuin-B was identified in a genome wide study as a significantly underexpressed gene in both poorly and moderately differentiated in hepatocellular carcinoma [167]. If fetuin-B regulates SAS1B in cancer as predicted, we would expect to see an inverse correlation between fetuin-B and active SAS1B levels (i.e. lacking propeptide region) in SAS1B^{pos} human tumors which could be assayed by RT-qPCR and Western blot. Downregulation of fetuin-B, via an unknown mechanism, would result in loss of SAS1B activation inhibition by fetuin-B. If a SAS1B substrate is identified in cancer, such as DMBT-1, whether fetuin-B inhibits SAS1B in cancer could be assayed by monitoring proteolysis of DMBT-1 *in vitro* in response to fetuin-B treatment of SAS1B^{pos}

cells. In this model, fetuin-B treatment would result in decreased proteolysis of DMBT-1 by SAS1B.

SAS1B is synthesized as an inactive zymogen with a propeptide region which is then proteolytically processed to become an active enzyme [43, 46]. Many astacins are activated extracellularly by trypsin-like serine proteases [168] which has been suggested to be the case for SAS1B *in vitro*, specifically by plasmin or plasminogen plus tissue plasminogen activator (tPA) (Karmilin et al., unpublished data). To determine if SAS1B is activated tPA-activated plasmin, tPA plus plasminogen can be incubated with rSAS1B *in vitro* and then Western blotted to look for accumulation of activated SAS1B (lacking the propeptide region). Within a cell line, an inhibitor of tPA-activated plasmin can be administered and then cell lysates and culture media assayed by Western blot for increased level of inactivate SAS1B zymogen.

4. Is SAS1B expressed in pancreatic cancer stem cells?

Once called “tumor-initiating” cells, cancer stem cells (CSCs) have been defined as malignant cells with functional properties similar to traditional stem cells: capacity for self-renewal, the potential to develop into any cell in the overall tumor population, and extensive proliferative potential [169] as well as the unique ability to seed tumors when transplanted into an animal host [170]. CSCs may produce all the malignant cells in the primary tumor and/or colonize distant metastases. Also considered drug-resistant, cancer stem cells may comprise the small pool of cells which will cause relapse after a chemotherapy-induced remission [169]. If we think of the population of cancer stem cell

as having the highest malignant potential, we may also consider this population to be the most de-differentiated, to have reverted the farthest back toward the undifferentiated mother cell. Genetic instability and drug resistance, features associated with tumor progression, are suggested to be associated with cancer stem cells [169]. It is reasonable then, to suggest, cancer stem cells may have acquired a higher degree of gametogenic programming than any other tumor cells which could theoretically include expression of SAS1B. Furthermore, some CTAs have shown preferential expression in CSCs [171] also supporting the hypothesis that SAS1B is expressed in CSCs. Clinical therapies targeting CSCs should eradicate tumors more effectively by reducing potential for relapse and metastasis. SAS1B may represent a potential novel therapeutic target for the elimination of the CSCs and therefore more effective treatment of SAS1B^{pos} cancers.

Pancreatic cancer stem cells have been defined as CD133^{pos} and are of high value in the treatment of the notoriously chemo- and radio-therapy resistant PDAC [172]. A preliminary experiment using pancreatic cancer cell lines co-stained with markers for pancreatic CSCs and SAS1B and analyzed by flow cytometry will determine if pancreatic CSCs are SAS1B^{pos}. This experiment will define what percent of CSCs are SAS1B^{pos} and what percent of SAS1B^{pos} cells are also CSCs. Additionally, a subpopulation of CD133^{pos} CXCR4^{pos} cells have been identified as essential for tumor metastasis [172]. PDAC cell lines will also be stained for CXCR4 to determine if these migrating CSCs are also SAS1B^{pos}. Pancreatic CSCs can also be co-stained for SAS1B and c-met, an additional known pancreatic CSC marker [173], to confirm presence or absence of cell surface-associated SAS1B in pancreatic CSCs.

If pancreatic CSCs show SAS1B cell surface localization by flow cytometry, a follow up cytotoxicity study will be completed. PDAC cell lines will be treated with a SAS1B-ADC, as described in Chapter 2 Methods section; after 72 hours, cells will be analyzed by flow cytometry to determine what percent of remaining viable cells are CSCs (defined by CD133^{POS}), and what proportion of those are SAS1B^{POS}, as compared to the control treated cells. Elimination of the pancreatic CSC pool in response to SAS1B-ADC treatment would validate SAS1B as potential therapeutic target for CSCs in pancreatic cancer.

5. What is the threshold of SAS1B surface expression needed for ADC cytotoxicity in PDAC cell lines and how does this relate to potential cutoff for which patients will be treated?

PDAC cell lines (mPanc96, 366, 608) showed a range of cell surface a SAS1B by flow cytometry which appeared to correlate with extent of cytotoxicity observed when treated with a SAS1B-ADC (Figure 2.5). However, the threshold of SAS1B surface expression needed to cause ADC induced cytotoxicity *in vitro* is unknown. Establishing a cutoff for SAS1B^{POS} cancer cells that will or will not respond to ADC treatment is vital for effective patient selection and clinical application. To assess firstly if a threshold exists, and secondly what level of surface-expressed SAS1B is sufficient to cause significant cytotoxicity, we propose collecting data on SAS1B density index versus cytotoxicity. Flow cytometry using anti-SAS1B mAb, SB2, can be used to assess cell surface SAS1B density of cell lines covering a range of SAS1B expression. A SAS1B knock-out or greatly knocked-down PDAC cell line(s) and a line(s) with overexpressed SAS1B will be used as

the lower and upper limits of surface expression. There is also likely an upper limit of surface expression which, once reached, will provide no greater cytotoxic results once surpassed. Multiple PDAC cell lines will be analyzed in addition to mPanc96, 608, and 366 which have been previously studied (Chapter 2); additional cell lines include those generated by the Bauer group, 738 and 450 [96], as well as BxPC-3 [174], Panc-1 [175], and AsPC-1 [176], which are well documented within the literature. SAS1B-ADC (mAb: SB2) cytotoxicity will be evaluated on each cell line according to the protocol established in Chapter 2: Methods. The density index of cell surface associated SAS1B and the LD50 for each cell line will be graphed to evaluate the potential SAS1B expression threshold required for cytotoxicity.

SAS1B surface density is likely only one of multiple components contributing to a successful ADC. Additional barriers and challenges to adequate ADC-mediated tumoricidal effects, related to the target, include antibody-antigen affinity, SAS1B membrane recycling rate, and internalization rate [177]. These other properties will need to be studied as well to develop the most effective clinical therapeutic. However, some ADC properties may be less relevant if SAS1B surface expression is not great enough to result in ADC cytotoxicity. Given that we have previously observed modest relative levels of cell surface SAS1B (Figure 2.5) and expression is heterogenous among tumor cells (Figure 2.1), we may consider ways to induce SAS1B expression at the cell surface to promote cell death. CTA expression has been shown to be highly inducible in cancer cell lines using the hypomethylating agents 5-Aza-2'-deoxycytidine or 5-Azacytidine and/or a histone deacetylase inhibitor LBH589 [178, 179]. We predict that treatment with either 5-Aza-2'-deoxycytidine or 5-Azacytidine in PDAC cell lines will induce expression of

SAS1B and suggest completing this experiment using flow cytometry to quantify changes in surface expressed SAS1B. The ADC cytotoxicity assay will then be used to determine if induced SAS1B expression leads to greater cytotoxic effects observed in PDAC cell lines. The implications from these results may advocate the use of hypomethylating agents as adjunctive therapy in combination with a SAS1B-ADC to achieve maximum tumoricidal effects.

6. Does a SAS1B-ADC effectively stop tumor growth or shrink tumors *in vivo*?

Cytotoxic effects of a SAS1B-ADC have been demonstrated *in vitro* in a uterine cancer cell line [41] and in neoplastic pancreatic cancer cell lines using a different SAS1B-ADC (Chapter 2, Figure 2.5) while non-neoplastic keratinocytes were not killed in the same assay. How a SAS1B-ADC potentially affects malignancies *in vivo* is unknown; these studies warrant further *in vivo* evaluation of SAS1B as an ADC therapeutic target. We propose utilization of PDAC PDX mouse models, from which tumors have been shown to be SAS1B^{pos} (Chapter 2, Figure 2.3), for *in vivo* SAS1B-ADC assessment as a logical progression from the *in vitro* studies presented in Chapter 2. Two of the PDAC cell lines, 366 and 608, which were sensitive to cell death by a SAS1B-ADC (Chapter 2, Figure 2.5), were generated from patient tumors also used for the orthotopic mouse models. Both 366 and 608 PDX orthotopic models have been published in the literature [89, 95, 96] and represent ideal models for *in vivo* testing of a SAS1B-ADC. The suggested PDAC PDX orthotopic mouse models, where fresh patient tumors are affixed directly into the mouse pancreas [96], have been shown to recapitulate the clinical, pathological, genetic, and molecular aspects of human disease [89] and are thus expected to be the best clinically

relevant model in which to study the effects of SAS1B therapies *in vivo*. Other models using freshly-derived human specimens have been described but have not validated that xenografted tumors maintain high phenotypic and genetic similarity with the patient tumor [180]. Both 366 and 608 PDX models are considered superior to PDAC models in which cancer cell lines are implanted heterotopically (subcutaneous) as the latter models poorly recapitulate the pancreatic tumor microenvironment [181] which plays a significant role in tumor cell behavior [182]. We predict that an ADC (with anti-SAS1B mAb SB2 conjugated to duocarmycin used previously in PDAC cell lines (Chapter2)) targeted against SAS1B will demonstrate tumoricidal activity in SAS1B^{pos} tumors whereas negative control arms will show limited or no tumoricidal activity.

Prior to the main study, we suggest an initial tolerance study in which immunocompromised mice to assess impact on mouse health. Animals will be observed daily for acute effects on respiration and behavior. A dose-escalation study will also be performed to determine the maximum, tolerated dose producing effective tumoricidal effects. The main drug efficacy study will determine if an SB2-duocarmycin ADC shows tumoricidal activity *in vivo*. The design of this study will recapitulate human situation by asking if the drug will shrink pre-existing tumors. Treatment will begin after implanted tumors have grown to a volume of 250 to 500 mm³ as assessed by volumetric magnetic resonance imaging (MRI). The tumoricidal activity of the SAS1B-ADC will be compared to control arms including 1) unlabeled SB2 mAb, 2) vehicle alone, 3) isotype matched mAb directed to an irrelevant antigen conjugated with duocarmycin (e.g. 3A4 used in Chapter 2), and 4) isotype matched mAb alone. ADCs will be delivered intravenously and tumor growth/regression will be assessed using MRI. Animal weights will be monitored at

weekly intervals. At the time of sacrifice, blood samples will be collected by cardiac puncture and tumors will be harvested for histopathology, Western blots, and for molecular studies (PCR) of SAS1B expression. Additionally, lung, kidney, liver, heart, brain, and mesenteric and peritoneal surfaces will be harvested and analyzed for any metastases and additional pathology to serve as an early safety and toxicity assessment. Ovaries will be harvested from female mice and studied by morphometrics for possible effects of drug treatment on oocyte growth and folliculogenesis. We anticipate that mice bearing pancreatic tumors treated with an ADC targeting SAS1B will show tumor shrinkage and will extend animal survival time. These studies will provide proof of concept that SAS1B can potentially be used as a therapeutic target for the treatment of pancreatic cancer using an ADC, opening an entirely new field of therapeutic targets.

FINAL SUMMARY

Immunotherapeutic options for the treatment of cancer, which remains a major global health challenge, offer the allure of greater tumor specificity and less associated toxicity than is typically achieved with traditional chemo- and radio-therapeutic strategies. The success of some immunotherapies, such as ADCs and CAR-Ts, rely on identification and selection of targets which are highly tumor-specific with limited or no expression in normal tissues. Cancer germline antigens represent potential ideal targets for targeted immunotherapy as CGAs are expressed in cancer cells but show limited or no expression among normal tissues. Although many cancer-testis antigens have been described, SAS1B is the first, and only, cancer-oocyte antigen identified to-date. Owing to the limited expression of SAS1B among normal tissue combined with expression in a number of cancer indications, we propose that SAS1B is an attractive immunotherapeutic target.

We have shown that, in addition to previous work published in female reproductive cancers, SAS1B is expressed in a majority of pancreatic and head and neck cancers. SAS1B localized to both the cytoplasm and the cell surface in PDAC and HNSCC cell lines by IIF and flow cytometry, suggesting potential utility of SAS1B targeted immunotherapeutic strategies. Furthermore, an ADC targeting SAS1B administered to pancreatic cancer cell lines was internalized and subsequently caused significant cell death in a manner correlated with SAS1B cell surface expression. Thus, SAS1B represents a novel therapeutic target for the treatment of PDAC and HNSCC. These data support further development of a SAS1B-ADC including *in vivo* assessment using mouse xenograft systems; however, some major questions regarding SAS1B need to be addressed prior to advancement to clinical utility.

While initial reports failed to detect ASTL/SAS1B in variety of normal tissues, recent data generated using more sensitive assays suggests some low level SAS1B expression in normal tissues, other than the ovary, including: keratinocytes, pancreas stromal cells, and leukocytes. For SAS1B to be considered a viable clinical therapeutic target, further studies are needed to fully characterize SAS1B expression in normal cells. *In vitro*, keratinocytes have been shown to express cell surface SAS1B but are insensitive to a SAS1B-ADC leading to the prediction that non-neoplastic SAS1B^{POS} cells will not be affected by a SAS1B-ADC. While ADCs need to be internalized to exert cytotoxic effects, CAR-Ts will potentially induce cell death in any cells expressing the target at the cell surface, independent of internalization. Unlike keratinocytes, pilot studies assessing SAS1B expression in leukocytes suggests SAS1B localizes to the cytoplasm in dendritic cells and a small population of B-cells and is not likely expressed at the cell surface. In theory, SAS1B expression limited to the cytoplasm of normal cells, would not preclude ADCs and CAR-Ts as viable SAS1B targeting approaches as these strategies rely on target expression at the cell surface. In addition to characterization of SAS1B expression in normal tissues, *in vivo* studies using a SAS1B ADC or CAR-T is needed to assess potential off-tumor cytotoxicity which will help guide development of SAS1B targeted immunotherapies.

Although we have shown proof of concept that SAS1B-ADC induces cytotoxicity in pancreatic cancer cell lines, addressing multiple fundamental biological questions which remain regarding SAS1B expression will also inform production of SAS1B targeted therapies. For example, we have identified six ASTL splice variants in cancer, known as SV-A to SV-F, and have shown differential cellular localization of recombinant SV-A and

SV-C proteins (cell surface vs. cytoplasm, respectively). Further studies characterizing major SAS1B protein isoform(s) expressed at the cell surface in cancers may lead to development of more effective immunotherapies utilizing mAbs generated against cell surface, cancer-associated form(s) of SAS1B.

Our work suggests SAS1B expression in a broad range of cancer indications and demonstrates efficacy of a SAS1B-ADC *in vitro*, thus supporting further assessment of SAS1B as an immunotherapeutic target for the treatment of cancer. While preliminary data suggests SAS1B to be a worthwhile cancer therapeutic target to study, potential complications arising from the basic biology of SAS1B need to be addressed in order to produce the most effective SAS1B targeted immunotherapy.

Chapter 5

References

1. Anonymous American Cancer Society: The Global Cancer Burden; <https://www.cancer.org/health-care-professionals/our-global-health-work/global-cancer-burden.html> , 2017.
2. Global Burden of Disease Cancer Collaboration, Fitzmaurice C, Allen C, Barber RM, Barregard L, Bhutta ZA, Brenner H, Dicker DJ, Chimed-Orchir O, Dandona R, Dandona L, Fleming T, Forouzanfar MH, et al. Global, Regional, and National Cancer Incidence, Mortality, Years of Life Lost, Years Lived With Disability, and Disability-Adjusted Life-years for 32 Cancer Groups, 1990 to 2015: A Systematic Analysis for the Global Burden of Disease Study. *JAMA oncology*. 2017; 3: 524-548.
3. Siegel RL, Miller KD, Jemal A. Cancer Statistics, 2017. *CA: a cancer journal for clinicians*. 2017; 67: 7-30.
4. Chabner BA, Thompson EC. Modalities of Cancer Therapy. Available at: <http://www.merckmanuals.com/professional/hematology-and-oncology/principles-of-cancer-therapy/modalities-of-cancer-therapy>. Merck Manual.
5. National Institute of Health. The website of the National Cancer Institute; available at: <https://www.cancer.gov>. 2017.
6. Chari RV. Targeted cancer therapy: conferring specificity to cytotoxic drugs. *Accounts of Chemical Research*. 2008; 41: 98-107.
7. Ducry L, Stump B. Antibody-drug conjugates: linking cytotoxic payloads to monoclonal antibodies. *Bioconjugate chemistry*. 2010; 21: 5-13.
8. Farkona S, Diamandis EP, Blasutig IM. Cancer immunotherapy: the beginning of the end of cancer?. *BMC medicine*. 2016; 14: 73-016-0623-5.
9. Yu X, Zhang Y, Chen C, Yao Q, Li M. Targeted drug delivery in pancreatic cancer. *Biochimica et Biophysica Acta (BBA) - Reviews on Cancer*. 2010; 1805: 97-104.
10. Pieczonka CM, Telonis D, Mouraviev V, Albala D. Sipuleucel-T for the Treatment of Patients With Metastatic Castrate-resistant Prostate Cancer: Considerations for Clinical Practice. *Reviews in urology*. 2015; 17: 203-210.
11. Rosenberg SA, Restifo NP. Adoptive cell transfer as personalized immunotherapy for human cancer. *Science (New York, N.Y.)*. 2015; 348: 62-68.
12. Brentjens RJ, Davila ML, Riviere I, Park J, Wang X, Cowell LG, Bartido S, Stefanski J, Taylor C, Olszewska M, Borquez-Ojeda O, Qu J, Wasielewska T, et al. CD19-targeted T cells rapidly induce molecular remissions in adults with chemotherapy-refractory acute lymphoblastic leukemia. *Science translational medicine*. 2013; 5: 177ra38.

13. Grupp SA, Kalos M, Barrett D, Aplenc R, Porter DL, Rheingold SR, Teachey DT, Chew A, Hauck B, Wright JF, Milone MC, Levine BL, June CH. Chimeric antigen receptor-modified T cells for acute lymphoid leukemia. *The New England journal of medicine*. 2013; 368: 1509-1518.
14. Kalos M, Levine BL, Porter DL, Katz S, Grupp SA, Bagg A, June CH. T cells with chimeric antigen receptors have potent antitumor effects and can establish memory in patients with advanced leukemia. *Science translational medicine*. 2011; 3: 95ra73.
15. Kochenderfer JN, Dudley ME, Kassim SH, Somerville RP, Carpenter RO, Stetler-Stevenson M, Yang JC, Phan GQ, Hughes MS, Sherry RM, Raffeld M, Feldman S, Lu L, et al. Chemotherapy-refractory diffuse large B-cell lymphoma and indolent B-cell malignancies can be effectively treated with autologous T cells expressing an anti-CD19 chimeric antigen receptor. *Journal of clinical oncology : official journal of the American Society of Clinical Oncology*. 2015; 33: 540-549.
16. Iyer U, Kadambi VJ. Antibody drug conjugates - Trojan horses in the war on cancer. *Journal of pharmacological and toxicological methods*. 2011; 64: 207-212.
17. Alley SC, Okeley NM, Senter PD. Antibody-drug conjugates: targeted drug delivery for cancer. *Current opinion in chemical biology*. 2010; 14: 529-537.
18. Walter RB, Raden BW, Kamikura DM, Cooper JA, Bernstein ID. Influence of CD33 expression levels and ITIM-dependent internalization on gemtuzumab ozogamicin-induced cytotoxicity. *Blood*. 2005; 105: 1295-1302.
19. Senter PD. Potent antibody drug conjugates for cancer therapy. *Current opinion in chemical biology*. 2009; 13: 235-244.
20. Lewis Phillips GD, Li G, Dugger DL, Crocker LM, Parsons KL, Mai E, Blattler WA, Lambert JM, Chari RV, Lutz RJ, Wong WL, Jacobson FS, Koeppen H, et al. Targeting HER2-positive breast cancer with trastuzumab-DM1, an antibody-cytotoxic drug conjugate. *Cancer research*. 2008; 68: 9280-9290.
21. Erickson HK, Park PU, Widdison WC, Kovtun YV, Garrett LM, Hoffman K, Lutz RJ, Goldmacher VS, Blattler WA. Antibody-maytansinoid conjugates are activated in targeted cancer cells by lysosomal degradation and linker-dependent intracellular processing. *Cancer research*. 2006; 66: 4426-4433.
22. Polson AG, Williams M, Gray AM, Fuji RN, Poon KA, McBride J, Raab H, Januario T, Go M, Lau J, Yu SF, Du C, Fuh F, et al. Anti-CD22-MCC-DM1: an antibody-drug conjugate with a stable linker for the treatment of non-Hodgkin's lymphoma. *Leukemia*. 2010; 24: 1566-1573.
23. Singh R, Erickson HK. Antibody-cytotoxic agent conjugates: preparation and characterization. *Methods in molecular biology (Clifton, N.J.)*. 2009; 525: 445-67, xiv.

24. Alley SC, Okeley NM, Senter PD. Antibody-drug conjugates: targeted drug delivery for cancer. *Current opinion in chemical biology*. 2010; 14: 529-537.
25. Teicher BA, Doroshow JH. The promise of antibody-drug conjugates. *The New England journal of medicine*. 2012; 367: 1847-1848.
26. Feld J, Barta SK, Schinke C, Braunschweig I, Zhou Y, Verma AK. Linked-in: design and efficacy of antibody drug conjugates in oncology. *Oncotarget*. 2013; 4: 397-412.
27. Hamblett KJ, Senter PD, Chace DF, Sun MM, Lenox J, Cervený CG, Kissler KM, Bernhardt SX, Kopcha AK, Zabinski RF, Meyer DL, Francisco JA. Effects of drug loading on the antitumor activity of a monoclonal antibody drug conjugate. *Clinical cancer research : an official journal of the American Association for Cancer Research*. 2004; 10: 7063-7070.
28. McDonagh CF, Turcott E, Westendorf L, Webster JB, Alley SC, Kim K, Andreyka J, Stone I, Hamblett KJ, Francisco JA, Carter P. Engineered antibody-drug conjugates with defined sites and stoichiometries of drug attachment. *Protein engineering, design & selection : PEDS*. 2006; 19: 299-307.
29. Feld J, Barta SK, Schinke C, Braunschweig I, Zhou Y, Verma AK. Linked-in: design and efficacy of antibody drug conjugates in oncology. *Oncotarget*. 2013; 4: 397-412.
30. Guglin M, Cutro R, Mishkin JD. Trastuzumab-induced cardiomyopathy. *Journal of cardiac failure*. 2008; 14: 437-444.
31. Balyasnikova IV, Wainwright DA, Solomaha E, Lee G, Han Y, Thaci B, Lesniak MS. Characterization and immunotherapeutic implications for a novel antibody targeting interleukin (IL)-13 receptor alpha2. *The Journal of biological chemistry*. 2012; 287: 30215-30227.
32. Debinski W, Obiri NI, Powers SK, Pastan I, Puri RK. Human glioma cells overexpress receptors for interleukin 13 and are extremely sensitive to a novel chimeric protein composed of interleukin 13 and pseudomonas exotoxin. *Clinical cancer research : an official journal of the American Association for Cancer Research*. 1995; 1: 1253-1258.
33. Joshi BH, Plautz GE, Puri RK. Interleukin-13 receptor alpha chain: a novel tumor-associated transmembrane protein in primary explants of human malignant gliomas. *Cancer research*. 2000; 60: 1168-1172.
34. Jarboe JS, Johnson KR, Choi Y, Lonser RR, Park JK. Expression of interleukin-13 receptor alpha2 in glioblastoma multiforme: implications for targeted therapies. *Cancer research*. 2007; 67: 7983-7986.

35. Kawakami K, Terabe M, Kawakami M, Berzofsky JA, Puri RK. Characterization of a novel human tumor antigen interleukin-13 receptor alpha2 chain. *Cancer research*. 2006; 66: 4434-4442.
36. Debinski W, Slagle B, Gibo DM, Powers SK, Gillespie GY. Expression of a restrictive receptor for interleukin 13 is associated with glial transformation. *Journal of neuro-oncology*. 2000; 48: 103-111.
37. Sachdev M, Mandal A, Mulders S, Digilio LC, Panneerdoss S, Suryavathi V, Pires E, Klotz KL, Hermens L, Herrero MB, Flickinger CJ, van Duin M, Herr JC. Oocyte specific oolemmal SAS1B involved in sperm binding through intra-acrosomal SLLP1 during fertilization. *Developmental biology*. 2012; 363: 40-51.
38. Pires ES, Hlavin C, Macnamara E, Ishola-Gbenla K, Doerwaldt C, Chamberlain C, Klotz K, Herr AK, Khole A, Chertihin O, Curnow E, Feldman SH, Mandal A, et al. SAS1B protein [ovastacin] shows temporal and spatial restriction to oocytes in several eutherian orders and initiates translation at the primary to secondary follicle transition. *Developmental dynamics : an official publication of the American Association of Anatomists*. 2013; 242: 1405-1426.
39. Burkart AD, Xiong B, Baibakov B, Jimenez-Movilla M, Dean J. Ovastacin, a cortical granule protease, cleaves ZP2 in the zona pellucida to prevent polyspermy. *The Journal of cell biology*. 2012; 197: 37-44.
40. Peng Q, Yang H, Xue S, Shi L, Yu Q, Kuang Y. Secretome profile of mouse oocytes after activation using mass spectrum. *Journal of assisted reproduction and genetics*. 2012; 29: 765-771.
41. Pires ES, D'Souza RS, Needham MA, Herr AK, Jazaeri AA, Li H, Stoler MH, Anderson-Knapp KL, Thomas T, Mandal A, Gougeon A, Flickinger CJ, Bruns DE, et al. Membrane associated cancer-oocyte neoantigen SAS1B/ovastacin is a candidate immunotherapeutic target for uterine tumors. *Oncotarget*. 2015; 6: 30194-30211.
42. NCBI. Website: human ASTL EST database, <http://www.ncbi.nlm.nih.gov/nucest/14468989> and <http://www.ncbi.nlm.nih.gov/UniGene/ESTProfileViewer.cgi?uglist=Hs.447993>.
43. Quesada V, Sanchez LM, Alvarez J, Lopez-Otin C. Identification and characterization of human and mouse ovastacin: a novel metalloproteinase similar to hatching enzymes from arthropods, birds, amphibians, and fish. *The Journal of biological chemistry*. 2004; 279: 26627-26634.
44. Bond JS, Beynon RJ. The astacin family of metalloendopeptidases. *Protein science : a publication of the Protein Society*. 1995; 4: 1247-1261.

45. Sterchi EE, Stocker W, Bond JS. Meprins, membrane-bound and secreted astacin metalloproteinases. *Molecular aspects of medicine*. 2008; 29: 309-328.
46. Gomis-Ruth FX. Structural aspects of the metzincin clan of metalloendopeptidases. *Molecular biotechnology*. 2003; 24: 157-202.
47. Guevara T, Yiallourous I, Kappelhoff R, Bissdorf S, Stocker W, Gomis-Ruth FX. Proenzyme structure and activation of astacin metallopeptidase. *The Journal of biological chemistry*. 2010; 285: 13958-13965.
48. Barnes K, Ingram J, Kenny AJ. Proteins of the kidney microvillar membrane. Structural and immunochemical properties of rat endopeptidase-2 and its immunohistochemical localization in tissues of rat and mouse. *The Biochemical journal*. 1989; 264: 335-346.
49. Beynon RJ, Shannon JD, Bond JS. Purification and characterization of a metallo-endoproteinase from mouse kidney. *The Biochemical journal*. 1981; 199: 591-598.
50. Sterchi EE, Green JR, Lentze MJ. Non-pancreatic hydrolysis of N-benzoyl-L-tyrosyl-p-aminobenzoic acid (PABA-peptide) in the human small intestine. *Clinical science (London, England : 1979)*. 1982; 62: 557-560.
51. Lottaz D, Hahn D, Muller S, Muller C, Sterchi EE. Secretion of human meprin from intestinal epithelial cells depends on differential expression of the alpha and beta subunits. *European journal of biochemistry*. 1999; 259: 496-504.
52. Becker-Pauly C, Howel M, Walker T, Vlad A, Aufenvenne K, Oji V, Lottaz D, Sterchi EE, Debela M, Magdolen V, Traupe H, Stocker W. The alpha and beta subunits of the metalloprotease meprin are expressed in separate layers of human epidermis, revealing different functions in keratinocyte proliferation and differentiation. *The Journal of investigative dermatology*. 2007; 127: 1115-1125.
53. Lottaz D, Maurer CA, Hahn D, Buchler MW, Sterchi EE. Nonpolarized secretion of human meprin alpha in colorectal cancer generates an increased proteolytic potential in the stroma. *Cancer research*. 1999; 59: 1127-1133.
54. Ishmael FT, Shier VK, Ishmael SS, Bond JS. Intersubunit and domain interactions of the meprin B metalloproteinase. Disulfide bonds and protein-protein interactions in the MAM and TRAF domains. *The Journal of biological chemistry*. 2005; 280: 13895-13901.
55. Ge G, Greenspan DS. Developmental roles of the BMP1/TLD metalloproteinases. *Birth defects research. Part C, Embryo today : reviews*. 2006; 78: 47-68.

56. Hopkins DR, Keles S, Greenspan DS. The bone morphogenetic protein 1/Tolloid-like metalloproteinases. *Matrix biology : journal of the International Society for Matrix Biology*. 2007; 26: 508-523.
57. Vadon-Le Goff S, Hulmes DJ, Moali C. BMP-1/tolloid-like proteinases synchronize matrix assembly with growth factor activation to promote morphogenesis and tissue remodeling. *Matrix biology : journal of the International Society for Matrix Biology*. 2015; 44-46: 14-23.
58. Boyse EA, Old LJ, Stockert E, Shigeno N. Genetic origin of tumor antigens. *Cancer research*. 1968; 28: 1280-1287.
59. Schumacher TN, Schreiber RD. Neoantigens in cancer immunotherapy. *Science (New York, N.Y.)*. 2015; 348: 69-74.
60. Akers SN, Odunsi K, Karpf AR. Regulation of cancer germline antigen gene expression: implications for cancer immunotherapy. *Future oncology (London, England)*. 2010; 6: 717-732.
61. Hofmann O, Caballero OL, Stevenson BJ, Chen YT, Cohen T, Chua R, Maher CA, Panji S, Schaefer U, Kruger A, Lehvaslaiho M, Carninci P, Hayashizaki Y, et al. Genome-wide analysis of cancer/testis gene expression. *Proceedings of the National Academy of Sciences of the United States of America*. 2008; 105: 20422-20427.
62. Scanlan MJ, Simpson AJ, Old LJ. The cancer/testis genes: review, standardization, and commentary. *Cancer immunity*. 2004; 4: 1.
63. Kalejs M, Erenpreisa J. Cancer/testis antigens and gametogenesis: a review and "brain-storming" session. *Cancer cell international*. 2005; 5: 4.
64. Grizzi F, Gaetani P, Franceschini B, Di Ieva A, Colombo P, Ceva-Grimaldi G, Bollati A, Frezza EE, Cobos E, Rodriguez y Baena R, Dioguardi N, Chiriva-Internati M. Sperm protein 17 is expressed in human nervous system tumours. *BMC cancer*. 2006; 6: 23.
65. Lin W, Zhou X, Zhang M, Li Y, Miao S, Wang L, Zong S, Koide SS. Expression and function of the HSD-3.8 gene encoding a testis-specific protein. *Molecular human reproduction*. 2001; 7: 811-818.
66. Simpson AJ, Caballero OL, Jungbluth A, Chen YT, Old LJ. Cancer/testis antigens, gametogenesis and cancer. *Nature reviews.Cancer*. 2005; 5: 615-625.
67. Caballero OL, Chen YT. Cancer/testis (CT) antigens: potential targets for immunotherapy. *Cancer science*. 2009; 100: 2014-2021.
68. Monk M, Holding C. Human embryonic genes re-expressed in cancer cells. *Oncogene*. 2001; 20: 8085-8091.

69. Simpson AJ, Caballero OL, Jungbluth A, Chen YT, Old LJ. Cancer/testis antigens, gametogenesis and cancer. *Nature reviews.Cancer*. 2005; 5: 615-625.
70. James SR, Link PA, Karpf AR. Epigenetic regulation of X-linked cancer/germline antigen genes by DNMT1 and DNMT3b. *Oncogene*. 2006; 25: 6975-6985.
71. Lorient A, De Plaen E, Boon T, De Smet C. Transient down-regulation of DNMT1 methyltransferase leads to activation and stable hypomethylation of MAGE-A1 in melanoma cells. *The Journal of biological chemistry*. 2006; 281: 10118-10126.
72. Wischniewski F, Pantel K, Schwarzenbach H. Promoter demethylation and histone acetylation mediate gene expression of MAGE-A1, -A2, -A3, and -A12 in human cancer cells. *Molecular cancer research : MCR*. 2006; 4: 339-349.
73. De Smet C, Lurquin C, Lethe B, Martelange V, Boon T. DNA methylation is the primary silencing mechanism for a set of germ line- and tumor-specific genes with a CpG-rich promoter. *Molecular and cellular biology*. 1999; 19: 7327-7335.
74. Woloszynska-Read A, Mhawech-Fauceglia P, Yu J, Odunsi K, Karpf AR. Intertumor and intratumor NY-ESO-1 expression heterogeneity is associated with promoter-specific and global DNA methylation status in ovarian cancer. *Clinical cancer research : an official journal of the American Association for Cancer Research*. 2008; 14: 3283-3290.
75. Gjerstorff MF, Burns J, Ditzel HJ. Cancer-germline antigen vaccines and epigenetic enhancers: future strategies for cancer treatment. *Expert opinion on biological therapy*. 2010; 10: 1061-1075.
76. Rahib L, Smith BD, Aizenberg R, Rosenzweig AB, Fleshman JM, Matrisian LM. Projecting cancer incidence and deaths to 2030: the unexpected burden of thyroid, liver, and pancreas cancers in the United States. *Cancer research*. 2014; 74: 2913-2921.
77. Becker AE, Hernandez YG, Frucht H, Lucas AL. Pancreatic ductal adenocarcinoma: risk factors, screening, and early detection. *World journal of gastroenterology*. 2014; 20: 11182-11198.
78. Li J, Wientjes MG, Au JL. Pancreatic cancer: pathobiology, treatment options, and drug delivery. *The AAPS journal*. 2010; 12: 223-232.
79. Siegel R, Ma J, Zou Z, Jemal A. Cancer statistics, 2014. *CA: a cancer journal for clinicians*. 2014; 64: 9-29.
80. Chiorean EG, Coveler AL. Pancreatic cancer: optimizing treatment options, new, and emerging targeted therapies. *Drug design, development and therapy*. 2015; 9: 3529-3545.

81. Feig C, Gopinathan A, Neesse A, Chan DS, Cook N, Tuveson DA. The pancreas cancer microenvironment. *Clinical cancer research : an official journal of the American Association for Cancer Research*. 2012; 18: 4266-4276.
82. Li D, Xie K, Wolff R, Abbruzzese JL. Pancreatic cancer. *Lancet (London, England)*. 2004; 363: 1049-1057.
83. Chauffert B, Mornex F, Bonnetain F, Rougier P, Mariette C, Bouche O, Bosset JF, Aparicio T, Mineur L, Azzedine A, Hammel P, Butel J, Stremmsdoerfer N, et al. Phase III trial comparing intensive induction chemoradiotherapy (60 Gy, infusional 5-FU and intermittent cisplatin) followed by maintenance gemcitabine with gemcitabine alone for locally advanced unresectable pancreatic cancer. Definitive results of the 2000-01 FFCO/SFRO study. *Annals of oncology : official journal of the European Society for Medical Oncology*. 2008; 19: 1592-1599.
84. Ghaneh P, Costello E, Neoptolemos JP. Biology and management of pancreatic cancer. *Postgraduate medical journal*. 2008; 84: 478-497.
85. Sultana A, Tudur Smith C, Cunningham D, Starling N, Tait D, Neoptolemos JP, Ghaneh P. Systematic review, including meta-analyses, on the management of locally advanced pancreatic cancer using radiation/combined modality therapy. *British journal of cancer*. 2007; 96: 1183-1190.
86. Moorcraft SY, Khan K, Peckitt C, Watkins D, Rao S, Cunningham D, Chau I. FOLFIRINOX for locally advanced or metastatic pancreatic ductal adenocarcinoma: the Royal Marsden experience. *Clinical colorectal cancer*. 2014; 13: 232-238.
87. Von Hoff DD, Ervin T, Arena FP, Chiorean EG, Infante J, Moore M, Seay T, Tjulandin SA, Ma WW, Saleh MN, Harris M, Reni M, Dowden S, et al. Increased survival in pancreatic cancer with nab-paclitaxel plus gemcitabine. *The New England journal of medicine*. 2013; 369: 1691-1703.
88. Mahadevan D, Von Hoff DD. Tumor-stroma interactions in pancreatic ductal adenocarcinoma. *Molecular cancer therapeutics*. 2007; 6: 1186-1197.
89. Walters DM, Stokes JB, Adair SJ, Stelow EB, Borgman CA, Lowrey BT, Xin W, Blais EM, Lee JK, Papin JA, Parsons JT, Bauer TW. Clinical, molecular and genetic validation of a murine orthotopic xenograft model of pancreatic adenocarcinoma using fresh human specimens. *PloS one*. 2013; 8: e77065.
90. Distler M, Aust D, Weitz J, Pilarsky C, Grutzmann R. Precursor lesions for sporadic pancreatic cancer: PanIN, IPMN, and MCN. *BioMed research international*. 2014; 2014: 474905.
91. Hruban RH, Adsay NV, Albores-Saavedra J, Compton C, Garrett ES, Goodman SN, Kern SE, Klimstra DS, Kloppel G, Longnecker DS, Luttges J, Offerhaus GJ. Pancreatic

intraepithelial neoplasia: a new nomenclature and classification system for pancreatic duct lesions. *The American Journal of Surgical Pathology*. 2001; 25: 579-586.

92. Capolla S, Garrovo C, Zorzet S, Lorenzon A, Rampazzo E, Sprez R, Pozzato G, Nunez L, Tripodo C, Macor P, Biffi S. Targeted tumor imaging of anti-CD20-polymeric nanoparticles developed for the diagnosis of B-cell malignancies. *International journal of nanomedicine*. 2015; 10: 4099-4109.

93. Hong H, Zhang Y, Sun J, Cai W. Molecular imaging and therapy of cancer with radiolabeled nanoparticles. *Nano today*. 2009; 4: 399-413.

94. Naaby-Hansen S, Mandal A, Wolkowicz MJ, Sen B, Westbrook VA, Shetty J, Coonrod SA, Klotz KL, Kim YH, Bush LA, Flickinger CJ, Herr JC. CABYR, a novel calcium-binding tyrosine phosphorylation-regulated fibrous sheath protein involved in capacitation. *Developmental biology*. 2002; 242: 236-254.

95. Stokes JB, Adair SJ, Slack-Davis JK, Walters DM, Tilghman RW, Hershey ED, Lowrey B, Thomas KS, Bouton AH, Hwang RF, Stelow EB, Parsons JT, Bauer TW. Inhibition of focal adhesion kinase by PF-562,271 inhibits the growth and metastasis of pancreatic cancer concomitant with altering the tumor microenvironment. *Molecular cancer therapeutics*. 2011; 10: 2135-2145.

96. Walters DM, Lindberg JM, Adair SJ, Newhook TE, Cowan CR, Stokes JB, Borgman CA, Stelow EB, Lowrey BT, Chopivsky ME, Gilmer TM, Parsons JT, Bauer TW. Inhibition of the growth of patient-derived pancreatic cancer xenografts with the MEK inhibitor trametinib is augmented by combined treatment with the epidermal growth factor receptor/HER2 inhibitor lapatinib. *Neoplasia (New York, N.Y.)*. 2013; 15: 143-155.

97. Strickland SW, Vande Pol S. The Human Papillomavirus 16 E7 Oncoprotein Attenuates AKT Signaling To Promote Internal Ribosome Entry Site-Dependent Translation and Expression of c-MYC. *Journal of virology*. 2016; 90: 5611-5621.

98. Yamada SS. Preparation of human epidermal keratinocyte cultures. *Current protocols in cell biology*. 2004; Chapter 2: Unit 2.6.

99. O'Rorke MA, Ellison MV, Murray LJ, Moran M, James J, Anderson LA. Human papillomavirus related head and neck cancer survival: a systematic review and meta-analysis. *Oral oncology*. 2012; 48: 1191-1201.

100. Lee J, Moon C. Current status of experimental therapeutics for head and neck cancer. *Experimental biology and medicine (Maywood, N.J.)*. 2011; 236: 375-389.

101. Rousseau A, Badoual C. Head and neck squamous cell carcinoma: an overview. *Atlas of Genetics and Cytogenetics in Oncology and Hematology*. 2011; 16: 145-155.

102. Licitra L, Felip E, ESMO Guidelines Working Group. Squamous cell carcinoma of the head and neck: ESMO clinical recommendations for diagnosis, treatment and follow-up. *Annals of oncology : official journal of the European Society for Medical Oncology*. 2009; 20 Suppl 4: 121-122.
103. Colevas AD. Chemotherapy options for patients with metastatic or recurrent squamous cell carcinoma of the head and neck. *Journal of clinical oncology : official journal of the American Society of Clinical Oncology*. 2006; 24: 2644-2652.
104. Vermorken JB, Specenier P. Optimal treatment for recurrent/metastatic head and neck cancer. *Annals of oncology : official journal of the European Society for Medical Oncology*. 2010; 21 Suppl 7: vii252-61.
105. Kim L, King T, Agulnik M. Head and neck cancer: changing epidemiology and public health implications. *Oncology (Williston Park, N.Y.)*. 2010; 24: 915-9, 924.
106. Segafort S, Van Cutsem E. Clinical signs, pathophysiology and management of skin toxicity during therapy with epidermal growth factor receptor inhibitors. *Annals of oncology : official journal of the European Society for Medical Oncology*. 2005; 16: 1425-1433.
107. Mehra R, Cohen RB, Burtness BA. The role of cetuximab for the treatment of squamous cell carcinoma of the head and neck. *Clinical advances in hematology & oncology : H&O*. 2008; 6: 742-750.
108. National Cancer Institute. SEER Cancer Stat Facts: Leukemia. Website: <https://seer.cancer.gov/statfacts/html/leuks.html>.
109. Mayo Clinic. Leukemia: Treatments and Drugs. Website: <http://www.mayoclinic.org/diseases-conditions/leukemia/basics/treatment/con-20024914>.
110. Pray LA. Gleevec: the breakthrough in cancer treatment. *Nature Education*. 2008; 1: 37.
111. Pajares MJ, Ezponda T, Catena R, Calvo A, Pio R, Montuenga LM. Alternative splicing: an emerging topic in molecular and clinical oncology. *The Lancet.Oncology*. 2007; 8: 349-357.
112. Skotheim RI, Nees M. Alternative splicing in cancer: noise, functional, or systematic?. *The international journal of biochemistry & cell biology*. 2007; 39: 1432-1449.
113. Tang JY, Lee JC, Hou MF, Wang CL, Chen CC, Huang HW, Chang HW. Alternative splicing for diseases, cancers, drugs, and databases. *TheScientificWorldJournal*. 2013; 2013: 703568.

114. Chen M, Manley JL. Mechanisms of alternative splicing regulation: insights from molecular and genomics approaches. *Nature reviews.Molecular cell biology*. 2009; 10: 741-754.
115. Pal S, Gupta R, Davuluri RV. Alternative transcription and alternative splicing in cancer. *Pharmacology & therapeutics*. 2012; 136: 283-294.
116. Feng H, Qin Z, Zhang X. Opportunities and methods for studying alternative splicing in cancer with RNA-Seq. *Cancer letters*. 2013; 340: 179-191.
117. Brinkman BM. Splice variants as cancer biomarkers. *Clinical biochemistry*. 2004; 37: 584-594.
118. Garces C, Ruiz-Hidalgo MJ, Bonvini E, Goldstein J, Laborda J. Adipocyte differentiation is modulated by secreted delta-like (dlk) variants and requires the expression of membrane-associated dlk. *Differentiation; research in biological diversity*. 1999; 64: 103-114.
119. Liu J, Hu B, Yang Y, Ma Z, Yu Y, Liu S, Wang B, Zhao X, Lu M, Yang D. A new splice variant of the major subunit of human asialoglycoprotein receptor encodes a secreted form in hepatocytes. *PloS one*. 2010; 5: e12934.
120. Venables JP. Aberrant and alternative splicing in cancer. *Cancer research*. 2004; 64: 7647-7654.
121. O'Keefe EP. A comprehensive review of siRNAs and shRNAs as tools for gene silencing. *Mater Methods*. 2013; 197.
122. Kleiveland CR. Peripheral Blood Mononuclear Cells In: Verhoeckx K, Cotter P, Lopez-Exposito I, Kleiveland C, Lea T, Mackie A, Requena T, Swiatecka D, Wichers H (eds). *The Impact of Food Bioactives on Health: in vitro and ex vivo models*. Springer International Publishing. 2015: 161-167.
123. Stockwin LH, McGonagle D, Martin IG, Blair GE. Dendritic cells: immunological sentinels with a central role in health and disease. *Immunology and cell biology*. 2000; 78: 91-102.
124. Heiser A, Coleman D, Dannull J, Yancey D, Maurice MA, Lallas CD, Dahm P, Niedzwiecki D, Gilboa E, Vieweg J. Autologous dendritic cells transfected with prostate-specific antigen RNA stimulate CTL responses against metastatic prostate tumors. *The Journal of clinical investigation*. 2002; 109: 409-417.
125. Ritchie D, Hermans I, Yang J, Walton J, Matthews K, Carter J, Findlay M, Dady P, Rawson P, Ronchese F. Autologous dendritic cells pulsed with eluted peptide as immunotherapy for advanced B-cell malignancies. *Leukemia & lymphoma*. 2006; 47: 675-682.

126. Di Nicola M, Zappasodi R, Carlo-Stella C, Mortarini R, Pupa SM, Magni M, Devizzi L, Matteucci P, Baldassari P, Ravagnani F, Cabras A, Anichini A, Gianni AM. Vaccination with autologous tumor-loaded dendritic cells induces clinical and immunologic responses in indolent B-cell lymphoma patients with relapsed and measurable disease: a pilot study. *Blood*. 2009; 113: 18-27.
127. Ohtsubo K, Marth JD. Glycosylation in cellular mechanisms of health and disease. *Cell*. 2006; 126: 855-867.
128. Roth Z, Yehezkel G, Khalaila I. Identification and quantification of protein glycosylation. *International Journal of Carbohydrate Chemistry*. 2012; 2012.
129. Kadowaki T, Tsukuba T, Bertenshaw GP, Bond JS. N-Linked oligosaccharides on the meprin A metalloprotease are important for secretion and enzymatic activity, but not for apical targeting. *The Journal of biological chemistry*. 2000; 275: 25577-25584.
130. Leuenberger B, Hahn D, Pischitzis A, Hansen MK, Sterchi EE. Human meprin beta: O-linked glycans in the intervening region of the type I membrane protein protect the C-terminal region from proteolytic cleavage and diminish its secretion. *The Biochemical journal*. 2003; 369: 659-665.
131. Stowell SR, Ju T, Cummings RD. Protein glycosylation in cancer. *Annual review of pathology*. 2015; 10: 473-510.
132. Trendowski M. The inherent metastasis of leukaemia and its exploitation by sonodynamic therapy. *Critical reviews in oncology/hematology*. 2015; 94: 149-163.
133. Caplan MJ. Chapter 2: Functional Organization of the Cell In: Boron WF and Boulpaep EL. (ed). *Medical Physiology: A Cellular and Molecular Approach*. Saunders Elsevier. Philadelphia, PA. 2012: 29.
134. Celis JE, Rasmussen HH, Madsen P, Leffers H, Honore B, Dejgaard K, Gesser B, Olsen E, Gromov P, Hoffmann HJ. The human keratinocyte two-dimensional gel protein database (update 1992): towards an integrated approach to the study of cell proliferation, differentiation and skin diseases. *Electrophoresis*. 1992; 13: 893-959.
135. Mutz KO, Heilkenbrinker A, Lonne M, Walter JG, Stahl F. Transcriptome analysis using next-generation sequencing. *Current opinion in biotechnology*. 2013; 24: 22-30.
136. Chen G, Wang C, Shi T. Overview of available methods for diverse RNA-Seq data analyses. *Science China.Life sciences*. 2011; 54: 1121-1128.
137. Shapiro IM, Cheng AW, Flytzanis NC, Balsamo M, Condeelis JS, Oktay MH, Burge CB, Gertler FB. An EMT-driven alternative splicing program occurs in human breast cancer and modulates cellular phenotype. *PLoS genetics*. 2011; 7: e1002218.

138. Matters GL, Manni A, Bond JS. Inhibitors of polyamine biosynthesis decrease the expression of the metalloproteases meprin alpha and MMP-7 in hormone-independent human breast cancer cells. *Clinical & experimental metastasis*. 2005; 22: 331-339.
139. Wu X, Liu T, Fang O, Leach LJ, Hu X, Luo Z. miR-194 suppresses metastasis of non-small cell lung cancer through regulating expression of BMP1 and p27(kip1). *Oncogene*. 2014; 33: 1506-1514.
140. Bastida-Ruiz D, Van Hoesen K, Cohen M. The Dark Side of Cell Fusion. *International journal of molecular sciences*. 2016; 17: 10.3390/ijms17050638.
141. Zhang S, Mercado-Uribe I, Xing Z, Sun B, Kuang J, Liu J. Generation of cancer stem-like cells through the formation of polyploid giant cancer cells. *Oncogene*. 2014; 33: 116-128.
142. Seyfried TN, Huysentruyt LC. On the origin of cancer metastasis. *Critical reviews in oncogenesis*. 2013; 18: 43-73.
143. Jovine L, Darie CC, Litscher ES, Wassarman PM. Zona pellucida domain proteins. *Annual Review of Biochemistry*. 2005; 74: 83-114.
144. Bernabeu C, Lopez-Novoa JM, Quintanilla M. The emerging role of TGF-beta superfamily coreceptors in cancer. *Biochimica et biophysica acta*. 2009; 1792: 954-973.
145. Margulis V, Maity T, Zhang XY, Cooper SJ, Copland JA, Wood CG. Type III transforming growth factor-beta (TGF-beta) receptor mediates apoptosis in renal cell carcinoma independent of the canonical TGF-beta signaling pathway. *Clinical cancer research : an official journal of the American Association for Cancer Research*. 2008; 14: 5722-5730.
146. Mollenhauer J, Helmke B, Muller H, Kollender G, Krebs I, Wiemann S, Holmskov U, Madsen J, Otto HF, Poustka A. An integrative model on the role of DMBT1 in epithelial cancer. *Cancer detection and prevention*. 2002; 26: 266-274.
147. Mori M, Shiraishi T, Tanaka S, Yamagata M, Mafune K, Tanaka Y, Ueo H, Barnard GF, Sugimachi K. Lack of DMBT1 expression in oesophageal, gastric and colon cancers. *British journal of cancer*. 1999; 79: 211-213.
148. Braidotti P, Nuciforo PG, Mollenhauer J, Poustka A, Pellegrini C, Moro A, Bulfamante G, Coggi G, Bosari S, Pietra GG. DMBT1 expression is down-regulated in breast cancer. *BMC cancer*. 2004; 4: 46.
149. Imai MA, Moriya T, Imai FL, Shiiba M, Bukawa H, Yokoe H, Uzawa K, Tanzawa H. Down-regulation of DMBT1 gene expression in human oral squamous cell carcinoma. *International journal of molecular medicine*. 2005; 15: 585-589.

150. Wu W, Kemp BL, Proctor ML, Gazdar AF, Minna JD, Hong WK, Mao L. Expression of DMBT1, a candidate tumor suppressor gene, is frequently lost in lung cancer. *Cancer research*. 1999; 59: 1846-1851.
151. Ambruosi B, Accogli G, Douet C, Canepa S, Pascal G, Monget P, Moros Nicolas C, Holmskov U, Mollenhauer J, Robbe-Masselot C, Vidal O, Desantis S, Goudet G. Deleted in malignant brain tumor 1 is secreted in the oviduct and involved in the mechanism of fertilization in equine and porcine species. *Reproduction (Cambridge, England)*. 2013; 146: 119-133.
152. Dix MM, Simon GM, Cravatt BF. Global mapping of the topography and magnitude of proteolytic events in apoptosis. *Cell*. 2008; 134: 679-691.
153. Egeblad M, Werb Z. New functions for the matrix metalloproteinases in cancer progression. *Nature reviews.Cancer*. 2002; 2: 161-174.
154. Freije JM, Balbin M, Pendas AM, Sanchez LM, Puente XS, Lopez-Otin C. Matrix metalloproteinases and tumor progression. *Advances in Experimental Medicine and Biology*. 2003; 532: 91-107.
155. Hojilla CV, Mohammed FF, Khokha R. Matrix metalloproteinases and their tissue inhibitors direct cell fate during cancer development. *British journal of cancer*. 2003; 89: 1817-1821.
156. Netzel-Arnett S, Hooper JD, Szabo R, Madison EL, Quigley JP, Bugge TH, Antalis TM. Membrane anchored serine proteases: a rapidly expanding group of cell surface proteolytic enzymes with potential roles in cancer. *Cancer metastasis reviews*. 2003; 22: 237-258.
157. Weber J, Salgaller M, Samid D, Johnson B, Herlyn M, Lassam N, Treisman J, Rosenberg SA. Expression of the MAGE-1 tumor antigen is up-regulated by the demethylating agent 5-aza-2'-deoxycytidine. *Cancer research*. 1994; 54: 1766-1771.
158. Coral S, Sigalotti L, Altomonte M, Engelsberg A, Colizzi F, Cattarossi I, Maraskovsky E, Jager E, Seliger B, Maio M. 5-Aza-2'-Deoxycytidine-Induced Expression of Functional Cancer Testis Antigens in Human Renal Cell Carcinoma: Immunotherapeutic Implications. *Clinical cancer research : an official journal of the American Association for Cancer Research*. 2002; 8: 2690-2695.
159. Kimmins S, Sassone-Corsi P. Chromatin remodelling and epigenetic features of germ cells. *Nature*. 2005; 434: 583-589.
160. Watanabe Y, Maekawa M. Methylation of DNA in cancer. *Advances in Clinical Chemistry*. 2010; 52: 145-167.

161. Gjerstorff M, Burns JS, Nielsen O, Kassem M, Ditzel H. Epigenetic modulation of cancer-germline antigen gene expression in tumorigenic human mesenchymal stem cells: implications for cancer therapy. *The American journal of pathology*. 2009; 175: 314-323.
162. Rajkovic A, Pangas SA, Ballow D, Suzumori N, Matzuk MM. NOBOX deficiency disrupts early folliculogenesis and oocyte-specific gene expression. *Science (New York, N.Y.)*. 2004; 305: 1157-1159.
163. Choi Y, Qin Y, Berger MF, Ballow DJ, Bulyk ML, Rajkovic A. Microarray analyses of newborn mouse ovaries lacking Nobox. *Biology of reproduction*. 2007; 77: 312-319.
164. Korschgen H, Kuske M, Karmilin K, Yiallourous I, Balbach M, Floehr J, Wachten D, Jahnen-Dechent W, Stocker W. Intracellular activation of ovastacin mediates pre-fertilization hardening of the zona pellucida. *Molecular human reproduction*. 2017; 23, No.9: 607-616.
165. Dietzel E, Wessling J, Floehr J, Schafer C, Ensslen S, Denecke B, Rosing B, Neulen J, Veitinger T, Spehr M, Tropartz T, Tolba R, Renne T, et al. Fetuin-B, a liver-derived plasma protein is essential for fertilization. *Developmental cell*. 2013; 25: 106-112.
166. Hsu SJ, Nagase H, Balmain A. Identification of Fetuin-B as a member of a cystatin-like gene family on mouse chromosome 16 with tumor suppressor activity. *Genome*. 2004; 47: 931-946.
167. Ge X, Yamamoto S, Tsutsumi S, Midorikawa Y, Ihara S, Wang SM, Aburatani H. Interpreting expression profiles of cancers by genome-wide survey of breadth of expression in normal tissues. *Genomics*. 2005; 86: 127-141.
168. Yiallourous I, Kappelhoff R, Schilling O, Wegmann F, Helms MW, Auge A, Brachtendorf G, Berkhoff EG, Beermann B, Hinz HJ, Konig S, Peter-Katalinic J, Stocker W. Activation mechanism of pro-astacin: role of the pro-peptide, tryptic and autoproteolytic cleavage and importance of precise amino-terminal processing. *Journal of Molecular Biology*. 2002; 324: 237-246.
169. Jordan CT, Guzman ML, Noble M. Cancer stem cells. *The New England journal of medicine*. 2006; 355: 1253-1261.
170. Rosen JM, Jordan CT. The increasing complexity of the cancer stem cell paradigm. *Science (New York, N.Y.)*. 2009; 324: 1670-1673.
171. Yamada R, Takahashi A, Torigoe T, Morita R, Tamura Y, Tsukahara T, Kanaseki T, Kubo T, Watarai K, Kondo T, Hirohashi Y, Sato N. Preferential expression of cancer/testis genes in cancer stem-like cells: proposal of a novel sub-category, cancer/testis/stem gene. *Tissue antigens*. 2013; 81: 428-434.

172. Hermann PC, Huber SL, Herrler T, Aicher A, Ellwart JW, Guba M, Bruns CJ, Heeschen C. Distinct populations of cancer stem cells determine tumor growth and metastatic activity in human pancreatic cancer. *Cell stem cell*. 2007; 1: 313-323.
173. Li C, Wu JJ, Hynes M, Dosch J, Sarkar B, Welling TH, Pasca di Magliano M, Simeone DM. c-Met is a marker of pancreatic cancer stem cells and therapeutic target. *Gastroenterology*. 2011; 141: 2218-2227.e5.
174. Tan MH, Nowak NJ, Loor R, Ochi H, Sandberg AA, Lopez C, Pickren JW, Berjian R, Douglass HO, Jr, Chu TM. Characterization of a new primary human pancreatic tumor line. *Cancer investigation*. 1986; 4: 15-23.
175. Lieber M, Mazzetta J, Nelson-Rees W, Kaplan M, Todaro G. Establishment of a continuous tumor-cell line (panc-1) from a human carcinoma of the exocrine pancreas. *International journal of cancer*. 1975; 15: 741-747.
176. Tan MH, Chu TM. Characterization of the tumorigenic and metastatic properties of a human pancreatic tumor cell line (AsPC-1) implanted orthotopically into nude mice. *Tumour biology : the journal of the International Society for Oncodevelopmental Biology and Medicine*. 1985; 6: 89-98.
177. Vasalou C, Helmlinger G, Gomes B. A mechanistic tumor penetration model to guide antibody drug conjugate design. *PloS one*. 2015; 10: e0118977.
178. Tarnowski M, Czerewaty M, Deskur A, Safranow K, Marlicz W, Urasinska E, Ratajczak MZ, Starzynska T. Expression of Cancer Testis Antigens in Colorectal Cancer: New Prognostic and Therapeutic Implications. *Disease markers*. 2016; 2016: 1987505.
179. Heninger E, Krueger TE, Thiede SM, Sperger JM, Byers BL, Kircher MR, Kosoff D, Yang B, Jarrard DF, McNeel DG, Lang JM. Inducible expression of cancer-testis antigens in human prostate cancer. *Oncotarget*. 2016; 7: 84359-84374.
180. Kim MP, Evans DB, Wang H, Abbruzzese JL, Fleming JB, Gallick GE. Generation of orthotopic and heterotopic human pancreatic cancer xenografts in immunodeficient mice. *Nature protocols*. 2009; 4: 1670-1680.
181. Rubio-Viqueira B, Jimeno A, Cusatis G, Zhang X, Iacobuzio-Donahue C, Karikari C, Shi C, Danenberg K, Danenberg PV, Kuramochi H, Tanaka K, Singh S, Salimi-Moosavi H, et al. An in vivo platform for translational drug development in pancreatic cancer. *Clinical cancer research : an official journal of the American Association for Cancer Research*. 2006; 12: 4652-4661.
182. Luo G, Long J, Zhang B, Liu C, Xu J, Ni Q, Yu X. Stroma and pancreatic ductal adenocarcinoma: an interaction loop. *Biochimica et biophysica acta*. 2012; 1826: 170-178.

